THE UNIVERSITY of ADELAIDE

Linear and Non-Linear Guided Waves for Damage Detection in Reinforced Concrete Structures

By

Ahmed Aseem

Thesis submitted for the degree of

Doctor of Philosophy

The University of Adelaide

School of Architecture and Civil Engineering

Faculty of Sciences, Engineering and Technology

Abstract

Reinforced concrete (RC) structures are a major part of our civil infrastructure and they provide valuable services in the sectors of residential, commercial, transport, defence, education and entertainment. RC structures can be subjected to debonding, corrosion and fire damage in unforeseen scenarios. The debonding and corrosion in RC reduce the bonding between steel rebar and concrete, which ultimately reduces the structural capacity of RC structure. Similarly, fire damage affects the structural and bond strength of RC structure. The fully established fire can cause temperature to rise above 1,000^{o}C, which can result in structural failure. Over the last decades, the fire damage has caused loss in structure, life and property. Structural health monitoring (SHM) of RC structures is a vital tool to detect damage in the early stages to avoid critical failure of such structures. Non-destructive testing using guided waves is an important technique for damage detection. Nonlinear features of guided waves are sensitive to material nonlinearity, cracks or debonding damage. The aim of this thesis is to utilize linear and nonlinear features of guided waves to detect debonding damage in rebar embedded in concrete. The work presented in this thesis has also investigated the effect of fire or heat damage on debonding between rebar and concrete in RC structures.

The thesis comprises published and prepared journal articles under the scope of damage detection in RC structures using linear and nonlinear guided waves. Chapter 1 highlights the importance of linear and nonlinear guided wave techniques to detect damage. The propagation of guided wave modes in cylindrical structures as rebar is also discussed. Nonlinear techniques, such as second harmonics and guided wave mixing, are introduced for damage detection, which has not been investigated for debonding damage in RC structures in the literature. Chapter 2 proposes to use the nonlinear feature of guided wave, second harmonic, to detect debonding damage in RC beam. Numerical and experimental investigations have shown the presence of

second harmonics in debonded specimens, which are generated due to contact acoustic nonlinearity (CAN) between the rebar and concrete surfaces. Chapter 2 also presents study to locate debonding damage using nonlinear guided waves.

In Chapter 3, an advanced nonlinear guided wave technique, guided wave mixing, is proposed to be used to detect debonding damage in ribbed reinforced concrete beams. Longitudinal mode pairs are mixed by satisfying synchronism conditions to generate sum combinational harmonics in longitudinal and torsional directions. Chapter 3 also proposes to use the phase reversal technique for magnifying the presence of sum combinational harmonics due to debonding damage. The sum combinational harmonics in the torsional direction are found to be more sensitive to damage than the longitudinal direction.

The impact of heat damage on reinforced concrete beams is investigated in Chapter 4. Nonlinear guided wave techniques have shown that second harmonics are produced due to debonding between rebar and concrete as the CAN effect. The debonding is generated due to heat damage in RC beam from 100^{o}C to 800^{o}C. The absence of second harmonics in bare steel rebar heated from 100^{o}C to 800^{o}C shows that second harmonics in RC beam are sourced from debonding or contact effect as compared to material nonlinearity in steel rebar. It is found that nonlinear features are more sensitive to debonding type damage as compared to the linear features.

Declaration

I, Ahmed Aseem, hereby declare that this work contains no material which has been accepted for the award of any other degree or diploma in my name, in any university or other tertiary institution and, to the best of my knowledge and belief, contains no material previously published or written by another person, except where due reference has been made in the text. In addition, I certify that no part of this work will, in the future, be used in a submission in my name, for any other degree or diploma in any university or other tertiary institution without the prior approval of the University of Adelaide and where applicable, any partner institution responsible for the joint-award of this degree.

I acknowledge that the copyright of published works contained within this thesis resides with the copyright holder(s) of those works. I also give permission for the digital version of my thesis to be made available on the web, via the University's digital research repository, the Library Search, and also through web search engines, unless permission has been granted by the University to restrict access for a period of time.

I acknowledge the support I have received for my research through the provision of Adelaide Government Research Training Program.

Signature:__ Date: 16/7/2023

Acknowledgment

First of all, I am honorary grateful to my God who gave me courage and skills to pursue my PhD. I will always be thankful to His blessings.

I am deeply grateful to my supervisor, Prof Ching Tai (Alex) Ng for his support and guidance. He had always encouraged me through my PhD journey. I've found him friendly and a great human being. I am also thankful to my co-supervisor A/Prof Hueng Fai Lam.

I am also thankful to my laboratory technician Mr. Ian Oger for his support. I would also like to mention the great support and valuable time from my fellow colleagues Dr. Carman Yeung, Dr. Juan Allen, Dr. Xianwen Hu, Dr. Tingyuan Yin, Mr. Jinhang Wu and Mr. Hankai Zhu.

Without the support from my family, my studies wouldn't have been easier. I would also like to credit my wife and my children for their encouragement and patience. Further, I am also grateful to my parents who believed in me to pursue these studies for the betterment. My PhD journey went through COVID-19 and I was also blessed with a beautiful daughter during this time. I would like to acknowledge Adelaide Graduate Research School who provided me additional time and support to carry on studies during these circumstances.

Lastly, I and thankful to Adelaide Graduate Research School, Faculty of Sciences, Engineering and Technology and the School of Architecture and Civil Engineering for providing any financial support to complete my studies.

I am delighted and grateful for this PhD experience. It is a roller coaster ride but it is worth riding on, if you are passionate about it.

List of Publications

The following articles presents a list of published and prepared journal and conference papers authored by the candidate.

Journal papers in the main research included in this thesis

1. **Aseem, A.** and C.T. Ng, *Debonding detection in rebar-reinforced concrete structures using second harmonic generation of longitudinal guided wave.* NDT & E International, 2021. **122**: 102496.
2. **Aseem, A.** and C.T. Ng, *Collinear nonlinear guided wave mixing for debonding detection in reinforced concrete beam using longitudinal and torsional wave modes.* Construction and Building Materials, 2023 (Under preparation)
3. **Aseem, A**. and C.T. Ng, *Detection and evaluation of heat damage in reinforced concrete beams using linear and nonlinear guided waves*. Structural Health Monitoring-an International Journal, 2023. (Submitted)

Relevant conference paper in the main research topic excluded in this thesis

1. **Aseem, A.** and C.T. Ng, *Debonding damage detection and monitoring using nonlinear guided wave for reinforced concrete beam subjected to bending*. 2021, Engineers Australia: BARTON, ACT.

Table of content

Contents

List of Figures

List of Tables

1. Chapter 1

1.1 Background

Civil structures provide valuable services to human society. In order to develop sustainable infrastructure, the integrity of such structures is a paramount factor. However, civil engineering structures are subjected to damages that can lead to the catastrophic failure of structures. The recent history has shown the sudden collapse of bridges and buildings due to unforeseen damages in structures, which have led to a fatality and economic loss [1-3] as seen in Figure 1.1. In reinforced concrete structures, the reinforced steel bar plays a vital role in providing strength to the structure. Various environmental factors such as carbonation due to the reaction of $Ca(OH)_2$ and CO_2 produce lime deteriorating the concrete and steel rebar by producing rust [4]. According to the Institute of Public Works Engineers Australia (2016), the economic loss due to corrosion in reinforced concrete structures is AUD30 Billion per year in Australia.

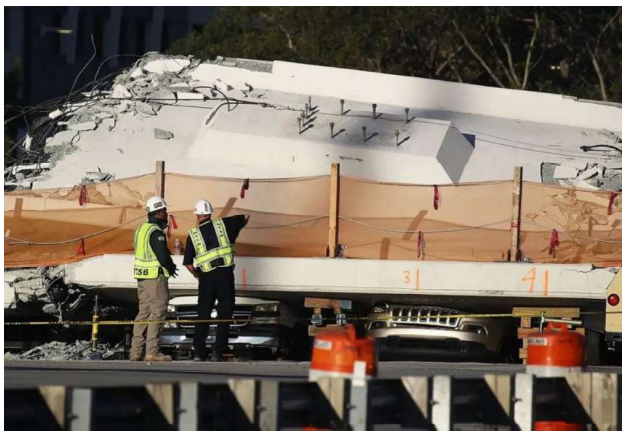

Figure 1.1 Collapse of pedestrian bridge [1]

The presence of loading and time-dependent corrosion in reinforced concrete beams increases the deflection profile, and reduces the time to reach the ultimate deflection limit and ductile behaviour and ultimate strength of the structure causing it to fail earlier without giving warning signs [5]. Apart from corrosion or debonding damage, the reinforced concrete

structures can be subjected to fire and heat damage, which reduces the young's modulus, compressive strength and tensile strength [6]. In last two decades, there has been a loss of more than one million life due to fire in buildings. In 2014, one percent of world GDP has been lost due to fire damage [7]. The RC structures can lose its strength and rigidity due to fire damage. Further, this loss in strength can result in irreversible structural damage which can lead to collapse of RC structure [8]. The bond strength and flexural capacity are also reduced due to heat damage in reinforced concrete structure [9].

The reliability of the structure must be evaluated to adopt precautions before any serious catastrophic failure. Various non-destructive techniques have been used to monitor damage [10, 11] and ultrasonic guided waves have proven to be a reliable technique for structural health monitoring (SHM) in concrete structures [12, 13]. In the literature, researchers have demonstrated to depict various types of damages using ultrasonic guided waves in reinforced concrete structures which include debonding [14-18], cracks [19, 20], surface cracks [21, 22], corrosion [23-30], delamination between rebar and concrete [31] and stress/strain monitoring [32] etc. Therefore, ultrasonic guided wave is considered to be a suitable technique for damage detection and quantification. However, limited research has been carried out to detect debonding in rebar reinforced concrete using various non-linear features of guided waves (GW). Further, guided wave techniques are not utilized to heat damage detection in reinforced concrete structures. The study in this project focus on the detection and quantification of debonding or heat damage in rebar reinforced concrete using advanced linear and non-linear guided wave methods. This detection can provide valuable information to avoid potential collapse of concrete structure.

1.2 Literature Review

Ultrasonic guided waves are mechanical stress waves and they travel along the surface of media with boundaries for guiding the waves. Initially, guided waves in plates were studied by Horace Lamb [33]. The guided waves differ from bulk waves and have many advantages as illustrated in Figure 1.2 [34]. The guided waves can travel a relatively long distance, and therefore, has the ability to scan larger areas with less attenuation. Unlike conventional bulk waves, where the transducer has to be moved to scan a particular location, guided waves can detect damage to areas that are inaccessible. Therefore, it gives a fair advantage for damage detection in reinforced concrete structures. The propagation characteristics of guided waves depend upon the excitation frequency of the wave, geometry and material properties of the structure.

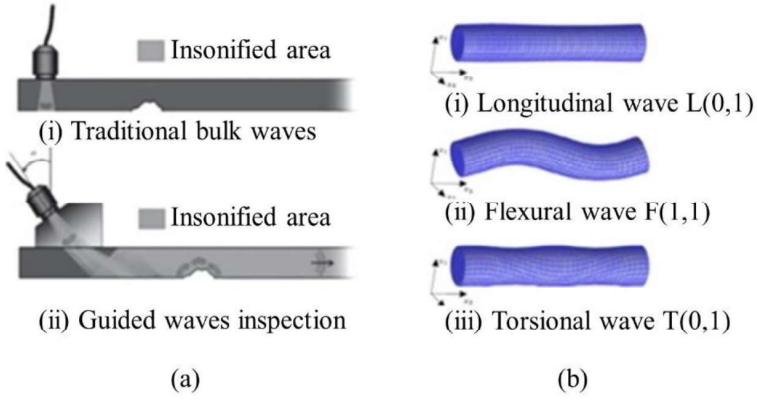

Figure 1.2 (a) Bulk waves vs guided waves [25] (b) Guided wave modes in cylinders

1.2.1 Guided Waves in Cylindrical Structure

Rebar is the key component providing strength to the structural element increasing yield strength, ultimate moment, tension and shear capacity and deflection capacity. It can reduce the design cross-sectional area. The defects in rebar can be caused by corrosion [4], fatigue loading [35] or fire [36] etc. Therefore, it is vital to monitor damage in rebar as it will affect the overall capacity of the structural element. Due to the cylindrical shape of the rebar,

ultrasonic guided wave has three wave modes in the cylindrical structure as shown in Figure 1.2 (b). Longitudinal wave mode has particle motion in the direction of wave propagation while flexural wave mode has particle motion in a perpendicular direction. The torsional mode tends to twist the particles of the cylinder along the direction of wave propagation.

The velocities for longitudinal and flexural waves can be expressed as Equation 1.1 and 1.2 respectively [37];

$$c_l = \sqrt{\frac{E(1-v)}{\rho(1+v)(1-2v)}} \qquad (1.1) \qquad\qquad c_S = \sqrt{\frac{E}{2\rho(1+v)}} \qquad (1.2)$$

where E is the elastic modulus of the material, ρ is the material density, c_l is the longitudinal wave speed, c_S is the shear wave velocity and v is the poison's ratio.

1.2.2 Linear methods

Ultrasonic guided waves has attracted a lot of researchers for damage detection in the past few decades. The damage detection through ultrasonic guided waves consists of wave generation, capture, signal processing and data processing. Therefore, the process requires an actuator to apply force for signal generated by function generator and a receiving sensor for signal capture. The receiving guided wave signal can have information regarding damage or material nonlinearity in the specimen. Ultrasonic guided wave damage detection methods can be classified into linear or non-linear. Linear ultrasonic methods detect the damage based on the variation of various linear features such as amplitude, time of arrival, signal energy, voltage, velocity and mode conversion [38];

These linear features are found to be more sensitive to gross defects in structures such as cracks, holes in plates, major corrosion, etc. as studied by Lu. et al. [38]. Linear ultrasonic features as time of flight of guided waves has been studied to detect damage in cracked concrete samples, and corrosion in rebar reinforced concrete [39]. Recently, Zima and Rucka (2018)

studied the dispersion of longitudinal waves for rebar partially embedded in a grout [40]. The longitudinal waves were excited at the free end and its diffraction and mode conversion from the embedded bar were studied. The delay in arrival time of diffracted waves from embedded bars with or without debonding indicated the presence of damage. Therefore, the variation in the arrival signature of various modes of guided waves in the embedded bar can indicate the presence of damage.

The linear ultrasonic parameters, such as pulse velocity, are found to be less sensitive to damage as compared nonlinear ultrasonic features [41, 42]. Non-linear features can be more sensitive and accurate in detecting damage in early stages such as corrosion initiation, minor cracks, excessive stress levels and fatigue crack. Further, the research has also indicated that the linear technique requires to establish baseline measurements to detect damage levels in the structure. The process of quantifying and locating damage is difficult in linear methods as they are insensitive to minor cracks and nonlinearities in the structure.

1.2.3 Nonlinear methods

In contrast to linear methods, nonlinear methods are able to detect minor cracks, nonlinearity and fatigue damage in the material. In the past decade, nonlinear methods have been studied by many researchers to detect damage in steel, concrete, aluminium, metals and other various materials. The nonlinear phenomenon for ultrasonic guided waves generates when they interact with material damage. Various nonlinear features have been used to detect and quantify damage [13, 43-45] such as;

- Second harmonic and higher harmonics
- Combinational harmonics due to guided wave mixing

When ultrasonic waves (fundamental) interact with microscale damage, fundamental wave energy converts into second harmonic [46]. The interaction of GW with contact-type damage

generates second harmonics. This type of phenomenon is known as Contact Acoustic Non-Linearity (CAN) [47]. Based on the presence of sub and higher harmonics, damage and material changes can be quantified and therefore serves as an important factor for SHM. The cracks in cement mortar were detected by the second harmonic generations (SHG) [48]. Recently, SHG were studied for detecting debonding in Carbon Fiber Reinforced Polymer (CFRP) Concrete [18, 49]. Apart from concrete and steel, damage detection has also been extended to aluminium plates and pipes. The increase in the density of cracks in aluminium plates has shown an increase in the amplitude of second harmonics. The acoustic nonlinearity parameter is also sensitive to fatigue loading in the aluminium plates [50-52]. The ability of nonlinear guided wave to detect debonding or contact type damage in embedded rebars in concrete using second harmonics are not studied in the literature.

Apart from material nonlinearity and contact type damage, higher harmonics can be sourced from system nonlinearities. To avoid system nonlinearities in damage detection and quantification, guided wave mixing is studied by many researchers.

Wave mixing technique has been adopted for damage detection in various structures. Initially, Jones et al. discussed that two intersecting longitudional or transverse waves interaction produce scattering wave provided certain resonant conditions are met [53]. The wave mixing can be collinear (waves travelling in parallel direction) and non-collinear (nonparallel coplanar directions), while collinear wave mixing has one-way mixing for waves travelling in the same direction and two-way mixing for waves travelling in opposite directions.

When primary elastic waves interact each other in nonlinearity or damage, resonant conditions needs to be met to produce resonant wave. The nonlinear parameters generated from wave mixing have the potential to be more sensitive than nonlinear parameters in second harmonic generation because wave mixing nullifies the effects of system nonlinearities and

only represents the material nonlinearity or damage [54]. Recently, wave mixing has been used to detect cracks in metals and the damage has been quantified with the help of nonlinearity parameter. The generation of frequency sidebands at sum and different frequencies of wave mixing indicate the presence of damage [55-58]. The study has also been extended to detect ageing, deformation and fatigue in plastics [59-61]. Similarly, fatigue and thermal ageing in aluminium have been studied using non-collinear wave mixing techniques [62, 63]. Unlike metal structures, in which researcher have been able to quantify the damage, nonlinear parameter for debonding damage using guided wave mixing have not been studied in concrete structures. Concrete has complex heterogeneous microstructure and many studies have shown the ability of wave mixing to detect alteration of concrete subjected to oxidation and alkali silica damage. Oxidation and alkali silica reaction tends to change the microstructural and mechanical properties and therefore tends to alter the nonlinear acoustic parameter [42, 64]. However, the debonding type damage between rebar and concrete is not studied using guided wave mixing in the literature. Nonlinear guided wave mixing has the potential to generate sum or different frequencies due to debonding or contact type damage in reinforced concrete structures.

1.3 Research project objectives

This PhD project focuses on linear and nonlinear guided wave techniques for damage detection in reinforced concrete structure. The conventional linear ultrasonic methods are less sensitive to debonding damage in reinforced concrete as compared to nonlinear methods proposed in this thesis. Numerical investigations using FE study to detect and locate debonding damage in RC are also unique in this research as compared to studies found in the literature. GW mixing study using numerical and experimental investigation for debonding damage in RC are not found in literature, which gives this research a distinctive objective for GW study. Further, the practical damage due to fire in RC is studied through experimental investigation via nonlinear

guided wave methods. These studies layout the notable objectives for GW study in RC structure. The debonding type damage is considered between rebar and concrete. The reinforced concrete beams are also studied for heat type damage. The effect of temperature increase on bonding between rebar and concrete is studied using linear and nonlinear guided waves. Second harmonic generation and guided wave mixing techniques are used to detect damage in rebar reinforced concrete structure. The project comprises the following objectives:

- To detect debonding damage in rebar reinforced concrete using second harmonic generation of longitudinal guided wave
- To estimate debonding damage location in embedded rebar with numerical and experimental investigation of longitudinal guided wave
- To investigate debonding damage using guided wave mixing of longitudinal and torsional wave modes in reinforced concrete beams
- To develop finite element (FE) model of reinforced concrete beam and conducting experimental investigation for carrying out damage detection using second harmonics generation and guided wave mixing of longitudinal mode pairs
- To study the effect of heat damage on linear and nonlinear guided wave propagation in bonded and debonded reinforced concrete beam

1.4 Thesis structure

This thesis comprises of three journal articles for detecting debonding and heat damage in reinforced concrete beams using linear and nonlinear guided wave techniques. Chapter 1 presents the background for SHM. The importance of guided wave techniques is highlighted to detect damage in order to avoid catastrophic failure in reinforced concrete structures. Linear and nonlinear guided wave methods are discussed to detect debonding or contact-type damage.

Later, the objectives of the thesis are defined to detect and locate damage in embedded rebar in concrete using second harmonic generation and guided wave mixing techniques.

Chapter 2 discusses the debonding damage detection and location estimation using the second harmonic generation of longitudinal guided wave in the reinforced concrete beam. With rebar embedded in concrete, the propagating guided wave energy is leaked into the surrounding concrete. Longitudinal mode pairs are utilized for the excitation and receiving of guided wave signals to maximize debonding damage detection. The circular piezoelectric transducers (PZTs) are attached to the cylinder shape rebar ends to effectively propagate longitudinal guided wave mode. After validation of longitudinal mode pair propagation in bare and embedded rebar, numerical and experimental investigations are carried out to detect debonding damage. This chapter has shown that second harmonic is generated in the debonded specimen, which is absent in fully bonded specimens. The debonding is created using Mylar sheet, which is wrapped around rebar embedded in concrete. The amplitude of the second harmonic received at the rebar end tends to increase with debonding size. In order to locate the debonding, time-frequency and wavenumber frequency analysis is conducted along with phase velocity curves of longitudinal mode pairs. This valuable analysis provided information for the difference in time of arrival of second harmonics to estimate debonding location. This technique is also experimentally verified to locate debonding damage in the reinforced concrete beam.

Chapter 3 discusses the nonlinear guided wave mixing of longitudinal wave modes to detect debonding damage in the reinforced concrete specimen. The ribbed steel rebars are used in this study. For guided wave mixing to generate second-order combinational harmonics, phase matching and synchronism conditions for longitudinal mode pairs are met. Two longitudinal mode pairs are selected for the wave mixing study. The numerical and experimental investigation shows the presence of sum combinational harmonics for both mode pairs in the debonded specimen, which is absent in the fully bonded specimen. The receiving

mode pair in the longitudinal and torsional direction both represent the presence of sum combinational harmonics due to debonding damage. To further amplify the debonding damage, phase reversal technique is applied using guided wave mixing. With the sum of original excited signal and phase reversed signal, the second harmonics and sum combinational harmonics are magnified in the frequency domain. By utilizing this technique and wavenumber frequency analysis, the location of debonding is also estimated. The sum combinational harmonics received in torsional wave mode is more sensitive to debonding damage as compared to longitudinal wave mode.

Chapter 4 investigates the heat damage on rebar and reinforced concrete beams using linear and nonlinear guided waves experimentally. Initially, the embedded sensors attached to rebar ends are used to detect heat damage using the second harmonic generation of longitudinal guided wave. The embedded sensors are functional to detect heat damage till 300^{o}C. To overcome this limit, the reinforced concrete specimen with exposed rebar ends are prepared. This type of specimen is heated till 800^{o}C to monitor the debonding damage due to elevated temperature. At 1,000^{o}C, the specimen is deteriorated and split into pieces due to heat damage. The bonded and debonded specimens have shown the presence of second harmonics due to heat damage at elevated temperatures, which is absent in fully bonded unheated specimens. In order to review the source of second harmonics due to heat damage, bare rebar is also heated and tested for nonlinear guided waves. The elevated temperature for bare rebar shows the absence of second harmonics, which depicts that nonlinearity is sourced from contact-type damage between rebar and concrete as compared to any material nonlinearity from bare rebar. The heat damage has an effect on the linear features of guided waves, which is observed in terms of the amplitude of guided wave signal.

Chapter 5 highlights the key factors of this research and their significance. It further recommends future studies.

1.5 References

1. *New York State settles in collapse of bridge. (New York State Thruway bridge into Schoharie Creek)*. 1990. p. 10.
2. *United States: Engineer on Florida Bridge Project Reported Cracks Days Before Collapse*. 2018: Bangkok.
3. Manik, J.A. and J. Yardley, *Building Collapse in Bangladesh Kills Scores of Garment Workers.(Foreign Desk)(Rana Plaza)*. 2013. p. A1.
4. Zhao, Y.a., *Steel corrosion-induced concrete cracking*, ed. W.a. Jin. 2016: Elsevier.
5. Du, Y.G., M. Cullen, and C.K. Li, *Structural performance of RC beams under simultaneous loading and reinforcement corrosion.* Construction and Building Materials, 2013. **38**: p. 472-481.
6. Ozbolt, J., et al., *3D numerical analysis of reinforced concrete beams exposed to elevated temperature.* Engineering Structures, 2014. **58**: p. 166-174.
7. Kodur, V.K.R., P. Kumar, and M.M. Rafi, *Fire hazard in buildings: review, assessment and strategies for improving fire safety.* PSU Research Review, 2019.
8. Qin, D., et al., *A comprehensive review on fire damage assessment of reinforced concrete structures.* Case Studies in Construction Materials, 2022. **16**: p. e00843.
9. Ghazaly, N., et al., *Evaluation of bond strength between steel rebars and concrete for heat-damaged and repaired beam-end specimens.* Engineering Structures, 2018. **175**: p. 661-668.
10. Salençon, J., W. Ostachowicz, and J.A. Güemes, *New Trends in Structural Health Monitoring*. Vol. 542. 2012, Vienna: Vienna: Springer.
11. Büyüköztürk, O.a., *Nondestructive Testing of Materials and Structures*, ed. M.A.a. Taşdemir, et al. 2013: Springer Netherlands : Imprint: Springer.
12. Chen, J., C.L. Yang, and Q.Q. Guo, *Evaluation of surface cracks of bending concrete using a fully non-contact air-coupled nonlinear ultrasonic technique.* Materials and Structures, 2018. **51**(4).
13. Kim, G., et al., *In situ nonlinear ultrasonic technique for monitoring microcracking in concrete subjected to creep and cyclic loading.* Ultrasonics, 2018. **88**: p. 64-71.
14. Xu, B., B. Li, and G.B. Song, *Active Debonding Detection for Large Rectangular CFSTs Based on Wavelet Packet Energy Spectrum with Piezoceramics.* Journal of Structural Engineering, 2013. **139**(9): p. 1435-1443.
15. Li, J.S., et al., *Guided waves for debonding identification in CFRP-reinforced concrete beams.* Construction and Building Materials, 2017. **131**: p. 388-399.
16. Wu, F. and F.K. Chang, *Debond detection using embedded piezoelectric elements in reinforced concrete structures - Part I: Experiment.* Structural Health Monitoring-an International Journal, 2006. **5**(1): p. 5-15.
17. Wu, F. and F.K. Chang, *Debond detection using embedded piezoelectric elements for reinforced concrete structures - Part II: Analysis and algorithm.* Structural Health Monitoring-an International Journal, 2006. **5**(1): p. 17-28.
18. Mohseni, H. and C.T. Ng, *Rayleigh wave propagation and scattering characteristics at debondings in fibre-reinforced polymer-retrofitted concrete structures.* Structural Health Monitoring-an International Journal, 2019. **18**(1): p. 303-317.
19. Pahlavan, L., et al., *Interaction of ultrasonic waves with partially-closed cracks in concrete structures.* Construction and Building Materials, 2018. **167**: p. 899-906.
20. Park, S., et al., *Multiple crack detection of concrete structures using impedance-based structural health monitoring techniques.* Experimental Mechanics, 2006. **46**(5): p. 609-618.
21. Zhu, J.S., C. Gao, and L.K. He, *Piezoelectric-based Crack Detection Techniques of Concrete Structures: Experimental Study.* Journal of Wuhan University of Technology-Materials Science Edition, 2012. **27**(2): p. 346-352.
22. Lee, F.W., et al., *Concrete Subsurface Crack Characterization by Means of Surface Rayleigh Wave Method.* Aci Materials Journal, 2019. **116**(1): p. 113-123.

23. Moustafa, A., et al., *Corrosion monitoring of post-tensioned concrete structures using fractal analysis of guided ultrasonic waves.* Structural Control & Health Monitoring, 2014. **21**(3): p. 438-448.
24. Mustapha, S., et al., *Damage detection in rebar-reinforced concrete beams based on time reversal of guided waves.* Structural Health Monitoring-an International Journal, 2014. **13**(4): p. 347-358.
25. Sriramadasu, R.C., Y. Lu, and S. Banerjee, *Identification of incipient pitting corrosion in reinforced concrete structures using guided waves and piezoelectric wafer transducers.* Structural Health Monitoring-an International Journal, 2019. **18**(1): p. 164-171.
26. Ervin, B.L. and H. Reis, *Longitudinal guided waves for monitoring corrosion in reinforced mortar.* Measurement Science and Technology, 2008. **19**(5).
27. Jiang, T.Y., et al., *Monitoring of Corrosion-Induced Degradation in Prestressed Concrete Structure Using Embedded Piezoceramic-Based Transducers.* Ieee Sensors Journal, 2017. **17**(18): p. 5823-5830.
28. Sharma, S. and A. Mukherjee, *Longitudinal Guided Waves for Monitoring Chloride Corrosion in Reinforcing Bars in Concrete.* Structural Health Monitoring-an International Journal, 2010. **9**(6): p. 555-567.
29. Sharma, S. and A. Mukherjee, *Monitoring Corrosion in Oxide and Chloride Environments Using Ultrasonic Guided Waves.* Journal of Materials in Civil Engineering, 2011. **23**(2): p. 207-211.
30. Sharma, A., et al., *Ultrasonic guided waves for monitoring corrosion of FRP wrapped concrete structures.* Construction and Building Materials, 2015. **96**: p. 690-702.
31. Reis, H., et al., *Estimation of corrosion damage in steel reinforced mortar using guided waves.* Journal of Pressure Vessel Technology-Transactions of the Asme, 2005. **127**(3): p. 255-261.
32. Miller, T.H., et al., *A new guided wave-based technique for corrosion monitoring in reinforced concrete.* Structural Health Monitoring-an International Journal, 2013. **12**(1): p. 35-47.
33. Lamb, H., *On waves in an elastic plate.* Proceedings of the Royal Society of London Series a-Containing Papers of a Mathematical and Physical Character, 1917. **93**(648): p. 114-128.
34. Rose, J.L.a. and J.L. Rose, *Ultrasonic guided waves in solid media*. 2014: Cambridge University Press.
35. Rocha, M., E. Brühwiler, and A. Nussbaumer, *Microstructural influence on the scatter in the fatigue life of steel reinforcement bars.* International Journal of Fatigue, 2015. **75**: p. 205-212.
36. Kumar, V., et al., *Effect of temperature on mechanical properties of pre-damaged steel reinforcing bars.* Construction and Building Materials, 2013. **46**: p. 19-27.
37. Zima, B. and R. Kędra, *Reference-free determination of debonding length in reinforced concrete beams using guided wave propagation.* Construction and Building Materials, 2019. **207**: p. 12.
38. Lu, Y., et al., *Guided waves for damage detection in rebar-reinforced concrete beams.* Construction and Building Materials, 2013. **47**: p. 370-378.
39. Chen, J., et al., *Characterization of thermal damage in sandstone using the second harmonic generation of standing waves.* International Journal of Rock Mechanics and Mining Sciences, 2017. **91**: p. 81-89.
40. Zima, B. and M. Rucka, *Guided ultrasonic waves for detection of debonding in bars partially embedded in grout.* Construction and Building Materials, 2018. **168**: p. 124-142.
41. Shah, A.A., Y. Ribakov, and C. Zhang, *Efficiency and sensitivity of linear and non-linear ultrasonics to identifying micro and macro-scale defects in concrete.* Materials & Design, 2013. **50**: p. 905-916.
42. Ju, T.H., et al., *Ultrasonic nondestructive evaluation of alkali-silica reaction damage in concrete prism samples.* Materials and Structures, 2017. **50**(1).
43. Chen, J., et al., *Characterization of concentrated and distributed cracks in concrete using a harmonic wave modulation technique.* Materials and Structures, 2018. **51**(1).
44. Thiele, S., et al., *Air-coupled detection of nonlinear Rayleigh surface waves to assess material nonlinearity.* Ultrasonics, 2014. **54**(6): p. 1470-1475.

45. Carcione, A., et al., *Modulated high frequency excitation approach to nonlinear ultrasonic NDT.* Journal of Sound and Vibration, 2019. **446**: p. 238-248.
46. Kim, G., et al., *Drying shrinkage in concrete assessed by nonlinear ultrasound.* Cement and Concrete Research, 2017. **92**: p. 16-20.
47. Soleimanpour, R., *Damage detection of defects using linear and nonlinear guided waves*, A.C.-T. Ng, E. School of Civil, and E. Mining, Editors. 2017.
48. Chen, J., J. Ren, and T.Y. Yin, *Nondestructive evaluation of notched cracks in mortars by nonlinear ultrasonic technique.* Nondestructive Testing and Evaluation, 2016. **31**(2): p. 109-121.
49. Ng, C.-T., H. Mohseni, and H.-F. Lam, *Debonding detection in CFRP-retrofitted reinforced concrete structures using nonlinear Rayleigh wave.(Report).* Mechanical Systems and Signal Processing, 2019. **125**: p. 245.
50. Pruell, C., et al., *Evaluation of fatigue damage using nonlinear guided waves.* Smart Materials & Structures, 2009. **18**(3).
51. Zhao, Y.X., et al., *Generation mechanism of nonlinear ultrasonic Lamb waves in thin plates with randomly distributed micro-cracks.* Ultrasonics, 2017. **79**: p. 60-67.
52. Zhang, M.Y., et al., *Damage detection of fatigue cracks under nonlinear boundary condition using subharmonic resonance.* Ultrasonics, 2017. **77**: p. 152-159.
53. Jones, G.L. and D.R. Korbett, *Interaction of Elastic Waves in an Isotropic Solid.* Journal of the Acoustical Society of America, 1963. **35**(1): p. 5-&.
54. Liu, M.H., et al., *Measuring acoustic nonlinearity parameter using collinear wave mixing.* Journal of Applied Physics, 2012. **112**(2).
55. Jiao, J.P., et al., *Micro-crack detection using a collinear wave mixing technique.* Ndt & E International, 2014. **62**: p. 122-129.
56. Jiao, J.P., et al., *Nonlinear Lamb wave-mixing technique for micro-crack detection in plates.* Ndt & E International, 2017. **85**: p. 63-71.
57. Liu, P., et al., *Noncontact detection of fatigue cracks by laser nonlinear wave modulation spectroscopy (LNWMS).* Ndt & E International, 2014. **66**: p. 106-116.
58. Lim, H.J., et al., *Reference-free fatigue crack detection using nonlinear ultrasonic modulation under various temperature and loading conditions (vol 45, pg 468, 2014).* Mechanical Systems and Signal Processing, 2015. **54-55**: p. 506-506.
59. Sun, M.X., et al., *Scanning non-collinear wave mixing for nonlinear ultrasonic detection and localization of plasticity.* Ndt & E International, 2018. **93**: p. 1-6.
60. Demcenko, A., et al., *Non-collinear wave mixing for non-linear ultrasonic detection of physical ageing in PVC.* Ndt & E International, 2012. **49**: p. 34-39.
61. Croxford, A.J., et al., *The use of non-collinear mixing for nonlinear ultrasonic detection of plasticity and fatigue.* Journal of the Acoustical Society of America, 2009. **126**(5): p. El117-El122.
62. Kim, Y., H.J. Lim, and H. Sohn, *Nonlinear ultrasonic modulation based failure warning for aluminum plates subject to fatigue loading.* International Journal of Fatigue, 2018. **114**: p. 130-137.
63. Ju, T., et al., *Nondestructive evaluation of thermal aging of adhesive joints by using a nonlinear wave mixing technique.* NDT and E International, 2019. **103**(2019): p. 62-67.
64. McGovern, M.E., W.G. Buttlar, and H. Reis, *Field estimation of oxidative ageing in asphalt concrete pavements using non-collinear wave mixing.* Insight, 2015. **57**(11): p. 625-634.

2. Chapter 2 (Paper 1). Debonding Detection in Rebar-reinforced Concrete Structures using Second Harmonic Generation of Longitudinal Guided Wave

Abstract

Nonlinear features of ultrasonic guided waves (GWs) is studied for debonding detection and location estimation in rebar reinforced concrete structure. The study shows that the presence of debonding between steel rebar and concrete surface produces breathing phenomenon causing contact acoustic nonlinearity (CAN), which generates second harmonics. Time-frequency analysis is used to estimate the location of debonding in this study. At a particular frequency, embedded rebar has much greater number of wave modes in bare rebar. To avoid unnecessary complexity, only longitudinal GW modes for bare and embedded rebar are excited and received to detect and locate debonding. To precisely determine the wave mode at excited frequency and frequency of second harmonics, frequency-wavenumber analysis is performed using 2D-Fast Fourier Transform of time-space data. Three-dimensional explicit finite element simulations are performed for various case studies and the model is validated by experimentally measured data. The results of this study show that the proposed method is practically viable and beneficial for debonding detection and location estimation in reinforced concrete structures.

Keywords: Debonding; Nonlinear guided wave; Reinforced concrete structure; Second harmonic; Contact acoustic nonlinearity

Statement of Authorship

Title of Paper	Debonding Detection in Rebar-reinforced Concrete Structures using Second Harmonic Generation of Longitudinal Guided Wave
Publication status	☒ Published ☐ Accepted for Publication ☐ Submitted for Publication ☐ Unpublished and unsubmitted work written in manuscript style
Publication Details	Aseem, A. and C.T. Ng, *Debonding detection in rebar-reinforced concrete structures using second harmonic generation of longitudinal guided wave.* Ndt & E International, 2021. **122**.

Principal Author

Name of Principal Author (Candidate)	Ahmed Aseem		
Contribution to the Paper	Conceptualization, Developing and validating numerical models, Conducting experimental measurements, Signal processing and data analysis, Writing the original draft and editing.		
Overall percentage (%)	80%		
Certification:	This paper reports on original research I conducted during the period of my Higher Degree by Research candidature and is not subject to any obligations or contractual agreements with a third party that would constrain its inclusion in this thesis. I am the primary author of this paper.		
Signature		Date	16-07-2023

Co-Author Contributions

By signing the Statement of Authorship, each author certifies that:

i. the candidate's stated contribution to the publication is accurate (as detailed above);

ii. permission is granted for the candidate in include the publication in the thesis; and

iii. the sum of all co-author contributions is equal to 100% less the candidate's stated contribution.

Name of Co-Author	Ching-Tai Ng		
Contribution to the Paper	Supervision, writing – review and editing.		
Signature		Date	18-07-2023

Please cut and paste additional co-author panels here as required.

2.1 Introduction

Civil engineering structures made by reinforced concrete are vital part of our infrastructure. These structures are subjected to environmental and external loading, along with corrosion and fatigue, which can lead to damage and degradation. The integrity of these structures cannot be neglected. The bonding between steel rebar and concrete develops required strength in reinforced concrete structures. Corrosion and debonding can significantly reduce the ultimate strength and serviceable life of the reinforced concrete structure [1]. Different Structural Health Monitoring (SHM) techniques have been developed by researchers to assess the integrity of various structures. Linear and nonlinear features of ultrasonic guided waves (GWs) have been proven to be reliable in damage detection. The linear features of ultrasonic GWs have been found to be sensitive to gross defects in structures, such as holes, notches and open cracks etc [2]. The nonlinear features have been recognised to be more sensitive to material nonlinearities, fatigue cracks, fatigue and material degradation [3, 4].

2.1.1 Linear features of ultrasonic guided waves

Linear features of ultrasonic GWs, for example, wave amplitude, velocity, energy and time-of-flight (ToF) were used by many researchers for detecting damage in reinforced concrete structures and composites. In the literature, GWs have been widely recognized as one of the promising techniques for damage detection in reinforced concrete structures. The surface cracks in reinforced concrete can be detected using linear features [5, 6]. Steel rebar damage in concrete was studied by Lu *et al*. and Mustapha *et al*. [7, 8] using linear features of ultrasonic GWs and they proposed a time reversal method to detect the damage. Similarly, GWs have also been used to monitor reinforced concrete beam subjected to damage using embedded and surface bonded piezo electric transducers [9]. Zhu *et al*. [10] demonstrated the use of linear features of GWs in detecting debonding between steel and concrete at various locations in reinforced concrete structures. Wu and Chang [11, 12] experimentally observed the linear

feature of GWs for steel debonding in concrete subjected to loading. The sensitivity of energy distribution of GWs for debonding detection using wavelet technique were studied for reinforced concrete [13]. Mohseni and Ng studied the scattering of linear GWs at surface debonding in fibre reinforced polymer (FRP) retrofitted concrete structure [14].

Ultrasonic GWs are also capable of monitoring accelerated corrosion at steel bar in reinforced concrete [15-19]. Recently, Zima and Kedra [20, 21] used one of the linear features of GWs, time-of-flight of different GW modes, for debonding size estimation in reinforced concrete beams. They used variation of group velocities in debonded region to detect damage. The effect of multiple debondings was also studied but the linear features were unable to detect the location of debonding. The aforementioned damage detection methods used the variation in voltage, velocity, time-of-flight, amplitude and energy of GWs to detect the damage. However, damage detection methods require baseline data as the damage detection is achieved by comparing the measured data from intact structures and the structures with the damage. The variation of environmental conditions, such as temperature and external loading, can make the baseline subtraction fail in extracting the damage information from the measured data. In the literature, nonlinear features of GWs have demonstrated their feasibility for damage detection without using the baseline data.

2.1.2 Nonlinear features of guided waves

When ultrasonic waves interact with material nonlinearity and/or contact type of damages, the fundamental wave energy converts into higher harmonics, which is one of the nonlinear features of GWs. In the literature, nonlinear features of GWs have been proven to be promising for damage identification and quantification. Soleimanpour and Ng [22] used second harmonic generation of GWs to detect and locate delamination in laminated composite beams. Mohseni and Ng demonstrated that the higher harmonic generation in FRP-retrofitted concrete structures can be used to detect debonding [23]. Chen *et al*. showed that the presence of surface cracks in

bending concrete also generate second harmonics due to the breathing effect [24]. But these studies were limited to detect debonding between FRP and concrete, or crack in reinforced concrete structures using second harmonics of GWs.

The presence of debonding between steel rebar and concrete can significantly reduce the stiffness of the reinforced concrete structures. In the literature, majority of the studies only used linear features of GWs to detect debonding and they require baseline data to extract the linear features, which are not sensitive to debonding. It has been recognized that second harmonic is potential to detect damage without using the baseline data. Therefore, an insight into the nonlinear features, such as second harmonic, is required to develop methods for debonding detection.

Second harmonics can be produced due to the presence of material nonlinearity and imperfections. When wave interacts with weak material nonlinearity, higher order harmonics are generated and they have been studied by many researchers [25-29]. The presence of imperfections in materials, such as micro cracks, holes, discontinuities and delamination produce contact surfaces within material, can lead to the second harmonic generation [30]. This phenomenon is known as contact acoustic nonlinearity (CAN). Solodov *et al*. have described the phenomenon of generation of higher harmonics due to clapping interfaces in detail [31]. It enables fundamental wave mode generating second harmonics while interacting with defects. These kinds of studies have been carried out to detect cracks, fatigue and other defects in plate-like structures [24, 32, 33]. Klepka *et al.* studied nonlinear vibro-acoustic wave interaction mechanism to detect contact damage in aluminium plate [34] . Guan *et al*. [35] detected fatigue cracks in pipe using nonlinear GWs. But the nonlinear features of GWs have not been widely studied for contact type damages for embedded rebar in concrete. The nonlinear features are baseline free techniques for damage detection and have therefore advantage over linear features. For embedded structures such as rebar in concrete, no significant research has been

reported to detect damage using nonlinear features. The paper also studies the time-frequency analysis, which is used for debonding location estimation. Although linear techniques are available for damage estimation in embedded rebar but the nonlinear baseline free technique is proposed to be a useful method in civil engineering applications. This paper focuses on the use of linear and nonlinear features, i.e. second harmonic of longitudinal GWs, to detect the debonding between in rebar and concrete. The exposed ends of embedded rebar are considered for excitation and receiving to understand wave propagation phenomenon for the fundamental study as mentioned in this paper.

This paper is organized as follows. The proposed methodology is presented in Section 2.2. Numerical and experimental investigations are described in Sections 2.3 and 2.4, respectively. The results are then discussed and used to elaborate the use of nonlinear features in detecting and locating debonding between steel rebar and concrete in Section 2.5.

2.2 Proposed Methodology

For reinforced concrete structures with debonding between rebar and concrete, there are two types of nonlinearity can generate second harmonics. They are weakly material nonlinearity and contact nonlinearity, which is caused by the debonding between steel rebar and concrete. The study focuses on CAN, which has proven to have much larger magnitude of second harmonic as compared to that generated by material nonlinearity. This makes it easier to be used for damage detection [36]. The debonding (contact damage) can be detected and quantified using a ratio of second harmonic amplitude (A_2) to fundamental frequency amplitude (A_1), i.e. $\beta = A_2/A_1$, where β is nonlinear acoustic parameter for contact type of damage.

2.2.1 Debonding detection using second harmonics

When GW propagates in embedded rebar, various wave modes are generated. Due to the presence of surrounding concrete, the energy of GW is leaked from rebar to concrete as shown in Figure 2.1. However, the energy will not be leaked into concrete if the phase velocity of propagating wave in rebar is less than the bulk shear and longitudinal velocities of the concrete. There are two cases of wave energy leakage, (a) when phase velocity is greater than the bulk shear wave and less than the bulk longitudinal wave velocity of concrete, only shear wave is leaked from rebar into concrete; (b) when phase velocity is greater than both the bulk shear and longitudinal wave velocity of concrete, both bulk and shear wave energy are leaked from rebar into concrete [37]. Considering the phase velocity of steel rebar is greater than either shear or longitudinal wave of concrete, the energy is likely to be leaked into concrete. However, the propagation of GW in embedded rebar produces multiple wave modes and this will be discussed later. The leaked energy will not provide enough information for debonding detection. The interaction of wave propagating in embedded rebar with debonding is the main focus of this study. The presence of debonding at rebar in concrete creates discontinuity between rebar and concrete surface and affects the GW propagation. The discontinuity behaves as contact surface and second harmonics are generated due to the CAN phenomenon as shown in Figure 1. When a GW with tension and compression components passes through a debonding region, the contact surfaces of rebar and concrete open due to tensile components of the wave and close due to compression components. When GW interact at the debonding, the opening and closing of contact surfaces generate second harmonics.

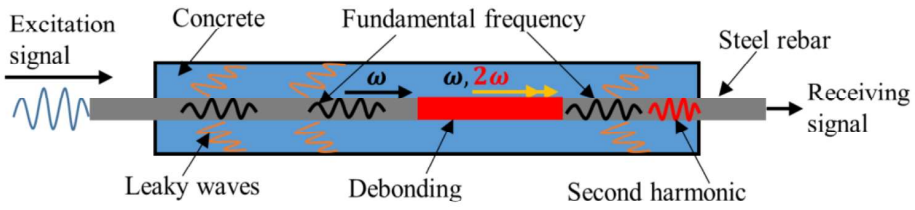

Figure 2.1 Generation of second harmonics at debonding between rebar and concrete

After the GW passed through the debonding, the propagating GW consists of fundamental and second harmonics. The presence of second harmonic provides valuable information for debonding detection. The debonding of varying sizes can be quantified using relative nonlinear acoustic parameter β discussed earlier of this section. Based on the generation of second harmonic, damages can be quantified, and therefore, serves as an important indicator for SHM.

2.2.2 Guided wave modes in bare rebar and rebar embedded in concrete

For debonding detection in steel rebar reinforced concrete, the GW propagation in bare rebar and embedded rebar is investigated in this section. It is necessary to understand different GW modes in bare steel rebar and embedded rebar as shown in Figure 1. Three GW modes can exist in circular waveguide, they are longitudinal L(0,*n*), torsional T(0,*n*) and flexural F(1,*n*) wave mode, where *n* represents the mode order, while 0 and 1 are for symmetric and asymmetric wave fields, respectively. For rebar embedded in concrete, the number of flexural GW modes is greater than longitudinal and torsional modes. Moreover, torsional GW modes have greater attenuation in embedded rebar than flexural and longitudinal modes. For simplicity in analysis, only longitudinal GW modes are excited and measured. The group velocity dispersion curve of longitudinal GW modes for 10mm radius bare circular steel rebar is calculated using DISPERSE software [37]. GW modes propagating in structures embedded in concrete have greater number of wave modes. For 10mm radius steel bar embedded in concrete having outer diameter of 100mm, the first 13 longitudinal wave modes were calculated using DISPERSE and the results are shown as L(0,1) – L(0,13) in Figure 2. The circular cross-section of concrete

was chosen because of simplicity in calculating the dispersion curves in DISPERSE. The properties of the steel and concrete are listed in Table 2.1.

Table 2.1 Material properties of steel and concrete

Material	Density (kg/m^3)	Elastic Modulus (GPa)	Poisson's ratio
Steel	7880	207	0.33
Concrete	2289	32.5	0.14

There are only two longitudinal GW modes existed in bare rebar shown as $L(0,1)_b$ and $L(0,2)_b$, while embedded rebar in concrete has 13 longitudinal GW modes within the frequency range of 0-200 kHz as shown in Figure 2.2. The subscript b means the results are for bare rebar. The fastest wave mode in bare rebar is $L(0,1)_b$, while the second order longitudinal wave mode $L(0,2)_b$ appears after 180 kHz. The group velocities of embedded rebar wave modes L(0,1) – L(0,7) have smaller value than that of $L(0,1)_b$ for frequency less than 132 kHz.

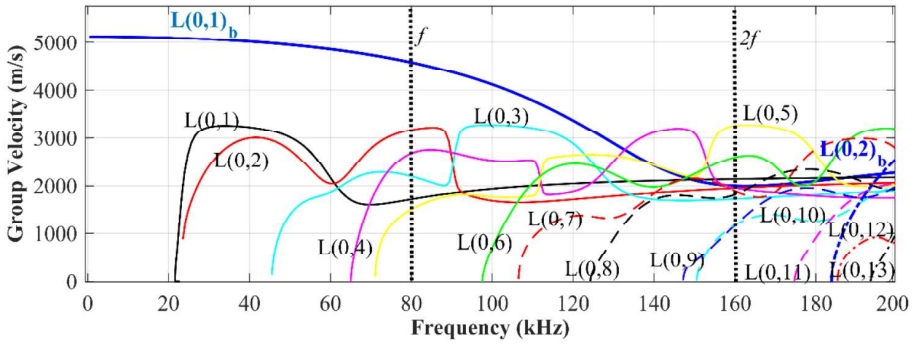

Figure 2.2 Group velocity dispersion curve for bare steel rebar and steel rebar embedded in concrete

2.2.3 Estimation of debonding location using second harmonic

The use of linear features for damage detection in rebar reinforced concrete requires baseline data from undamaged specimen [38]. Nonlinear feature, such as second harmonic, is proposed in this study to overcome the shortcomings of linear features. The behaviour of GWs in bare rebar and rebar embedded in concrete is different in terms of various mode generation. A schematic diagram of reinforced concrete beam specimen is shown in Figure 2.3. When wave

is excited at the end of bare steel rebar, GW modes propagate. Upon entrance into intact concrete, various wave modes are generated, which can be observed in the dispersion curve of rebar embedded in concrete. These wave modes at fundamental frequency (f) travel at different wave speeds with few wave modes arriving earlier than the others. When these wave modes interact with debonding (contact nonlinearity), second harmonics are produced. The group velocity of second harmonic wave modes is different to first harmonic and they have different wavelengths at second harmonics ($2f$). Due to the change in velocity, the first harmonic wave arrives the other end of the rebar at a time different to the second harmonic.

The presence of arrival time delay in first and second harmonics provides valuable information to determine the debonding location. The second harmonics are not produced instantly at the interaction of respective fundamental wave mode with contact damage. There is time delay in generation of second harmonics at debonding when the wave interacting with contact surfaces. It needs to be taken into account for accurate estimation of the debonding location. This will be further discussed in Section 2.5. After passing from concrete into steel at receiving end, the wave travel at group velocity of wave mode in bare steel bar at respective frequency.

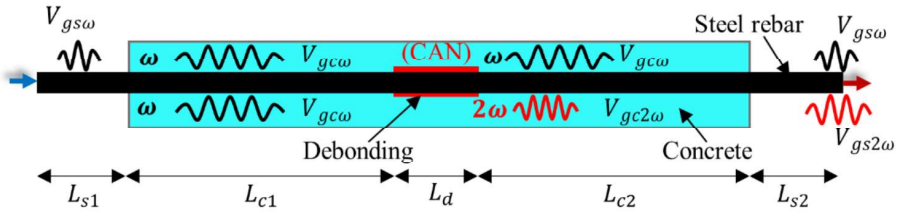

Figure 2.3 Schematics for fundamental and second harmonic wave propagation in reinforced concrete

The arrival time of first and second harmonics using parameters in Figure 2.3 can be calculated

$$T_{\omega} = \frac{L_{s1}}{V_{gs\omega}} + \frac{L_{s2}}{V_{gs\omega}} + \frac{L_{c1}}{V_{gc\omega}} + \frac{L_{c2}}{V_{gc\omega}} + \frac{L_{d}}{V_{gc\omega}} \quad (2.1)$$

$$T_{2\omega} = \frac{L_{s1}}{V_{gs\omega}} + \frac{L_{s2}}{V_{gs2\omega}} + \frac{L_{c1}}{V_{gc\omega}} + \frac{L_{c2}}{V_{gc2\omega}} + \frac{L_{d}}{V_{gc2\omega}} + t_{d} \quad (2.2)$$

where

T_{ω} = arrival time of first harmonics

$T_{2\omega}$ = arrival time of second harmonics

L_{s1} = length of bare steel at excitation end

L_{s2} = length of bare steel at receiving end

L_{d} = length of debonding

L_{c1} = length of embedded steel from excitation end till debonding

L_{c2} = length of embedded steel from debonding till receiving end

$V_{gs\omega}$ = group velocity of first harmonic in bare steel

$V_{gs2\omega}$ = group velocity of second harmonic in bare steel

$V_{gc\omega}$ = group velocity of first harmonic for embedded steel in concrete

$V_{gc2\omega}$ = group velocity of second harmonic for embedded steel in concrete

t_{d} = time delay in generation of second harmonic at debonding

Δt = difference in time of arrival of first harmonics T_{ω} and second harmonics $T_{2\omega}$

By knowing Δt as delay in second harmonics ($T_{2\omega} - T_{\omega}$), location of debonding as d_l can be found using equation (2.1) and (2.2) as

$$d_l = \frac{(\Delta t - t_d - c)\left(V_{gc2\omega}.V_{gc\omega}\right)}{V_{gc\omega} - V_{gc2\omega}} \quad (2.3)$$

where $d_l = L_{c2} + L_d$ and c = $\frac{L_{s2}}{V_{gs2\omega}}$ - $\frac{L_{s2}}{V_{gs\omega}}$ is treated as time difference between first and second harmonics waves in bare steel bar at receiving end. The location of debonding estimated using equation (2.3) can be used to identify the debonding region. The effect of varying debonding length at different locations in debonding location estimation is studied using numerical and experimental analysis.

2.3 Finite Element Simulations

2.3.1 Finite element model of plain rebar and effect of ribs

The pattern on the surface of the ribbed steel rebar provides better bonding and slip resistance with concrete surface. The maximum bond stress of ribbed rebar is 2-3 times greater than that of plain rebar [39]. It is, therefore, important to observe the propagation of GWs in plain and ribbed rebar. The ribbed and plain rebar are modelled in Abaqus/Explicit. The plain rebar is modelled as circular cross-section with 20mm diameter while the ribbed rebar is modelled using spiral solid as ribs on the plain rebar. Typical dimensions of ribbed rebar are selected for the ribs on plain rebar in the model. The 20mm diameter of plain rebar is reduced to 19mm diameter with circular cross-section of spiral being 1mm in radius. The spiral is given 69 revolutions throughout 700mm length of plain rebar with10mm spacing between the ribs. With one complete circular revolution as 360°, total 24,840° of revolution are applied to spiral rib. The inner diameter of hollow spiral with 1mm thickness is the same as outside diameter of plain rebar. This allows them to be bonded together perfectly. Using tie constraints, the spiral ribs are perfectly bonded to the plain rebar to form the ribbed rebar as shown in Figure 2.4.

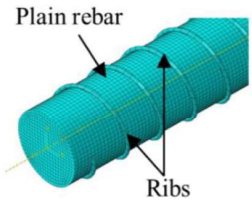

Figure 2.4 Meshing of ribbed rebar in ABAQUS

The Hanning windowed 8-cycle sinusoidal tone burst signal with central frequency of 80kHz was used as excitation pulse. At this frequency, the longitudinal wave mode $L(0,1)_b$ is well separated from higher order modes. Excitation signal was applied as the pressure to the cross-section of at the bar end. The hexagonal mesh type of 1mm size was chosen type for meeting quality meshing and this gives $L_e = \frac{\lambda}{20}$, where λ is the wavelength and L_e is the mesh size[40]. The finite element (FE) was chosen as C3D8R with three-dimensional (3D) stress and 8-noded solid element with reduced integration. The duration of the simulation is 0.7ms. The longitudinal GWs received at the other end of the plain and ribbed rebar were obtained by calculating the displacement in the direction of pressure applied. The obtained signals are shown in Figure 2.5. The signals received at the end of the plain and ribbed rebar are similar. The ribbed pattern on plain rebar does not have any significant effect on the GW propagation property. The wavelength of the excited pulse is 55mm, which is much larger than the rib spacing (10mm) on ribbed rebar. Therefore, the longitudinal GWs do not interact with ribs and generate other wave modes or reflection. In view of this, the plain rebar was used for debonding study in reinforced concrete due to ease of FE modelling, geometrical and practical considerations.

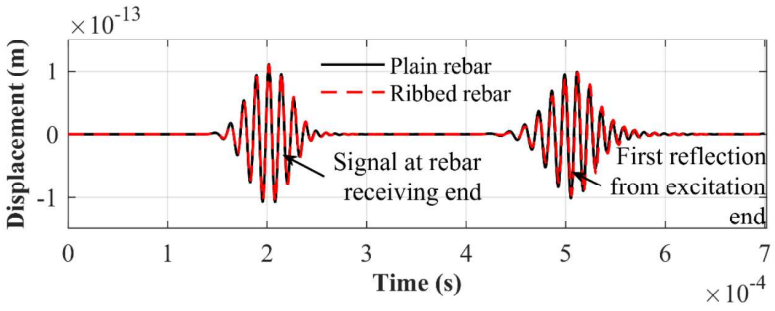

Figure 2.5 Comparison of L(0,1)b wave mode propagation in plain and ribbed rebar

The group velocity of the wave propagation can be calculated using $V_G = \frac{\Delta d}{\Delta t}$, where Δd and Δt are the distance and time difference between two measurement points of propagating wave, respectively. The group velocities of $L(0,1)_b$ at various frequencies calculated using FE model are plotted against theoretical dispersion curve, which were also validated through experimental study in Section 4. For the rebar embedded in concrete, various longitudinal GW modes were observed at a single frequency, which makes it complicated to separate the wave modes and calculate the group velocities. Considering this complexity, the group velocity dispersion was only validated for bare rebar.

2.3.2 Finite element model of reinforced concrete beam

A reinforced concrete beam with cross-section of 100mm×100mm and length of 700mm was selected for the study. The reinforcing rebar has 10mm radius with total length of 900mm and similar properties as listed in Table 1. The reinforcing rebar is extruding 100mm outside from each end of the beam for the ease of installation, wave excitation and measurement. A schematic diagram of the specimen is shown in Figure 2.6.

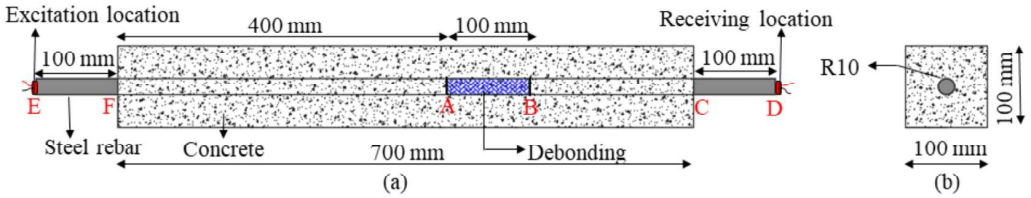

Figure 2.6 Reinforced concrete beam specimen (a) longitudinal view (b) cross-section

A 3D explicit FE method was used to study the generation and propagation of longitudinal GW in reinforced concrete beam as shown in Figure 2.7. The model is developed in Abaqus/CAE and is solved using Abaqus/Explicit. In reinforced concrete beam, the steel used for bare rebar FE model is restrained by increasing its length to 900 mm. For developing a reinforced concrete beam model, the steel rebar and rectangular concrete cross-section having 20mm Ø hole in centre is perfectly bonded together using tie constraints on the concrete and steel interfacial surfaces. A Hanning windowed 8-cycle tone burst signal at central frequency of 80 kHz is used as excitation signal from one end of extruding rebar by applying pressure on the surface of rebar at Point E. The mesh size for steel and concrete is 1mm as $L_e = \frac{\lambda}{20}$ [40]. The element for meshing is set to be three-dimensional eight-noded (C3D8R) having sweep hexagonal mesh type. For understanding the propagation of longitudinal GWs through the reinforced concrete beam, the displacement in the direction of rebar is measured at Point D. Initially, two reinforced concrete beam models with and without debonding are considered.

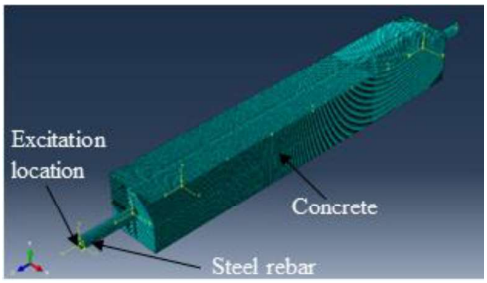

Figure 2.7 3D view of the finite element model for reinforced concrete beam

To create the debonding between the rebar and concrete, the tie constraint between steel rebar and concrete surface is removed for the length of the debonding. To model the CAN effect for debonding, the circumferential surface of rebar for the debonding length was made to be clapped with concrete surface to generate second harmonic due to breathing effect. The simulation of the surface–surface contact interaction with frictionless surface was solved using penalty contact method. The perfectly bonded model is referred as Case N0. While, the debonded specimen with debonding length of 100mm from region A-B shown in Figure 2.6 is referred as Case N1. The time-domain signal for cases N0 and N1 are shown in Figure 2.8, which are longitudinal GW modes with the estimated of arrival time using the group velocity dispersion curves as shown in Figure 2.2.

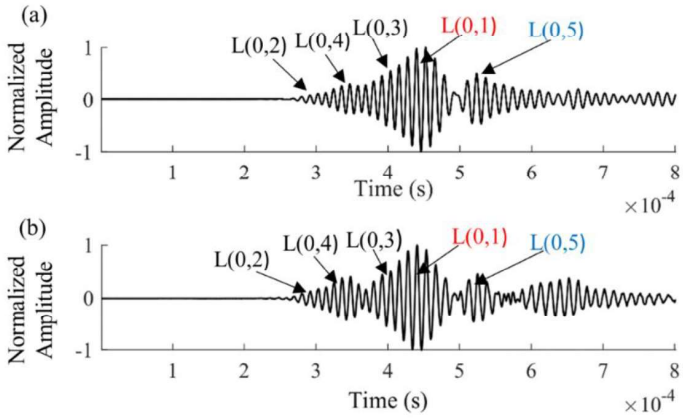

Figure 2.8 Time domain signal for numerical model (a) Case N0 without debonding (b) Case N1 with debonding

It is clearly represented that the L(0,1) wave mode arrives later than other higher order wave modes at the measurement location. The location of longitudinal wave modes i.e. L(0,1 – L0,5) on time domain signal is defined based on the group velocity dispersion curve for longitudinal wave. The higher order longitudinal wave modes, i.e. L(0,2), L(0,3) & L(0,4), arrive before L(0,1). The wave mode L(0,5) has group velocity slower than L(0,1) and it arrives

after the L(0,1) wave. The variation in linear feature as time of arrival of various GW modes in debonded specimen requires baseline measurements from fully bonded specimen [7, 8]. Therefore, the time domain signal for debonded beam model alone does not provide significant information for the damage identification. The nonlinear features of second harmonics needs to be analysed for debonding detection and location estimation.

The simulation for representing behaviour of longitudional GWs with debonding in rebar reinforced concrete is performed in shorter beam model to reduce the computation cost. For simulation purpose, the reinforced concrete beam specimen is reduced to 500mm in total length with 100mm length of plain rebar extruding out from each end leaving 300mm of embedded rebar in concrete. The cross-section of concrete and steel rebar is retained as same as in Figure 2.6(b) with similar material properties. The debonding length is chosen to be 100mm at the center embedded rebar in concrete. The numerical simulation for debonded specimen clearly represents the CAN effect at the location of debonding as shown in Figure 2.9. At the location of perfect bonding, the steel and concrete interfaces have compression and tension motion of GWs together, while the debonded region represents the opening and closure of debonded surface due to the breathing effect. The generation of secondary GW modes is studied using frequency analysis of time domain data after the discussion and comparison with experimental data in Section 2.4.

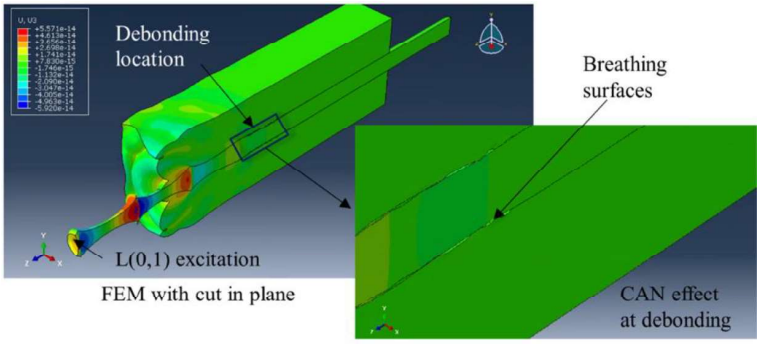

Figure 2.9 Numerical simulation representing CAN for debonding between steel rebar and concrete interface

2.4 Experimental Verification

In experimental study, the investigation for presence of debonding is carried out for the reinforced concrete beam specimen. As observed in time domain signal obtained from the FE model of specimen with the debonding, the information about presence of debonding is not obvious. Therefore, the time-frequency analysis is used to analyse the signal obtained from debonded and fully bonded reinforced concrete beam specimens. The experimentally measured time domain signals for bare and embedded plain rebar in concrete are compared with FE models.

2.4.1 Longitudinal guided wave in plain rebar

The propagation of longitudinal GW in plain rebar is compared with FE model described in Section 2.3.1. The plain steel rebar of 450mm in length and 20mm diameter is selected and has the same properties as those used in the numerical study for plain rebar. The longitudinal GW in steel rebar is actuated and received using 2mm thick and 10mm diameter circular piezoceramic transducers, which were attached to the centre of the cross-section located at the ends of the plain rebar as shown in Figure 2.10(a). The attached circular transducer at excitation location applies pressure to surface of rebar end and this is modelled in the numerical simulations. The signal is generated using National Instrument (NI) PXIe-1073, which has

arbitrary waveform generator NI PXI-5412 and measured using signal digitizer NI PXI-5105. The NI system was connected with computer to generate and record the data. The same system setup was used for study in reinforced concrete beam specimen. A similar signal, which is a 8-cycle 80kHz sinusoidal tone burst modulated by Hanning windowed, was used in numerical case study and it was excited at the end of the plain rebar. The generated signal has 5V (peak-to-peak) amplitude, which was further amplified ten times using KRON-HITE 7500 amplifier.

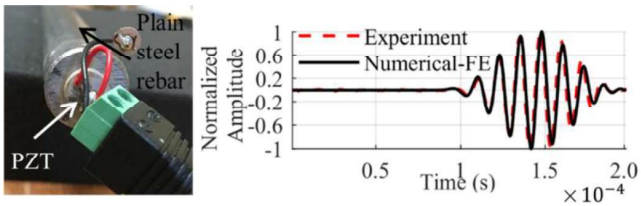

Figure 2.10 (a) PZT installed at the end of the plain rebar (b) comparison of experimentally measured longitudinal GW signal with FE calculated signal from bare plain rebar

The signals obtained from bare rebar was normalized so that they can be compared with the data obtained from the FE simulations. The normalized signals are shown in Figure 2.10(b). The experimentally measured signal has good agreement with the numerical results. In this study, the group velocity of $L(0,1)_b$ wave was calculated using the time of arrival of the absolute peak amplitude for the rebar. The excitation frequency from 50 kHz to 200 kHz were calculated for bare plain rebar and shown in the group velocity dispersion curve in Figure 2.11. The results of the theoretical dispersion curve from DISPERSE are also shown in the same figure. The group velocity dispersion curve for numerical, experimental and theoretical values have good agreement as shown in Figure 2.11.

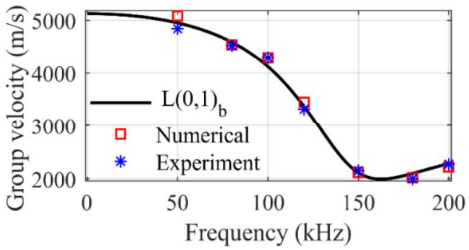

Figure 2.11 Group velocity dispersion curves for plain rebar

2.4.2 Longitudinal guided wave in reinforced concrete beam

To carry out experimental investigations, the reinforced concrete beam specimens with and without debonding were casted. The reinforced concrete beam has the same dimensions, i.e. 100mm×100mm×900mm, as the FE model shown in Figure 2.6. There is a section of 100mm of plain rebar extruding out from both ends. Before pouring concrete, the 900mm long plain rebar was placed at centre of 100mm×100mm cross-section formwork having the length of 700mm. In this manner, the remaining 200mm length of the plain rebar is extruded outside the formwork at both ends. The normal strength concrete was prepared with cement, sand and coarse aggregate with ratio as 1:2.5:4. The maximum size of coarse aggregate is 10mm. Two specimens were casted, in which one of them has debonding and the other is fully bonded (without debonding), to investigate the presence of second harmonic. The debonding in the specimen was created using Mylar sheet, which was wrapped around the whole surface of plain rebar at the location of 500mm from excitation location. The length of the debonding is 100mm as shown in Figure 2.12, which is the same as the debonding considered in the numerical model. The sheet was tightly held in place to avoid the passage of cementitious material below the Mylar.

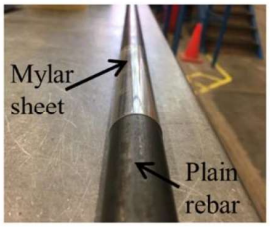

Figure 2.12 Debonding using Mylar sheet in plain rebar reinforced concrete specimen

The circular piezoceramic transducers are attached to the reinforced concrete beam specimens with and without debonding using epoxy glue. The experimental setup for generating and receiving of longitudinal GWs in beam specimens is shown in Figure 2.13. The 8-cycle sinusoidal tone burst signal with central frequency of 80kHz excited at left end of rebar had 5V (peak-to-peak) amplitude, which is amplified 50 times using KRON-HITE amplifier to ensure the wave has large enough amplitude to generate CAN phenomenon at the debonding. Before taking measurements, it has been confirmed that there is no source of external interference at the frequencies of interest. Along with debonded sample, fully bonded sample is also tested to further confirm the nonlinearity generated due to the debonding.

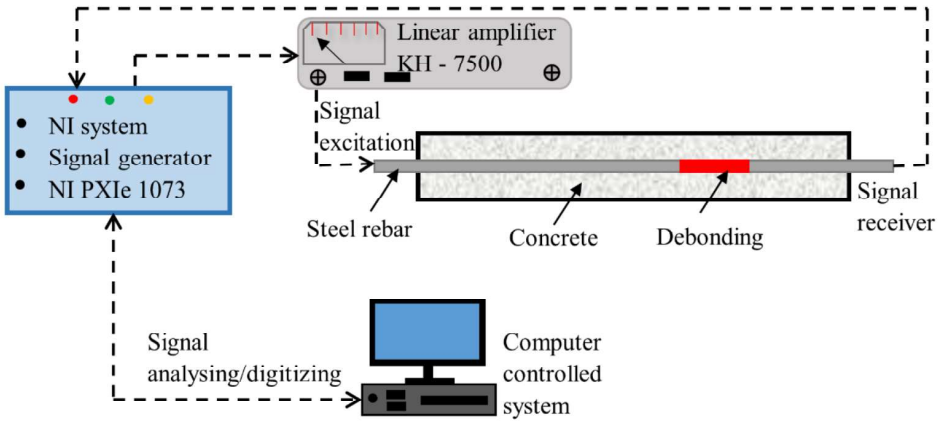

Figure 2.13 Experimental setup for debonding detection in reinforced concrete beam

The time domain signals for fully bonded and debonded specimens, which are experimental cases E0 and E1, were acquired in the experiment, are compared with the FE results as shown in Figures 2.14(a) and 2.14(b), respectively. The NI system has sampling rate of 6×10^7 samples per second with 14-bit depth. There is no significant difference in time domain signal between the fully bonded and debonded specimen.

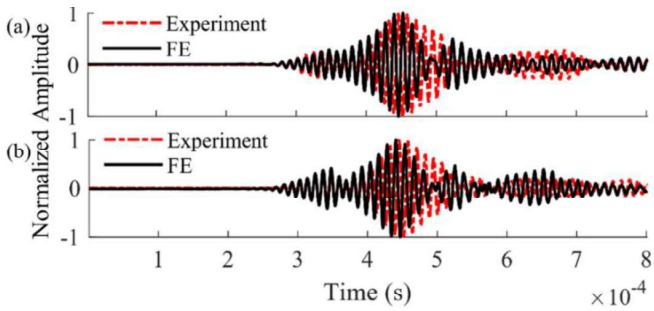

Figure 2.14 Experiment and FE time domain signal obtained from specimen (a) without bonding, and (b) with a debonding

The time domain signal is analysed in frequency domain using Fast Fourier Transform (FFT) with sample length of 65536 samples. The results of FFT transform are shown in Figure 2.15. A_1 and A_2 represents the normalized amplitude of FFT at excitation frequency (80kHz) and second harmonics (160kHz) respectively. The second harmonic can be clearly oberseved in the data obtained from debonded specimen.

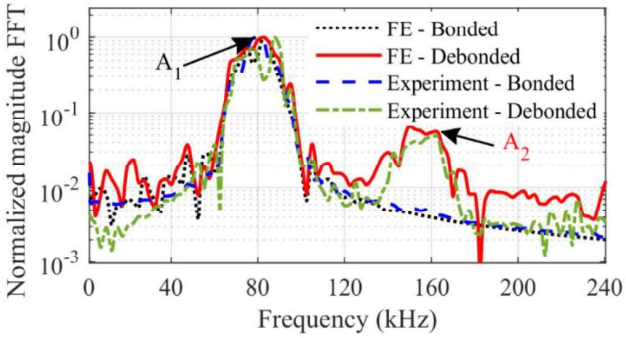

Figure 2.15 FFT transformed experimental and FE data obtained from the bonded and debonded specimens

For fully bonded specimens, the amplitude of frequency spectrum at the frequency of the second harmonic (160 kHz) is negligible as compared to the debonded speicmens. The observed peak at second harmonic frequency for debonded speicmen obviously indicates the presence of the debonding. For debonded sample, the nonlinear acoustic parameter β was calculated to be 0.048 and 0.054 for FE and experiment, respectively. The generation of the second harmonic is due to the CAN effect when the wave interacts at the debonding. Therefore, the presence of various wave modes in reinforced concrete can be adavantageous in a way that the amplitude of second harmonic is amplified due to multiple wave modes generating second harmonics. Therefore, the second harmonic can be used to detect debonding.

For locating debonding, the arrival time of second harmonic wave due to the debonding provides valuable information of the debonding location. The time domain signal is converted into time-frequency spectrum using Short-Time Fourier Transform (STFT). For time-frequency analysis, other methods as Wavelet Transform (WT) continuous or discrete co-exists. They can be used for good time-scale resolution as an alternative for future consideration. However, due to the uniform distribution of windowing function and segments, STFT was adopted. STFT utilizes the short duration time window τ and applies FFT on windowing function, which is sweeped across the whole time domain signal t. It is mathematically described as [41]

$$S(t,\omega) = \int_{-\infty}^{+\infty} f(\tau).W(\tau - t)e^{-2\pi i\omega\tau}d\tau \qquad (2.4)$$

where $S(t,\omega)$ represents the time-frequency spectrum, $f(\tau)$ is the FFT function and $W(\tau - t)$ is Hanning windowed function selected on time domain signal. The time-frequency spectrum of experimentally measured and FE simulated data for fully bonded specimen are shown in Figures 2.16(a) and 2.16(b), respectively. The window length for STFT was selected to be 4096. The excitation frequency is f=80kHz and $2f$=160kHz is the second harmonic frequency.

In Figure 2.16, the absence of the second harmonic wave at $2f$ shows that there is no debonding or contact type of damage in fully bonded specimen.

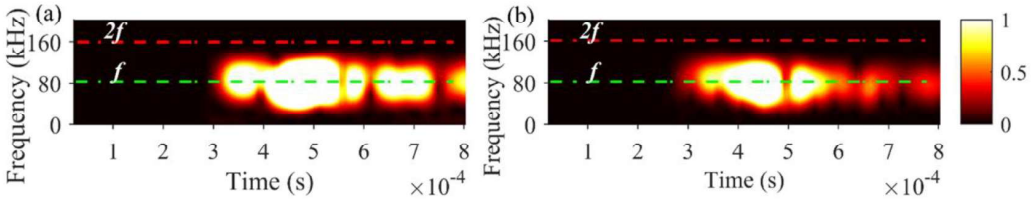

Figure 2.16 Time frequency spectrum of (a) experimentally measured and (b) FE simulated data for fully bonded specimen

For debonding specimen, the time-frequency analysis was also used to process the experimentally measured and FE calculated data. As observed from Figure 15, the normalized amplitude of the second harmonic is smaller than the amplitude at the excitation frequency. To clearly observe the spectrum around f and $2f$, the time-frequency spectrum is plotted at different scales for the debonded specimens. So, the second harmonic waves are detected at $2f$ for both experimentally measured and FE calculated data as shown in Figures 2.17(a) and 2.17(b), respectively.

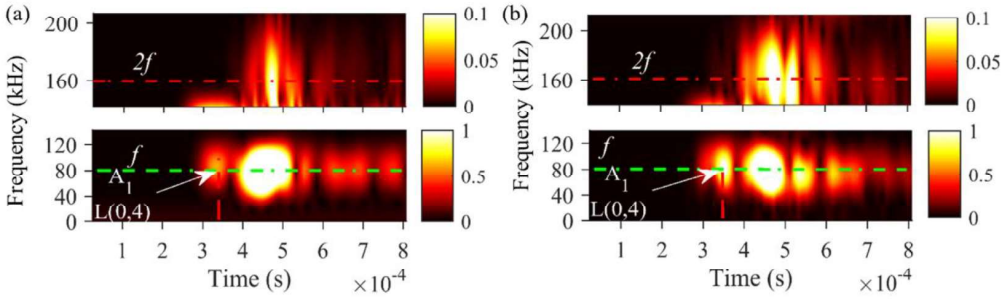

Figure 2.17 Time frequency spectrum of (a) experimentally measured and (b) FE simulated data for debonded specimen

From the group velocity dispersion curve of the rebar embedded in concrete, L(0,2) is the fastest and L(0,4) is the second fastest longitudinal wave mode at 80kHz. In bare rebar, only $L(0,1)_b$ is the propagating wave mode. Using the group velocity of the longitudinal wave modes

for the rebar in embedded in concrete and bare rebar, the arrival time of L(0,4) is estimated to be around 0.35ms and appears to be more dominant than L(0,2) which arrives just before L(0,4) as seen in Figure 17. For time-frequency spectrum around $2f$, there are multiple wave modes propagating, which makes it complicated to identify second harmonic wave using only the information of the group velocities because the location of debonding is unknown. Therefore, the identification of multiple wave modes at second harmonic frequency for debonding location estimation is more challenging. It requires more physical insights into the presence of the wave modes propagating at f and $2f$, which is discussed using frequency wavenumber analysis in Section 2.5. By carefully looking into the arrival times of the corresponding wave mode at f and $2f$, the location of debonding can be determined in the case studies in Section 2.5.

2.5 Case Studies

In Section 2.4, the FE model has been verified that it can be used to accurately predict the wave propagation and second harmonic generation due to CAN at the debonding. This section provides a series of numerical case studies using this experimentally verified FE model to study the effect of varying debonding length on the amplitude of the second harmonic. The determination of debonding location using the second harmonic wave generated at the debonding is also demonstrated in this section.

2.5.1 Second harmonics for debonding damage detection

A series of numerical case studies considered in this study are summarised in Table 2.2, in which different lengths and locations of debondings are considered. The setup of the FE model is the same as the model shown in Figure 2.6. The wave is excited at location E and the wave signal is measured at the Point D.

Table 2.2 Summary of debonding cases in reinforced concrete beam

Debonding Cases	Debonding length (mm)	Midpoint of debonding from receiving location i.e. Point D (mm)
N1	100	350
N2	50	375
N3	100	550
N4	100	450
N5	150	375

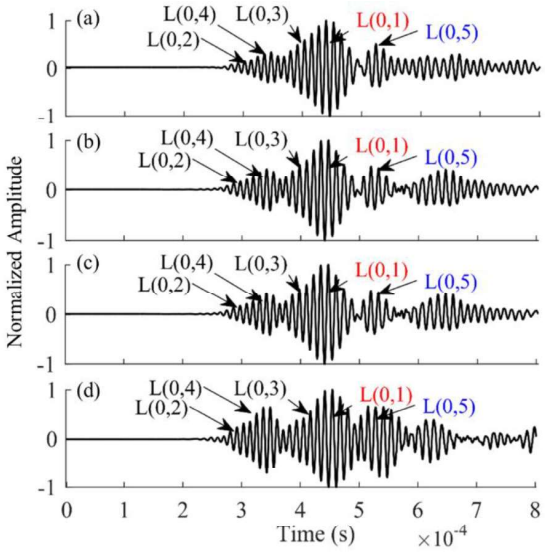

Figure 2.18 Time domain signals for debonding cases (a) N2, (b) N3, (c) N4, (d) N5 (results for debonding case N1 can be found in Figure 8(b))

The signals received at end of the rebar for debonded cases N2-N5 shown in Figure 2.18 are converted into frequency domain to identify the presence of any debonding. The FFT was performed using sample length of 65536 samples. As discussed in Section 2.2, the second harmonics are generated due to the CAN when the wave interact with the debonding. With complexity of various wave modes presented in time domain, it is challenging to identify any secondary wave generated in time domain signal. However, the frequency component of time domain can clearly distinguish the secondary wave generated due to the interaction between the fundamental frequency wave modes and debonding as shown in Figure 2.19 for debonded cases N2-N5. The variation in debonding length has impact on the amplitude of the second

harmonic generation. The amplitudes of the frequency spectrum are plotted in logarithmic scale, where A_1 and A_2 represents the amplitude of fundamental and second harmonic, respectively. The second harmonic is presence in the frequency domain of the signal in all debonding cases.

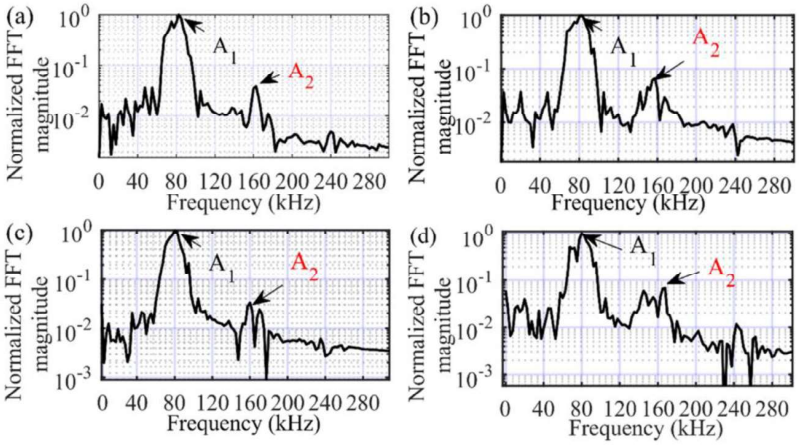

Figure 2.19 FFT analysis for debonded cases (a) N2, (b) N3, (c) N4, (d) N5 (results of debonding case N1 can be found in Figure 15)

The contact phenomenon generates the secondary waves and it gives valuable information about the presence of any damage without any baseline measurements. However, for locating damage, the information about wave modes at second harmonics is essential. Before developing information about wave mode content in debonded specimens, we must be aware of the presence of various wave modes for the selected reinforced concrete beam specimen as shown in Figure 2.6. When GW enters into reinforced concrete, $L(0,1)_b$ wave mode is converted into five longitudinal GW modes i.e. L(0,1) - L (0,5) at 80kHz as seen from dispersion curve comparison in Figure 2.2.

For excitation frequency f i.e. 80kHz $L(0,1)_b$ travelling at 4500m/s reduces to L(0,1) at 1780m/s for embedded rebar with higher order generated wave modes travelling at greater group velocity. At second harmonic frequency of $2f$ i.e. 160kHz, various higher order wave modes are presented. When all propagating wave modes at f interact with debonding region,

the second harmonic wave modes are generated. The longitudinal GW modes increase from 5 to 10 at $2f$. The presence of wave modes at $2f$ entirely depends upon the interaction of fundamental wave modes with debonding, which is not the case with wave modes at f for which signal is excited. It is necessary to understand that upon interaction with contact surfaces, which dominant second harmonic wave modes will propagate in embedded rebar. The characteristics of wave mode content propagating after debonding is studied using frequency wavenumber analysis.

2.5.2 Frequency Wavenumber analysis for bare and embedded rebar in concrete

The wave data extracted over space for known time provides valuable information about presence of wave modes propagating in space [42]. The two-dimensional Fast Fourier transform (2D-FFT) is implemented on time-space wavefield to acquire frequency wavenumber representation. In the time-space wave data analysis, frequency is the representation of time and wavenumber is the representation of space for the propagating wave. The longitudinal GW data over time-space can be transformed into frequency wavenumber representation and it is mathematically defined as

$$U(f,k) = \int_{-\infty}^{+\infty} \int_{-\infty}^{+\infty} u(t,x) e^{-j(2\pi ft - kx)} dt dx \tag{2.5}$$

where $U(f,k)$ is frequency wavenumber representation obtained using 2D-FFT of time-space data. u represents displacement of propagating longitudinal wave. t and x is time and distance data, respectively. The presence of dominating wave mode content can be reflected in time-frequency spectrum.

Frequency wavenumber spectrum analysis is carried out for a distance of 200mm in the rebar embedded in concrete, which is the region between Point B and C as shown in Figure 2.6(a) and the region is located after the debonding. The longitudinal displacement is obtained for 0.8ms at every 2mm in this region. In Figure 2.20(a), the frequency wavenumber spectrum

for various wave modes propagating from frequency 0 to 200kHz is plotted together with the results obtained from DISPERSE. The spectrum clearly shows the presence of fundamental frequency wave modes at 80kHz and second harmonic wave modes at 160kHz. The spectrum for rebar embedded in concrete shows the presence of L(0,1) – L(0,5) GW modes at f=80kHz with L(0,4) having the most dominant wave mode content. At $2f$=160kHz, L(0,6) – L(0,10) GW modes are generated, which have small amplitude in the spectrum, and hence, the L(0,4) is the dominant wave mode at $2f$. Therefore, this make it easy to identify its time of arrival for L(0,4). The value of the group velocity of L(0,4) at $2f$ is less than that at f. This means that L(0,4) GW mode at $2f$ arrives after L(0,4) GW mode at f in the time-frequency spectrum.

After debonding region, all GW modes for the rebar embedded in concrete at f and $2f$ upon entering into bare rebar travel with group velocity of $L(0,1)_b$ at f and $2f$, respectively. This is confirmed by performing the frequency wavenumber analysis from the data obtained in the bare rebar region C-D as shown in Figure 2.6(a). Similarly, the time-space data is acquired for 1ms at every 2mm in this 100mm long section of the extruding rebar. The frequency wavenumber spectrum for bare rebar has only one propagating GW mode $L(0,1)_b$ as shown in Figure 2.20(b) at f and $2f$. The information about GW mode content in embedded and bare rebar regions is essential for choosing dominant wave mode content in debonding location estimation using time-frequency analysis.

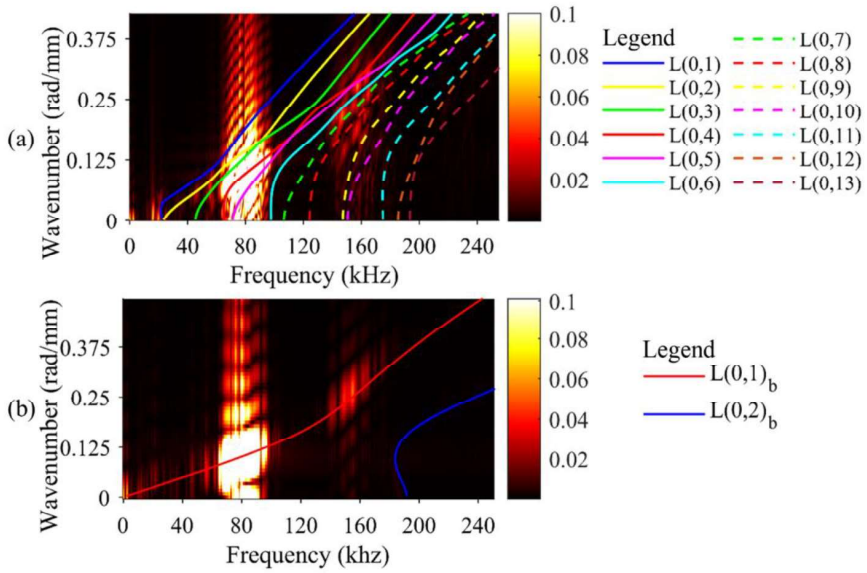

Figure 2.20 Frequency-wavenumber spectrum for propagating longitudinal wave (a) after debonding for rebar embedded in concrete, and (b) extruding bare rebar

2.5.3 Time delay in second harmonic generation for dominant wave mode

The fundamental GW modes propagating in embedded rebar generates secondary wave modes upon interaction with debonding damage. As shown in Figure 2.2, L(0,2) is the fastest wave mode for embedded rebar at f and is followed by L(0,4), L(0,3), L(0,1,) and L(0,5) in order. However, L(0,4) has proven to be the more dominant as compared to L(0,2) frequency wavenumber analysis. Upon interaction with debonding, the L(0,4) wave mode at f generates second harmonic L(0,4) wave mode, which is also the most dominant wave mode at $2f$ as proven from frequency wavenumber analysis. To accurately determine the location of debonding, the time delay in generation of second harmonic needs to be taken into account.

For verifying the presence of time delay, time-frequency spectrum analysis is carried out using STFT for the data obtained at Point A as shown in Figure 2.6(a). The time-frequency spectrum is analysed at $2f$. The arrival time of L(0,4) wave mode at f depends upon the group velocity of $L(0,1)_b$ wave mode at f in bare rebar (region E-F in Figure 2.6) and L(0,4) wave mode at f in embedded rebar (region F-A in Figure 2.6). The arrival time is estimated to be

2.36×10^{-4}s as shown by solid line in Figure 2.21. From results in frequency-wavenumber analysis, the dominant L(0,4) second harmonic wave mode will be propagating after debonding. The dominant wave mode content at $2f$ shall appear at the arrival time of L(0,4) at f. However, the time-frequency spectrum shows a time delay in the arrival time of L(0,4) second harmonic wave mode. The time delay is 6×10^{-5}s as shown in Figure 2.21 which is calculated by measuring the delayed arrival time at peak amplitude of $2f$. The delay is due to the time for generating the second harmonic wave when the incident wave interact with the debonding.

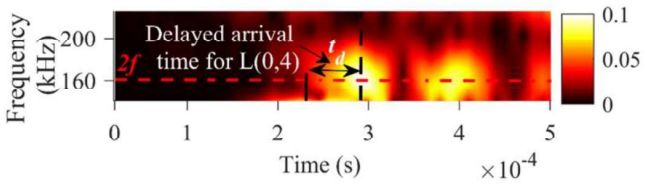

Figure 2.21 Time-frequency spectrum of the data obtained at Point A from the rebar embedded in concrete

The calculated time delay t_d is used to estimate the location of debonding. For the embedded rebar, the group velocity L(0,4) wave mode at f is around 2700m/s while for L(0,5) wave mode at $2f$ is around 1900m/s, which indicates that the dominant second harmonic L(0,4) wave mode arrive after L(0,4) wave mode at f in time-frequency spectrum.

2.5.4 Debonding location estimation

The analysis in Section 2.5.3 has provided valuable information on the dominant wave mode content at $2f$ and time-delay in the generation of second harmonic wave mode. For estimating the location of debonding, the arrival times of L(0,4) wave mode at f and $2f$ are utilized. Time-frequency spectrum of debonding cases N2-N5, which are individually analysed at different scales for distinguishing the spectrum at f and $2f$ as 0-1 and 0-0.1, are shown in Figures 2.22(a)-2.22(d). The amplitudes at the f and $2f$ of the time-frequency spectrum are shown in Figure 2.23 and the amplitudes are normalized.

The arrival times of L(0,4) wave mode at f and $2f$ are estimated by the respective peak amplitudes. For the data at the excitation frequency f=80kHz, although the magnitudes of the peaks appear to be more dominant than the first peak, which is the arrival time of L(0,4) wave mode, it is entirely due to the presence of L(0,3), L(0,1) and L(0,5) wave modes enlarging the amplitudes of the waves arrived after L(0,4).

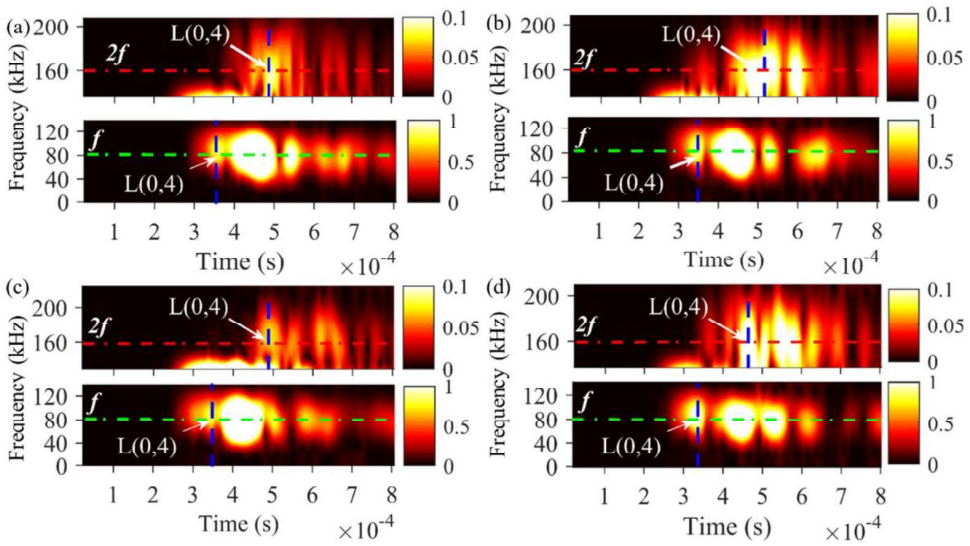

Figure 2.22 Time-frequency spectrum for debonding cases (a) N2, (b) N3, (c) N4, (d) N5 (results of debonding case N1 can be found in Figure 17(b))

At $2f$, the peak amplitude lies at L(0,4) wave mode and its time of arrival is estimated using peak amplitude of time frequency spectrums and their respective FT plots. The arrival time of L(0,4) at f and $2f$ is selected at the center of L(0,4) wave mode time frequency spectrum. The difference in arrival time of L(0,4) at f and $2f$ gives Δt as defined in section 2.2. Using equation 2.3 derived in section 2.2.3 and utilizing the time delay t_d, the debonding location estimated for debonding cases N2-N5 are shown in Table 2.3.

Table 2.3 Debonding location estimation using second harmonic wave

Debonding Cases	Wave Frequency (kHz)	Arrival time (s) of L(0,4) at Point D, (receiving location)	Estimated debonding location from Point D (mm)	Actual debonding location from Point D (mm) (Start – End location of debonding)
N1	160	4.78×10^{-4}	351	300-400
	80	3.50×10^{-4}		
N2	160	4.90×10^{-4}	371	350-400
	80	3.60×10^{-4}		
N3	160	5.10×10^{-4}	560	500-600
	80	3.50×10^{-4}		
N4	160	4.92×10^{-4}	448	400-500
	80	3.50×10^{-4}		
N5	160	4.70×10^{-4}	371	250-400
	80	3.40×10^{-4}		

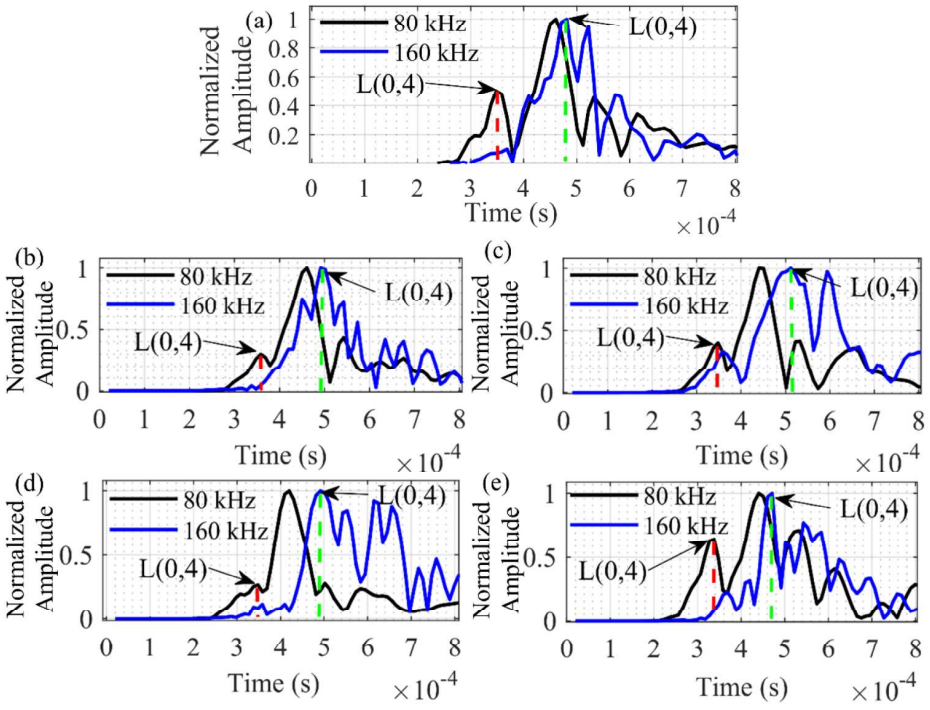

Figure 2.23 Amplitudes at f and 2f of the frequency-time spectrum for debonding cases (a) N1, (b) N2, (c) N3, (d) N4 and (e) N5

The locations of debondings for all debonded cases are accurately estimated and lie within the debonding region as shown in Table 2.3. For varying debonding lengths, the estimation of location is around the center of debonding. For experimental case E1 with debonding, the

arrival time of L(0,4) wave mode at f and $2f$ is estimated as 3.52× 10^{-4}s and 4.80× 10^{-4}s, respectively, as shown in Figure 2.17(a). The estimated debonding location is 356mm from Point D, which is within the actual debonding start-end location, 300mm–400mm, from Point D. Therefore, the nonlinear features of longitudinal guided waves can be used to accurately determine the location of debonding in rebar reinforced concrete.

2.5.5 Relationship between nonlinear acoustic parameter and debonding length

The presence of second harmonic is sensitive to the size of debonding. The amplitude of second harmonic generated varies with the length of debonding as observed in FFT analysis. The nonlinear acoustic parameter β as defined in section 2.2 is used to understand the relation for varying debonding sizes with generated second harmonic.

Three debonded cases N1, N2 and N5 with varying debonding lengths at fixed location are selected. The peak normalized amplitude around excitation frequency f i.e. A_1 and normalized amplitude around second harmonic frequency $2f$, i.e. A_2 is used to calculate β, which is plotted against debonding length for selected cases as shown in Figure 2.24. With increasing debonding length, the nonlinear acoustic parameter β also increases. By looking at Figure 2.24, the relation between β and debonding length appear to be nonlinear and increasing. Therefore, the amplitude of second harmonic generated is larger for greater debonding lengths.

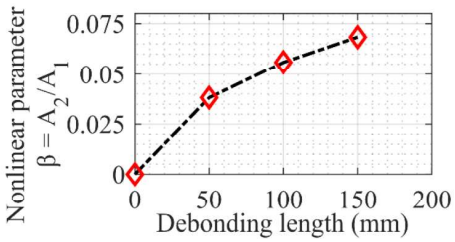

Figure 2.24 Relative nonlinear acoustic parameter for different debonding lengths

2.6 Conclusion

In this study, the nonlinear feature of longitudinal GW has been proposed to detect and locate debonding in reinforced concrete beam. The nonlinear feature, second harmonic, is generated due to CAN effect at debonding. Both numerical and experimental studies have been carried out in this study. The FE model of reinforced concrete beam with and without debonding has been developed to predict the presence of second harmonic due to CAN at debonding. The FE model has also been experimentally verified. The experimental study has also shown the presence of second harmonic in debonded specimen. The numerical and experimental studies have provided physical insights into the second harmonic generation at debonding.

It has been found that the time delay in generating the second harmonic wave when the incident wave interacts with debonding needs to be considered for estimating the debonding location. Due to the presence of multiple longitudinal GW modes in reinforced concrete beam at excitation frequency and second harmonics frequency, frequency-wavenumber analysis has been performed to understand various propagating wave modes.

Five different debonded cases with varying debonding size and location have been studied. Time-frequency spectrum has been used to analyse signals for location estimation. The results have shown that second harmonic can be used to accurately detect the existence of debonding and the debonding location. Finally, the study has also shown that there is a relationship between the relative nonlinear acoustic parameter to the debonding size and it can be used as an indicator of the debonding size.

Acknowledgement

This work was supported by Australian Research Training Program and Australian Research Council through DP200102300. The support is greatly appreciated.

2.7 References

1. Zhao, Y.a., *Steel corrosion-induced concrete cracking*, ed. W.a. Jin. 2016: Elsevier.
2. Sriramadasu, R.C., S. Banerjee, and Y. Lu, *Detection and assessment of pitting corrosion in rebars using scattering of ultrasonic guided waves.* Ndt & E International, 2019. **101**: p. 53-61.
3. Salençon, J., W. Ostachowicz, and J.A. Güemes, *New Trends in Structural Health Monitoring*. Vol. 542. 2012, Vienna: Vienna: Springer.
4. Büyüköztürk, O.a., *Nondestructive Testing of Materials and Structures*, ed. M.A.a. Taşdemir, et al. 2013: Springer Netherlands : Imprint: Springer.
5. Kim, G., et al., *In situ nonlinear ultrasonic technique for monitoring microcracking in concrete subjected to creep and cyclic loading.* Ultrasonics, 2018. **88**: p. 64-71.
6. Chen, J., C. Yang, and Q. Guo, *Evaluation of surface cracks of bending concrete using a fully non-contact air-coupled nonlinear ultrasonic technique.* Materials and Structures, 2018. **51**(4): p. 1-9.
7. Mustapha, S., et al., *Damage detection in rebar-reinforced concrete beams based on time reversal of guided waves.* Structural Health Monitoring-an International Journal, 2014. **13**(4): p. 347-358.
8. Lu, Y., et al., *Guided waves for damage detection in rebar-reinforced concrete beams.* Construction and Building Materials, 2013. **47**: p. 370-378.
9. Sabet Divsholi, B. and Y. Yang, *Combined embedded and surface-bonded piezoelectric transducers for monitoring of concrete structures.* NDT & E International, 2014. **65**: p. 28-34.
10. Zhu, X.Q., H. Hao, and K.Q. Fan, *Detection of delamination between steel bars and concrete using embedded piezoelectric actuators/sensors.* Journal of Civil Structural Health Monitoring, 2013. **3**(2): p. 105-115.
11. Wu, F. and F.K. Chang, *Debond detection using embedded piezoelectric elements in reinforced concrete structures - Part I: Experiment.* Structural Health Monitoring-an International Journal, 2006. **5**(1): p. 5-15.
12. Wu, F. and F.K. Chang, *Debond detection using embedded piezoelectric elements for reinforced concrete structures - Part II: Analysis and algorithm.* Structural Health Monitoring-an International Journal, 2006. **5**(1): p. 17-28.
13. Ou, G., et al., *Identifi cation of de-bonding between steel bars and concrete using wavelet techniques: Comparative study.* Australian Journal of Structural Engineering, 2013. **14**(1): p. 43-56.
14. Mohseni, H. and C.-T. Ng, *Rayleigh wave propagation and scattering characteristics at debondings in fibre-reinforced polymer-retrofitted concrete structures.* Structural Health Monitoring, 2019. **18**(1): p. 303-317.
15. Sriramadasu, R.C., Y. Lu, and S. Banerjee, *Identification of incipient pitting corrosion in reinforced concrete structures using guided waves and piezoelectric wafer transducers.* Structural Health Monitoring-an International Journal, 2019. **18**(1): p. 164-171.
16. Sharma, A., et al., *Investigation of deterioration in corroding reinforced concrete beams using active and passive techniques.* Construction and Building Materials, 2018. **161**: p. 555-569.
17. Sharma, S. and A. Mukherjee, *Longitudinal Guided Waves for Monitoring Chloride Corrosion in Reinforcing Bars in Concrete.* Structural Health Monitoring-an International Journal, 2010. **9**(6): p. 555-567.
18. Majhi, S., et al., *Corrosion detection in steel bar: A time-frequency approach.* Ndt & E International, 2019. **107**.
19. Reis, H., et al., *Estimation of corrosion damage in steel reinforced mortar using waveguides.* Nondestructive Evaluation and Health Monitoring of Aerospace Materials, Composites, and Civil Infrastructure Iv, 2005. **5767**: p. 98-107.

20. Zima, B. and R. Kędra, *Reference-free determination of debonding length in reinforced concrete beams using guided wave propagation.* Construction and Building Materials, 2019. **207**: p. 12.
21. Beata, Z. and K. Rafał, *Debonding Size Estimation in Reinforced Concrete Beams Using Guided Wave-Based Method.* Sensors, 2020. **20**(2): p. 389.
22. Soleimanpour, R. and C.T. Ng, *Locating delaminations in laminated composite beams using nonlinear guided waves.* Engineering Structures, 2017. **131**: p. 207-219.
23. Mohseni, H. and C.T. Ng, *Higher harmonic generation of Rayleigh wave at debondings in FRP-retrofitted concrete structures.* Smart materials and structures, 2018. **27**(10): p. 105038.
24. Chen, J., C.L. Yang, and Q.Q. Guo, *Evaluation of surface cracks of bending concrete using a fully non-contact air-coupled nonlinear ultrasonic technique.* Materials and Structures, 2018. **51**(4).
25. Hikata, A., B.B. Chick, and C. Elbaum, *Dislocation Contribution to the Second Harmonic Generation of Ultrasonic Waves.* Journal of Applied Physics, 1965. **36**(1): p. 229-236.
26. Ding, X., et al., *Experimental and Numerical Study of Nonlinear Lamb Waves of a Low-Frequency S 0 Mode in Plates with Quadratic Nonlinearity.* Materials, 2018. **11**(11).
27. Li, W. and Y. Cho, *Thermal Fatigue Damage Assessment in an Isotropic Pipe Using Nonlinear Ultrasonic Guided Waves.* Experimental Mechanics, 2014. **54**(8): p. 1309-1318.
28. Thiele, S., et al., *Air-coupled detection of nonlinear Rayleigh surface waves to assess material nonlinearity.* Ultrasonics, 2014. **54**(6): p. 1470-1475.
29. Bermes, C., et al., *Nonlinear Lamb waves for the detection of material nonlinearity.* Mechanical Systems and Signal Processing, 2008. **22**(3): p. 638-646.
30. Wang, K., et al., *Analytical insight into "breathing" crack-induced acoustic nonlinearity with an application to quantitative evaluation of contact cracks.* Ultrasonics, 2018. **88**: p. 157-167.
31. Solodov, I.Y., N. Krohn, and G. Busse, *CAN: an example of nonclassical acoustic nonlinearity in solids.* Ultrasonics, 2002. **40**(1): p. 621-625.
32. Broda, D., et al., *Generation of higher harmonics in longitudinal vibration of beams with breathing cracks.* Journal of Sound and Vibration, 2016. **381**: p. 206-219.
33. Wang, K., et al., *Nonlinear aspects of "breathing" crack-disturbed plate waves: 3-D analytical modeling with experimental validation.* International Journal of Mechanical Sciences, 2019. **159**: p. 140-150.
34. Klepka, A., et al., *Nonlinear acoustics for fatigue crack detection – experimental investigations of vibro-acoustic wave modulations.* Structural health monitoring, 2012. **11**(2): p. 197-211.
35. Guan, R.Q., et al., *Fatigue crack detection in pipes with multiple mode nonlinear guided waves.* Structural Health Monitoring-an International Journal, 2019. **18**(1): p. 180-192.
36. Radecki, R., et al., *Modelling nonlinearity of guided ultrasonic waves in fatigued materials using a nonlinear local interaction simulation approach and a spring model.* Ultrasonics, 2018. **84**: p. 272-289.
37. Pavlakovic, B., et al., *Disperse: A general purpose program for creating dispersion curves.* Review of Progress in Quantitative Nondestructive Evaluation, Vols 16a and 16b, 1997. **16**: p. 185-192.
38. Shah, A.A., Y. Ribakov, and C. Zhang, *Efficiency and sensitivity of linear and non-linear ultrasonics to identifying micro and macro-scale defects in concrete.* Materials & Design, 2013. **50**: p. 905-916.
39. *Local Bond-Stress to Slip Relationships for Hot Rolled Deformed Bars and Mild Steel Plain Bars.* ACI Journal Proceedings, 1979. **76**(3).
40. Wan, X., et al., *Numerical Simulation of Nonlinear Lamb Waves Used in a Thin Plate for Detecting Buried Micro-Cracks.* Sensors, 2014. **14**(5): p. 8528-8546.
41. Sharma, G.K., et al., *Short time Fourier transform analysis for understanding frequency dependent attenuation in austenitic stainless steel.* NDT and E International, 2013. **53**: p. 1-7.
42. Michaels, T.E., J.E. Michaels, and M. Ruzzene, *Frequency–wavenumber domain analysis of guided wavefields.* Ultrasonics, 2011. **51**(4): p. 452-466.

3. Chapter 3 (Paper 2). Collinear nonlinear guided wave mixing for debonding detection in reinforced concrete beam using longitudinal and torsional wave modes

Abstract

Nonlinear guided wave (GW) mixing of longitudinal wave is proposed to detect and locate debonding damage between rebar and concrete in reinforced concrete beam. Two wave mode pairs are chosen based on phase matching and synchronism condition for observing sum combinational harmonics, and longitudinal GW as the excitation signal while the longitudinal and torsional wave as the receiving signal. The study is carried out numerically and experimentally for bonded and debonded reinforced concrete specimens. For bonded specimen, the second order combinational harmonics are absent in all bonded cases. The contact effect due to debonding can generate second and higher order combination harmonics. The indication of debonding damage is determined in debonded specimens by the presence of sum combinational harmonics. The use of phase reversal approach in this study clearly observes the increase in amplitude of the sum combinational harmonics in the debonded cases. By utilizing phase reversal approach and wavenumber frequency analysis, the dominant longitudinal GW modes can be used to accurately determine the location of debonding. The amplitude of the nonlinear parameter of longitudinal and torsional GW modes increases with debonding length. In this study, the results show that the torsional GW modes have better performance than longitudinal GW modes for debonding detection because the torsional GW modes have larger amplitudes than the longitudinal GW modes.

Keywords: Wave mixing, combination harmonic, debonding detection, reinforced concrete, longitudinal wave, torsional wave

Statement of Authorship

Title of Paper	Collinear nonlinear guided wave mixing for debonding detection in reinforced concrete beam using longitudinal and torsional wave modes
Publication status	☐ Published ☐ Accepted for Publication ☐ Submitted for Publication ☒ Under Preparation
Publication Details	Aseem, A. and C.T. Ng, *Collinear nonlinear guided wave mixing for debonding detection in reinforced concrete beam using longitudinal and torsional wave modes.*

Principal Author

Name of Principal Author (Candidate)	Ahmed Aseem		
Contribution to the Paper	Conceptualization, Developing and validating numerical models, Conducting experimental measurements, Signal processing and data analysis, Writing the original draft and editing.		
Overall percentage (%)	80%		
Certification:	This paper reports on original research I conducted during the period of my Higher Degree by Research candidature and is not subject to any obligations or contractual agreements with a third party that would constrain its inclusion in this thesis. I am the primary author of this paper.		
Signature		Date	16-07-2023

Co-Author Contributions

By signing the Statement of Authorship, each author certifies that:

i. the candidate's stated contribution to the publication is accurate (as detailed above);

ii. permission is granted for the candidate in include the publication in the thesis; and

iii. the sum of all co-author contributions is equal to 100% less the candidate's stated contribution.

Name of Co-Author	Ching-Tai Ng		
Contribution to the Paper	Supervision, writing – review and editing.		
Signature		Date	18-07-2023

Please cut and paste additional co-author panels here as required.

3.1 Introduction

In recent years, the damage detection using nonlinear guided waves has attracted increasing attention. The potential of nonlinear guided waves to detect early damage without using baseline measurement is promising. The nonlinear features of guided waves as higher harmonics and combinational harmonics have been widely used in identifying material nonlinearity, fatigue and debonding [1-5]. The debonding between steel rebar and concrete can reduce the serviceability of reinforced concrete structures. Therefore, early damage detection can avoid the risk of unforeseeable collapse. For damage detection in concrete structures, the impression of nonlinear guided wave is found to be very limited in literature [2, 6, 7], for which the main focus of studies has been on higher harmonics, especially the nonlinear guided wave in plate like structures. One of the important factors of guided wave mixing over higher harmonics is that it nullifies the effect of system nonlinearities. In contrast to this, combinational harmonics are generated purely due to the interaction of different frequency guided waves in mixing zone from the sources of nonlinearities in specimen, such as material, fatigue, damage etc. [8]. In this regard, the guided wave mixing is preferred and more reliable technique for damage detection. It was first studied by Jones et al. that two primary waves interacting in presence of nonlinearity or damage can produce nonlinear scattering waves provided that synchronism conditions are met [9]. They are categorized as collinear (parallel) and non-collinear (nonparallel coplanar) wave mixing with one-way and two-way mixing directions for collinear wave mixing. The analytical solutions for one-way and two-way mixing of longitudinal and transverse waves were explicitly derived by Chen et al., where they showed numerically and experimentally that combinational harmonics are generated by one-way collinear wave mixing of longitudinal and transverse pulses [10].

The applications of wave mixing techniques for studying material damage and nonlinearities in plate like structures was well established. Croxford et al. demonstrated that

resonant wave is generated in plates having fatigue and deformation due to non-collinear Lamb wave mixing of shear horizontal wave modes [11]. Guided wave mixing can generate second order and third combinational harmonics. Allen and Ng studied bolt loosening condition in plates using guided wave mixing [12]. At loosen bolted joint, contact surfaces are generated between plates enabling guided wave mixing to generate second and third order combinational harmonics. Hasanian and Lissenden analytically, numerically and experimentally validated the presence of second order combinational harmonics using shear horizontal wave mixing [13]. They used counter-propagating collinear guided wave mixing of fundamental shear horizontal wave modes (SH_0) to demonstrate the presence of second and third order combinational harmonics due to material nonlinearity.

For circular waveguides such as pipes, Yeung and Ng have recently studied the material nonlinearity using nonlinear guided waves [14]. The study showed that torsional guided wave modes in hollow circular pipes can generate combinational harmonic due to material nonlinearity. Li et al. (2021) carried out numerical study using longitudinal guided wave modes for characterising material degradation in circular pipe by co-directional one-way guided wave mixing [15]. Under synchronism condition for longitudinal guided wave modes, sum and difference combinational harmonics are produced. In this study, the secondary longitudinal wave modes are generated from mixing of primary longitudinal wave mode. If phase matching conditions are met, it is possible to observe secondary wave modes in circular structures, such as rebar. The nonlinear parameter of difference combinational harmonic also increases with the size of mixing zone in a pipe with degradation. This was also verified by Zhao et al. [16]. However, this phenomenon is not discussed in literature for embedded circular structures as in reinforced concrete. In embedded circular structures, the possibility of secondary wave generated from the mixing zone to be registered at either rebar ends or scattered completely in surrounding concrete is yet to be investigated.

While considering damage in reinforced concrete, many studies used linear features of guided waves. To detect corrosion and debonding in rebar embedded in concrete, researchers proposed to use linear guided waves [17-23]. These techniques rely on baseline measurements and linear features of guided wave, such as amplitude, time-of-flight, and magnitude of the wave etc. To avoid comparison of linear feature at different states of specimen for damage detection, nonlinear features of guided waves were proposed by Aseem and Ng to detect damage [24]. The nonlinear feature as second harmonics can detect damage without reference data. If the reference data is not considered for damage detection, the nonlinearities as second or higher harmonics can be contaminated by instrumental nonlinearities. Therefore, these nonlinearities must be checked before carrying out these studies. To avoid these unnecessary complications and limitations, guided wave mixing can be used to detect debonding type damage in rebar reinforced concrete. Guided wave mixing could generate combination harmonics, which are at different frequency to the fundamental and second harmonic. Guided wave mixing is an advanced technique which is more sensitive to material nonlinearity and damages as compared to system nonlinearities [25]. In wave mixing technique, the certain synchronism conditions need to be met to generate combinational harmonics as studied in literature [26, 27]. Croxford et al. has also shown that guided wave mixing is less sensitive to system nonlinearities [28]. Hence, the combination harmonic would not be affected by the instrumental nonlinearities.

In this paper, nonlinear guided wave mixing is proposed to detect and locate debonding damage in reinforced concrete beam. Section 3.2 presents the guided wave mixing phenomenon. Section 3.3 describes the details of finite element simulation that is used to model the guided wave mixing in the rebar of the reinforced concrete beam, in which the longitudinal guided wave is used as the excitation. Phase matching synchronism conditions and mode pairs are established to observe generation of nonlinear scattered secondary wave in longitudinal and

torsional direction. In Section 3.3, a series of numerical studies are carried out on ribbed rebar embedded in concrete, in which various bonded and debonded cases are considered. The simulated numerical model is explained for excitation and receiving of guided waves mixed signals. In Section 3.4, phase reversal approach is defined to clearly observe the presence of sum combinational harmonics. The damage is located using time frequency spectrum analysis having insight of wavenumber frequency analysis and phase reversal approach. The numerical cases are experimentally studied in section 3.5. In last section, it is concluded that wave mixing of longitudinal guided wave modes can detect debonding damage by using longitudinal and torsional direction wave guides.

3.2 Methodology

For using combinational harmonics for damage detection, there can be two sources for its presence; a) material nonlinearity b) contact nonlinearity e.g. debonding between rebar and concrete interface. The study has already shown that amplitude of higher or combinational harmonics produced due to damage is greater than the amplitude from material nonlinearity [29]. The presence of combinational harmonics serves as an indicator for damage. It is worth to mention that damage between steel rebar and concrete serves as mixing zone for mixed wave, from which nonlinear scattered wave can be generated and propagated. To understand the generation of nonlinear wave from damage, we consider a schematic for steel rebar reinforced concrete beam as shown in Figure 3.1, which shows the phenomenon of collinear one-way mixing. When the propagating guided wave has two excitation frequencies travelling from bare ribbed rebar to the embedded rebar interacts with debonding or damaged zone, it generates nonlinear scattered wave. This nonlinear scattered wave can have nonlinear feature of second order or higher order combinational harmonics. The combinational harmonics are observed at the far rebar end. It also observes higher harmonics of the excitation frequencies because of contact acoustic nonlinearity (CAN) effect at debonding. The guided wave modes

for mixing frequencies are mixed and interacted in the debonding zone to produce combinational harmonics meaning that they arrive at same time at debonding location. Without either knowing the debonding location or time delay, the wave modes for mixing frequencies should have similar group velocities in embedded rebar to be mixed in debonding zone. This will be discussed in Section 3.3 & 3.4 in detail while defining mode pairs and investigating debonding damage location.

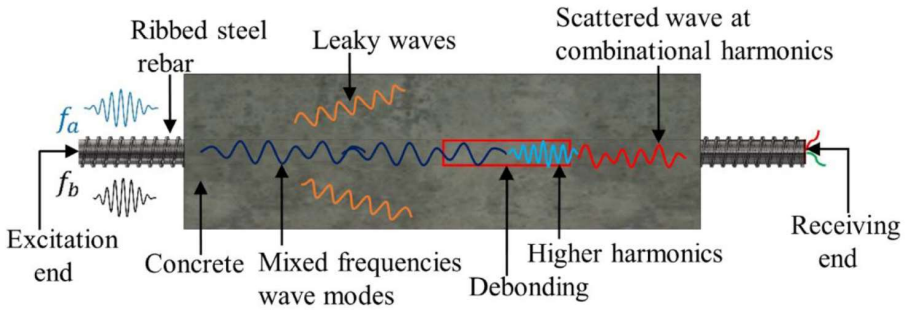

Figure 3.1 Schematics for guided wave mixing in debonded reinforced concrete beam

The choice of excitation frequencies is not straightforward. It requires synchronism conditions to be met to produce combinational harmonics. Consider two longitudinal guided waves ω_a and ω_b, propagating through mixing zone can produce second order combined harmonic [30]. The field $u^{(2)}$ generated due to the mixing of two primary wave field $u^{(a)}$ and $u^{(b)}$ can be written as a linear combination of series of excitation frequencies ω_a and ω_b;

$$u^{(2)} = \sum_m A_m(z) u_m^{\omega_a \pm \omega_b}(y) e^{[-j(\omega_a \pm \omega_b)t]} \tag{3.1}$$

where $u_m^{\omega_a \pm \omega_b}(y)$ is the field function of mth harmonics at mixing frequency $\omega^{(2)} = \omega_a \pm \omega_b$ with $k_m^{(2)}$ as the wavenumber. $A_m(z)$ is the corresponding expansion co-efficient can be written as

$$A_m(z) = \frac{[f_{s(m)}^2 + f_{b(m)}^2]}{4P_{mm}} \frac{\sin(\Delta_m z)}{\Delta_m} e^{[j(k_m^{(2)} + \Delta_m)z]} \tag{3.2}$$

where $\Delta_m = [(k_a \pm k_b) - k_m^{(2)}]/2$. $f_{s(m)}^2$ and $f_{b(m)}^2$ are surface driving traction and bulk driving forces. P_{mm} is the average power flow per unit width of beam for mth wave at mixing frequency $\omega^{(2)}$. For synchronism condition to be met perfectly, $\Delta_m = 0$ i.e. $k_m^{(2)} = (k_a \pm k_b)$ and nonzero power flux i.e. $f_{s(m)}^2 + f_{b(m)}^2 \neq 0$ in order to generate second order combinational harmonics.

It has been found in literature that magnitude of $A_m(z)$ increases linearly with propagation distance if $\Delta_m = 0$ perfectly. Therefore, we are bound to observe second order combinational harmonics at rebar receiving end following that $k_m^{(2)} = (k_a \pm k_b)$ [31].

To achieve synchronism condition, phase velocity dispersion and frequency wavenumber curves are plotted for reinforced concrete beam using DISPERSE [32] as shown in Figure 3.2 for longitudinal guided waves. In DISPERSE, the beam is considered as rebar embedded in concrete. The concrete is defined with circular shape as outer diameter of 150mm and inside diameter of 24mm, which is defined as the diameter of steel rebar inside concrete. The properties of steel and concrete are shown in Table 3.1. The two mode pairs are considered having phase matching condition for second order combinational harmonic at sum frequencies as represented in Figure 3.2(a). Wavenumber against frequency data is plotted for longitudinal (L) and torsional (T) mode pairs in Figure 3.2(b) and 3.2(c) respectively.

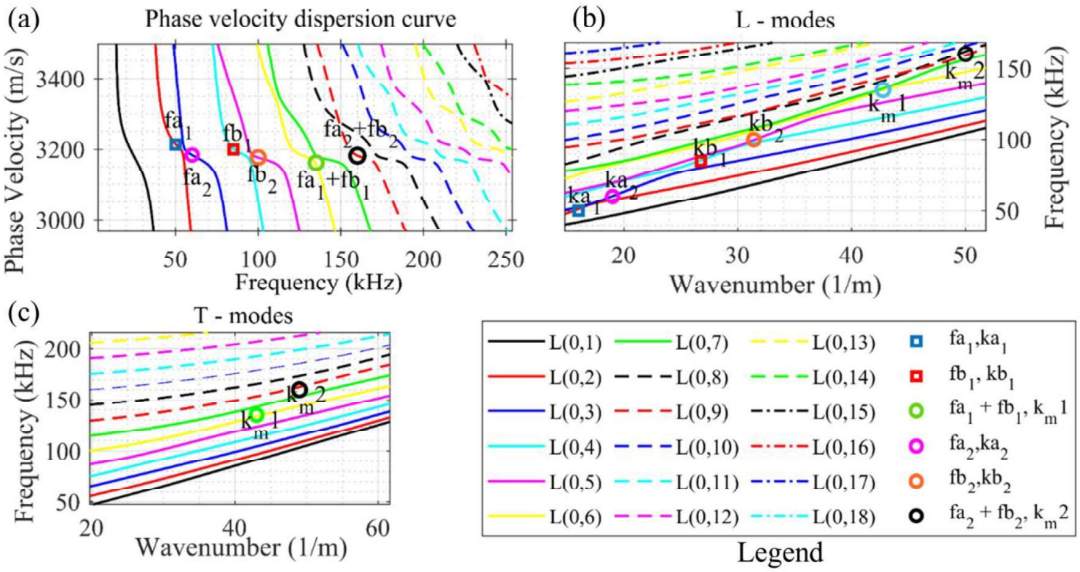

Figure 3.2 Synchronism condition for sum combinational harmonics (a) Phase matching for L mode pairs (b) Wavenumber frequency match for L mode pairs and (c) T mode pairs

Table 3.1 Mode pairs with synchronism condition for sum combinational harmonics

Mode Pairs	f_a (kHz)	f_b (kHz)	$f_a + f_b$ (kHz)	k_a (1/m)	k_b (1/m)	$k_a + k_b$ (1/m)	$k_m^{(2)}$ (1/m) L mode	$k_m^{(2)}$ (1/m) T mode
1	50	85	135	15.75	26.6	42.35	42.45	43
2	60	100	160	18	31	49	50	48

Considering mode pair 1, the phase velocities for excitation frequencies f_{a1}at L(0,2) wave mode and f_{b1} at L(0,4) wave mode is almost similar to the phase velocity of sum combinational harmonic f_{a1} + f_{b1} at L(0,7) wave mode around 3200 m/s. For second mode pair, the phase velocities for excitation frequencies f_{a2} at L(0,3) wave mode and f_{b2} at L(0,5) wave mode is also equal to the phase velocity of sum combinational harmonic f_{a2} + f_{b2} at L(0,9) wave mode around 3200 m/s. Apart from phase matching condition, the synchronism condition for second order combinational harmonics are also met as shown in Table 3.1. For both mode pairs, the wavenumber at sum combinational harmonic ($k_m^{(2)}$) is equal to the sum of wavenumber at excitation frequencies i.e., $k_a + k_b$.

It can be summarized as two primary longitudinal guided waves interacting through debonded region in rebar reinforced concrete beam. Satisfying the phase matching and synchronism conditions, it produces nonlinear scattering wave combinational harmonic at sum frequency in longitudinal direction and torsional direction. Jones and Kobett (1963) have mentioned in their study that primary interacting waves either in longitudinal or transverse direction upon satisfying synchronism condition can generate nonlinear scattering wave in either direction [9]. In our study, we aims at investigating nonlinear scattering wave generation in torsional and longitudinal direction at rebar end due to debonding. Once nonlinear scattered wave is generated from guided wave mixing in debonding zone, guided wave modes of combinational harmonics at sum frequency are expected to propagate as predicted by the dispersion curve.

3.3 Numerical Simulations

The numerical study is undertaken on reinforced concrete beam specimen. The reinforced concrete beam specimen has ribbed rebar embedded in the concrete. This section explains the numerical modelling of ribbed rebar and concrete surrounding the rebar. Fully bonded and

debonded cases are created to understand the phenomenon of guided wave mixing in intact and damaged specimen. The numerical study is carried out in ABAQUS 2017.

3.3.1 Modelling of ribbed steel rebar

The steel ribbed rebar considered has longitudinal and transverse ribs. Ribbed or deformed rebar is selected for the study because of wide acceptability of deformed bars in civil engineering structures. These ribs provide bond strength with concrete and more resistance to slip and shear failure as compared to plain bars without ribs.

A circular plain bar with 24mm ∅ and 700mm long is used in this study. Only 500mm length of rebar is embedded at centre in concrete and the cross-section of concrete is 150mm × 150mm. The ribbed rebar has longitudinal and transverse ribs. The transverse ribs are created using spiral part having 15120^{o} or 42 revolutions to revolve the transverse ribs around 700mm length of plain bar as shown in Figure 3.3(a). The pitch for transverse ribs is 16mm with cross-section of 2mm×2mm. The transverse ribs are connected to the plain bar using tie constraints. As the longitudinal ribs are throughout the length of rebar on top and bottom, it can coincide with concrete infill within the transverse ribs. To avoid this conflict, the longitudinal ribs are created at the exposed ends of the rebar only, i.e. outside the embedded zone. The cross-section of longitudinal ribs is also 2mm×2mm.

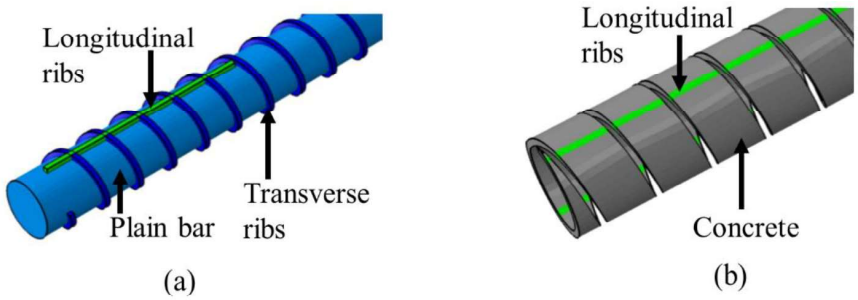

Figure 3.3 Numerical modelling of (a) ribbed rebar and (b) concrete within ribs of rebar

3.3.2 Modelling of concrete infill and beam

After modelling steel ribbed rebar, the infill part within transverse ribs is modelled using hollow circular cylinder having 2mm thickness and inner diameter equal to the outer diameter of plain rebar. The profile of spiral/transverse ribs is used to cut the concrete out of hollow cylinder which can be later filled with transverse ribs as shown in Figure 3.3(b) and Figure 3.4. As longitudinal ribs are throughout the length of rebar, the cross-section of longitudinal ribs as 2mm×2mm is defined at center of infill. It is represented as green region in Figure 3.3(b). The longitudinal ribs exist on top and bottom surfaces of the infill part. The longitudinal ribs are defined with material properties of steel. The rest of infill part is considered as concrete material as shown in grey in Figure 3.3(b). The longitudinal ribs and concrete infill are tie constrained with plain bar for fully bonded specimen.

A square concrete cross-section 150mm×150mm is created for the embedded zone of rebar with the length of 500mm. The square concrete section is hollow at the centre to allow for ribbed rebar with concrete infill. The concrete infill and square concrete cross-section beam are tie constrained for fully bonded specimen. Figure 3.4 shows sliced view of reinforced concrete beam with concrete infill and ribbed rebar. The outer square concrete cross-section is cut into half to show the concrete infill within transverse ribs along with longitudinal ribs in the embedded zone.

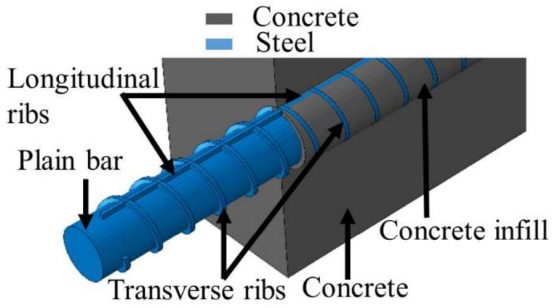

Figure 3.4 Sliced section of numerical model representing ribbed rebar, concrete infill and beam

Steel and concrete material are presented in blue and grey colours in Figure 3.4, respectively. For meshing, all parts are meshed using eight-node elements, C3D8R, with reduced integration. The mesh is swept having hexagonal shape with element size of 1mm. For quality meshing, it was shown that $L_e = \frac{\lambda}{20}$, where λ is the wavelength and L_e is the mesh size [33].

3.3.3 Debonding between steel ribbed rebar and concrete

To create debonding in reinforced concrete beam, contact surfaces are generated between steel rebar and concrete. In debonded region, the outer surface of transverse and longitudinal ribs are defined surface-surface contact interaction properties with concrete beam surface. Further, the surface of plain bar in debonded region is allowed to have similar contact type interaction with inner surface of concrete infill. These surfaces are considered frictionless. The interaction properties are simulated using penalty contact method. It is understood that this contact type interaction can generate higher harmonics. However, the guided wave mixing mode pairs satisfying the synchronism condition also generate sum combinational harmonics as discussed in section 3.2.

3.3.4 Case studies

One fully bonded and two debonded specimens are considered for the study. Initially, numerical study is undertaken. Numerical and experimental cases are defined in Table 3.2 based on different specimens, excitation-receiving modes and mode pairs as defined in section 3.2. The abbreviation of different cases in Table 3.2 indicates that N is for numerical, E is for experimental, L and T represents the receiving mode as longitudinal and torsional, respectively, 1 and 2 represents the excitation mode pair 1 and mode pair 2, respectively, as defined in section 3.2.

Table 3.2 Bonded and debonded specimen cases for guided wave mixing

Beam specimens	**Numerical Cases**	**Experiment Cases**	**Excitation – Receiving Mode**	**Debonding length d_l (mm)**	**Distance to debonding from excitation end l_a + l_{br} (mm)**
Bonded	N-B-L1	E-B-L1	L-L	0	-
	N-B-L2	E-B-L2	L-L	0	-
	N-B-T1	E-B-T1	L-T	0	-
	N-B-T2	E-B-T2	L-T	0	-
`Debonded	N-D1-L1	E-D1-L1	L-L	200	250
	N-D1-L2	E-D1-L2	L-L	200	250
	N-D1-T1	E-D1-T1	L-T	200	250
	N-D1-T2	E-D1-T2	L-T	200	250
	N-D2-L1	E-D2-T1	L-L	150	350
	N-D2-L2	E-D2-T2	L-L	150	350
	N-D2-T1	E-D2-T1	L-T	150	350
	N-D2-T2	E-D2-T2	L-T	150	350

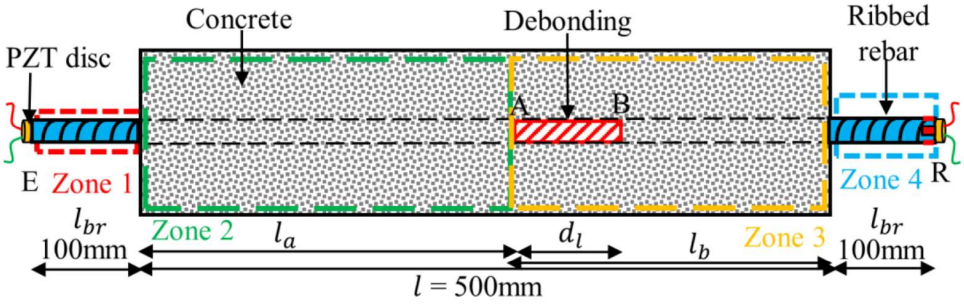

Figure 3.5 Schematics for debonded reinforced concrete specimen with excitation and receiving PZTs

The guided wave signal is excited at excitation end E as shown in Figure 3.5. Two guided wave signals are used, which are two separate mode pairs in section 3.2. For mode pair 1, 8-cycle hanning windowed signal with 50 kHz and 85 kHz frequencies are premixed, while for mode pair 2, 8-cycle hanning windowed signal with 60 kHz and 100 kHz frequencies are premixed as shown in Figure 3.6. The mixing frequencies of mode pairs are premixed with delay in the excitation time for frequency, which has faster group velocity. This ensures the wave modes for both frequencies arrive at the same time at the start of embedded rebar. The signal is applied as pressure on the bar planar surface. The magnitude of pressure is determined using experimental study via 1D laser Vibrometer at the excitation end. For selected 240V, the

order of magnitude pressure is 1×10^7 for excitation in FE. The material properties of steel and concrete used in FE are listed in Table 3.3 [34, 35].

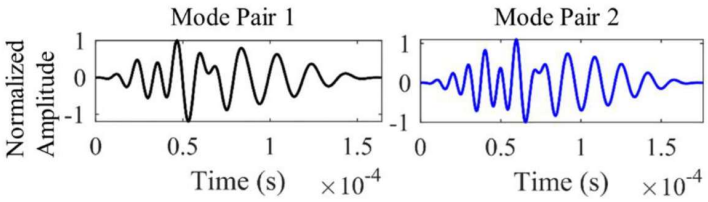

Figure 3.6 Mode pairs for guided wave mixing

Table 3.3 Material properties for concrete and steel

Material	Density (kg/m^3)	Elastic Modulus (GPa)	Poisson's ratio	λ (N/m^2)	μ (N/m^2)	l (N/m^2)	m (N/m^2)	n (N/m^2)
Steel	7890	210	0.33	1.06×10^{11}	7.9×10^{10}	-3.32×10^{11}	-5.84×10^{11}	-7.18×10^{11}
Concrete	2300	32.5	0.13	8×10^{9}	1.38×10^{10}	-4.32×10^{10}	-5.09×10^{11}	-3.04×10^{11}

Since the rebar is embedded in concrete, the guided wave energy propagating in embedded rebar is leaked into the surrounding concrete [32]. In regard to this, material damping for concrete is considered. Rayleigh damping is considered, which is a linear combination of mass-proportional (α) and stiffness proportional (β) damping. As the wave energy dissipates into concrete, the attenuation co-efficient k_i is defined as [36];

$$\frac{A_1}{A_2} = e^{k_i(x_2 - x_1)} \tag{3.3}$$

The damping constants α and β are frequency dependent and can be written based on particular angular frequency as;

$$\alpha_\omega = 2k_i C_g \tag{3.4}$$

$$\beta_\omega = \frac{2k_i C_g}{\omega^2} \tag{3.5}$$

where A_1 and A_2 are the amplitudes of propagating signal at location x_1 and x_2, respectively. Based on experimental setup defined in this study, the receiving signal is measured at one location only which is the rebar end R. Due to this limitation, the attenuation constant cannot

be found experimentally using equation 3.3. The attenuation constant is derived using trial-and-error method between numerical and experimental receiving signal. After matching the amplitude of numerical and experimental signal using varying values of damping constants, the attenuation constant is found numerically using amplitudes of guided wave signal (A_1 and A_2) at two locations (x_1 and x_2) in embedded rebar. Attenuation constant for mode pair 1 and 2 are 4.84 Np/m and 1.45 Np/m, respectively. By using equation 3.4 and 3.5, damping constant for mode pair 1 are α_ω = 29,000 rad/s and 1.02 × 10^{-7}s/rad, while for mode pair 2 are 8,700 rad/s and 2.2 × 10^{-8}s/rad. The comparison of time domain signal for numerical and experimental results are shown in Section 3.5.

3.3.4.1 Time domain signal

For receiving signal in longitudinal direction in FE, the displacement is measured along the direction of rebar. To receive only torsional wave mode, the displacements are measured in the direction of the circumference of rebar. The time domain signals of all cases for bonded and debonded specimen D1 are shown in Figures 3.7 and 3.8, respectively.

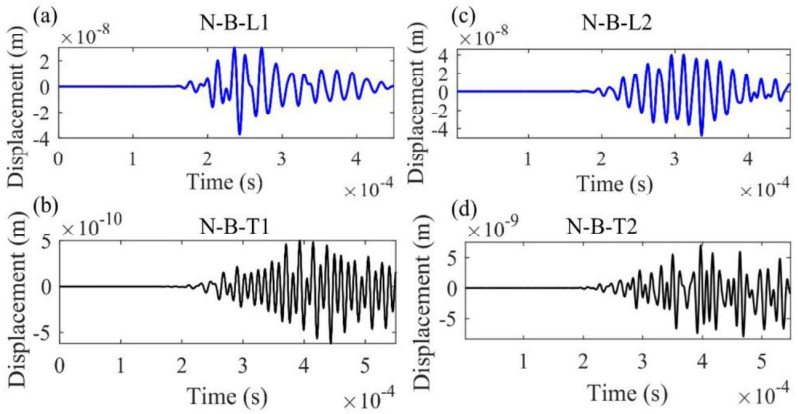

Figure 3.7 FE Time domain signal for bonded case (a) longitudinal and (b) torsional receiving for mode pair 1 excitation, (c) longitudinal and (d) torsional receiving for mode pair 2 excitation

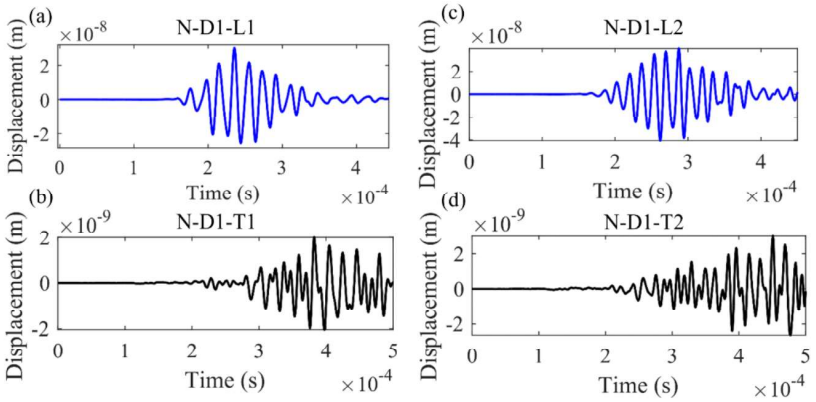

Figure 3.8 FE Time domain signal for debonded case (a) longitudinal and (b) torsional receiving for mode pair 1 excitation, (c) longitudinal and (d) torsional receiving for mode pair 2 excitation

For time domain signal of guided wave mixing, linear features alone do not provide enough information for the presence of damage. As per group velocity dispersion curves for the specimen, the longitudinal wave modes have greater group velocity as compared to the torsional wave mode. The longitudinal wave mode arrives earlier than the torsional wave mode as seen in Figures 3.7 and 3.8. The data obtained for debonded specimen 2 is not presented for simplicity. For observing the ability of nonlinear guided wave mixing to detect damage, the frequency analysis is carried out.

3.3.4.2 Frequency analysis

The frequency analysis is carried out for time domain signal using Fast Fourier Transform (FFT). For bonded specimen, frequency domain results for both mode pairs do not show any presence of higher and sum combinational harmonics as shown in Figures 3.9(a) and 3.9(b). In the debonded specimen D1, the presence of sum combinational harmonics for both mode pairs shows the presence debonding damage in the specimen. The sum combinational harmonics are observed for both longitudinal and torsional receiving modes. It should be noted that second and higher harmonics are also observed, which are generated due to contact damage in the

specimen. However, sum combinational harmonics are the point of interest for nonlinear guided wave mixing in this study.

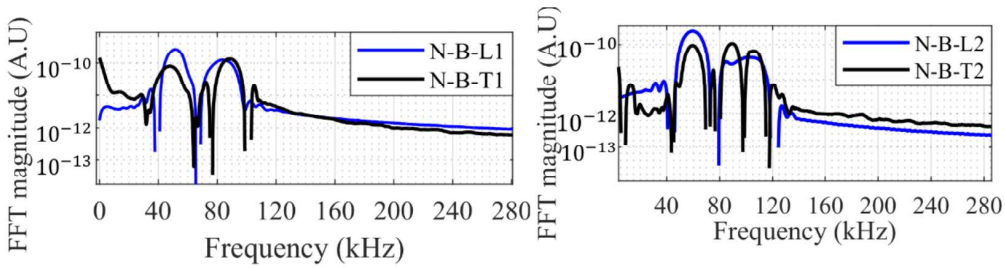

Figure 3.9 FFT for bonded specimen with longitudinal and torsional receiving modes (a) mode pair 1 excitation (b) mode pair 2 excitation

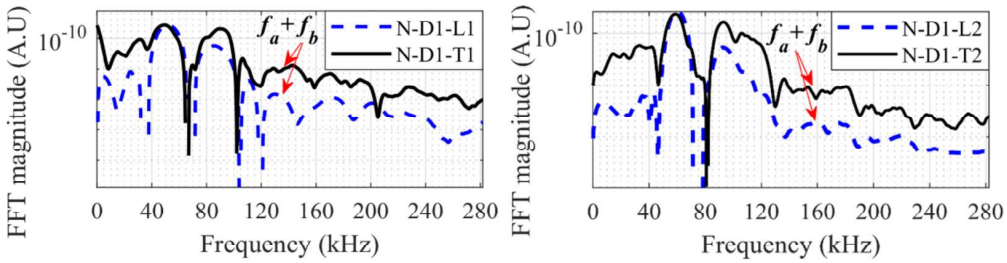

Figure 3.10 FFT for debonded specimen D1 with longitudinal and torsional receiving modes (a) mode pair 1 excitation (b) mode pair 2 excitation

For torsional receiving mode pairs, sum combinational harmonics appear to have larger amplitudes as compared to the longitudinal receiving mode pair. The torsional receiving mode pair can therefore be more effective in damage detection. In order to quantify damage for both mode pairs and receiving mode types, nonlinear parameter is calculated for all cases listed in Table 3.2 is shown in Figure 3.11. The nonlinear parameter is defined as $\beta' = (A_{a_{nb_n}})/A_{a_n}A_{b_n}$, where $A_{a_{nb_n}}$ represents the amplitude of sum combination harmonics, A_{a_n} and A_{b_n}represents the amplitude of mixed frequencies a and b respectively. The subscript *n* in each case represents the mode pair type as there are two mode pairs used for this study. The nonlinear parameter for each debonded case is plotted against its respective bonded case. The nonlinear parameter obtained assures a significant increase for all damaged cases as compared

to the bonded case. In Figure 3.11, N represents numerical results, B represent bonded, D1 and D2 are debonded specimens, L1 and L2 are longitudinal receiving modes for mode pair 1 and 2 excitations respectively, T1 and T2 are torsional receiving modes for mode pair 1 and 2 excitations respectively. In debonded specimens, for longitudinal and torsional receiving modes, mode pair 2 has greater nonlinear parameter as compared to mode pair 1. The graph also represents that torsional receiving modes have larger amplitude of nonlinear parameter as compared to their longitudinal receiving mode cases.

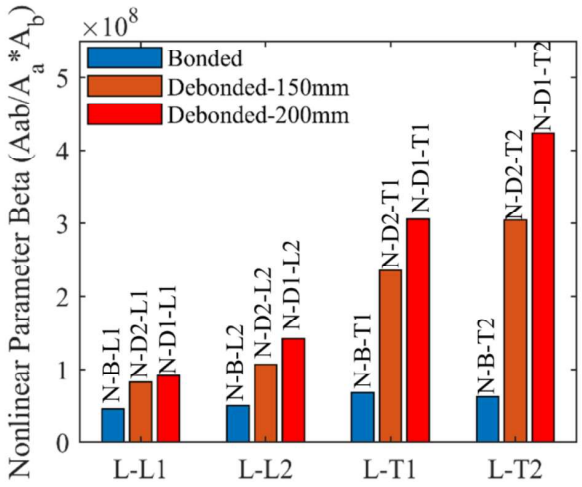

Figure 3.11 Nonlinear parameter for numerically bonded and debonded cases

It is imperative that nonlinear guided wave mixing can detect debonding damage in reinforced concrete beam. The information about the location of damage is registered within the mode pairs generated at sum combinational harmonics. Due to presence of multiple modes in embedded rebar in concrete, it is challenging to identify the dominant wave mode at sum combinational harmonics. The existence of other wave modes at excitation frequencies can be reduced by adopting the technique of phase reversal [37], which is discussed in detail in Section 3.4.

3.3.5 Debonding location estimation using phase reversal and frequency-wavenumber analysis

3.3.5.1 Phase reversal approach

The fundamental of phase reversal approach is to clearly observe the second order nonlinear harmonics by cancelling out the effect of excitation frequencies. For simplicity, the equation for propagation of wave field in nonlinear guided wave mixing is the combination of excitation frequencies, higher harmonics, and sum and combination harmonics [38]. The guided wave mixing signal received without any phase reversal can be written as

$$u^0(x,t) = A_a \cos(f_a t - k_a x) + A_b \cos(f_b t - k_b x) + x\beta \left[-\frac{A_a^2 k_a^2}{8} \cos(2f_a t - 2k_a x) - \frac{A_b^2 k_b^2}{8} \cos(2f_b t - 2k_b x) + \frac{A_a A_b k_a k_b}{4} \{ cos[(f_a - f_b)t - (k_a - k_b)x] - cos[(f_a + f_b)t - (k_a + k_b)x] \} \right] \quad (3.6)$$

where A_a and A_b are the amplitudes of excitation frequencies for a mode pair type with their respective frequencies f_a and f_b and wavenumbers k_a and k_b. x and t are the distance and time respectively. By applying 180^0 phase reversal for the excitation frequencies, the propagating guided wave mixed signal received can be written as

$$u^\pi(x,t) = A_a \cos(f_a t - k_a x + \pi) + A_b \cos(f_b t - k_b x + \pi) + x\beta \left[-\frac{A_a^2 k_a^2}{8} \cos(2f_a t - 2k_a x) - \frac{A_b^2 k_b^2}{8} \cos(2f_b t - 2k_b x) + \frac{A_a A_b k_a k_b}{4} \{ cos[(f_a - f_b)t - (k_a - k_b)x] - cos[(f_a + f_b)t - (k_a + k_b)x] \} \right] \quad (3.7)$$

It should be noted that similar conditions are maintained in Equations 3.6 and 3.7. By adding Equations 3.6 and 3.7, the excitation frequencies are counteracted and left with the addition of second harmonics, sum and combinational harmonics.

$$u^0(x,t) + u^\pi(x,t) = 2x\beta \left[-\frac{A_a^2 k_a^2}{8} \cos(2f_a t - 2k_a x) - \frac{A_b^2 k_b^2}{8} \cos(2f_b t - 2k_b x) + \frac{A_a A_b k_a k_b}{4} \{ cos[(f_a - f_b)t - (k_a - k_b)x] - cos[(f_a + f_b)t - (k_a + k_b)x] \} \right] \quad (3.8)$$

For phase reversal approach, only debonded specimen D1 is studied to clearly observe the presence of combinational harmonics in both mode pairs. The case studies N-D-L1 and N-

D1-L2 for mode pairs 1 and 2, respectively, are excited with original and phase reversed wave mixing signal. The original and phase reversed signal are plotted together for both cases as shown in Figures 3.12(a) and 3.12(b). The sum of original and phase reversed nonlinear guided wave mixed signal for both cases N-D-L1 and N-D1-L2 are represented in Figures 3.12 (c) and 3.12 (d), respectively.

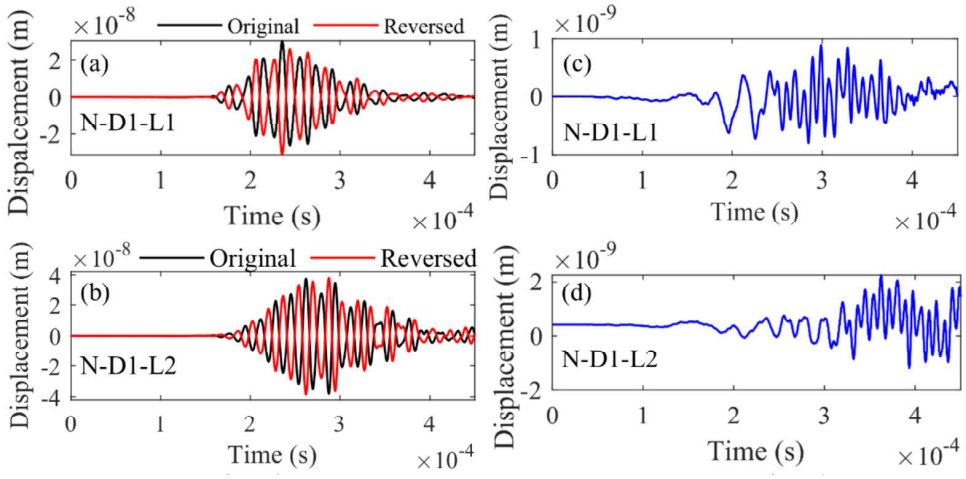

Figure 3.12 : FE D1 debonded specimen time domain data for original and phase reversed signal for (a) mode pair 1 and (b) mode pair 2, phase reversal sum signal for (c) mode pair 1 and (d) mode pair 2

The time domain signal contains the second order nonlinear features of guided waves. For observing the presence of higher harmonics and sum and difference combinational harmonics, FFT is applied on the sum signal. The FFT results of sum signal for both cases N-D1-L1 and N-D1-L2 are represented in Figures 3.13(a) and 3.13(b), respectively. It clearly shows the reduction in excitation frequencies at mode pair 1 i.e. 50 kHz and 85 and mode pair 2 i.e. 60 kHz and 100 kHz. Due to addition, the second harmonics and sum and difference combinational harmonics are clearly observed as shown in Figure 3.13.

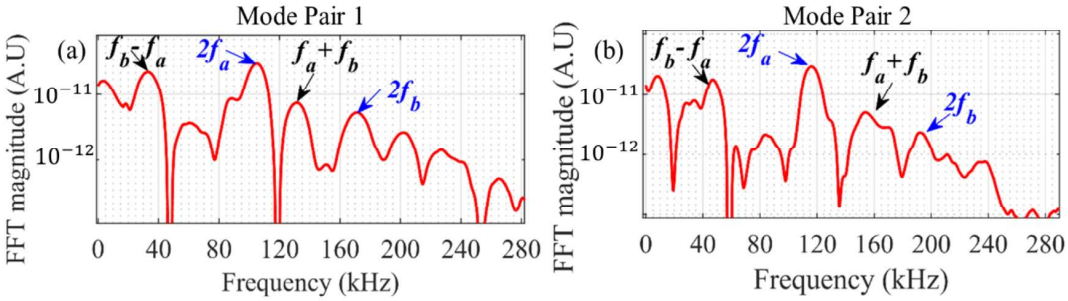

Figure 3.13 FE D1 debonded specimen FFT for (a) mode pair 1 and (b) mode pair 2 using phase reversal approach

In order to locate the debonding damage using sum combinational harmonics, time frequency spectrum analysis is performed. The information about the presence of dominant wave mode pair at sum combinational harmonics helps identify the location of debonding damage. The evidence of wave mode can be attained from frequency-wavenumber analysis.

3.3.5.2 Debonding location estimation

For locating the damage, the arrival time of sum combinational harmonics is utilized from time frequency spectrum of phase reversal technique. The use of phase reversal approach in locating damage in this scenario helps identify the time of arrival of sum combinational harmonics. As the guided wave is excited at the end E of reinforced concrete beam shown in Figure 3.5, the time of arrival of sum combinational harmonics $t_{f(a+b)}$ can be written as

$$t_{f(a+b)} = t_{fab}^{lbr} + t_{fab}^{la} + t_{f(a+b)}^{lb} + t_{f(a+b)}^{lbr} \tag{3.9}$$

which can be written as;

$$t_{f(a+b)} = \frac{l_{br}}{V_{fab}^{lbr}} + \frac{l_a}{V_{fab}^{la}} + \frac{l_b}{V_{f(a+b)}^{lb}} + \frac{l_{br}}{V_{(a+b)}^{lbr}} \tag{3.10}$$

where V_{fab}^{lbr} and V_{fab}^{la} are the group velocity of dominant guided wave mode of either frequencies f_a or f_b in zone 1 and zone 2 respectively. $V_{f(a+b)}^{lb}$ is the group velocity of dominant guided wave mode at sum combinational harmonics in embedded rebar for zone 3, while $V_{f(a+b)}^{lbr}$ is the group velocity of guided wave mode at sum combinational harmonics in bare

rebar for zone 4. l_{br} is bare rebar length in zone 1 and 4. l_a is the length of embedded rebar from concrete excitation end to the start of debonding i.e. zone 2, while l_b i.e $l - l_a$ is the length of embedded rebar from the start of debonding to concrete receiving end i.e. zone 3. Since the values of bare rebar length and group velocities are known in advance, $\frac{l_{br}}{V_{fab}^{lbr}} + \frac{l_{br}}{V_{f(a+b)}^{lbr}}$ can be treated as a constant C.

The location of debodning l_a from concrete excitation end A can be written as

$$l_a = \frac{(t_{f(a+b)})(V_{fab}^{la})(V_{f(a+b)}^{lb}) - C(V_{fab}^{la})(V_{f(a+b)}^{lb}) + l(V_{fab}^{la})}{(V_{f(a+b)}^{lb}) - (V_{fab}^{la})} \quad (3.11)$$

For Zone 1, the excitation frequencies are premixed with delayed time interval due to difference in their group velocities allowing the mode pairs to arrive same time at concrete excitation end. In Zone 1, $L(0,1)_{br}$ bare rebar wave mode exists. Group velocity of $L(0,1)_{br}$ wave mode at 85 kHz and group velocity of L(0,1) at 100 kHz is selected as V_{fab}^{lbr} for mode pairs 1 and 2 respectively. To determine dominant propagating wave mode in Zone 2, wavenumber frequency analysis is carried out for original signal as studied by Aseem & Ng (2021) [24]. It is found that L(0,4) at 85 kHz is dominant wave mode for mode pair 1 and L(0,5) at 100 kHz is the dominant wave mode for mode pair 2. The group velocity dispersion curve for rebar embedded in concrete is shown in Figure 3.14.

The combinational harmonics are generated at the start of debonding location A. The information about time of arrival of sum combination harmonics i.e. $t_{f(a+b)}$ at the receiving end is obtained from phase reversed signal. To find out dominant propagating wave mode at sum combinational harmonics in Zone 3, wave number frequency analysis is carried out on phase reversed signal. The original and phase reversal time domain signals are acquired every 2mm for a distance of 50mm in the debonding Zone 3, which are then used to attain phase reversed signal for wavenumber frequency analysis. It is found by frequency-wavenumber analysis of phase reversed signal that L(0,11) and L(0,16) are the dominant propagating wave

modes at sum combinational harmonics for mode pair 1 and 2 respectively. The group velocity at sum combinational harmonics i.e. $V_{f(a+b)}^{lb}$ for mode pair 1 at L(0,11) wave mode is 1730 m/s and for mode pair 2 at L(0,16) wave mode is 1200 m/s.

Lastly, the frequency-wavenumber analysis of phase reversed signal in zone 4 yields the dominant propagating wave mode as $L(0,1)_{br}$ at 135 kHz for mode pair 1 and $L(0,2)_{br}$ at 160 kHz for mode pair 2. Therefore, the group velocity $V_{f(a+b)}^{lbr}$ for sum combinational harmonics for bare rebar is 1999 m/s at 135 kHz for mode pair 1 and 1800 m/s at 160 kHz for mode pair 2.

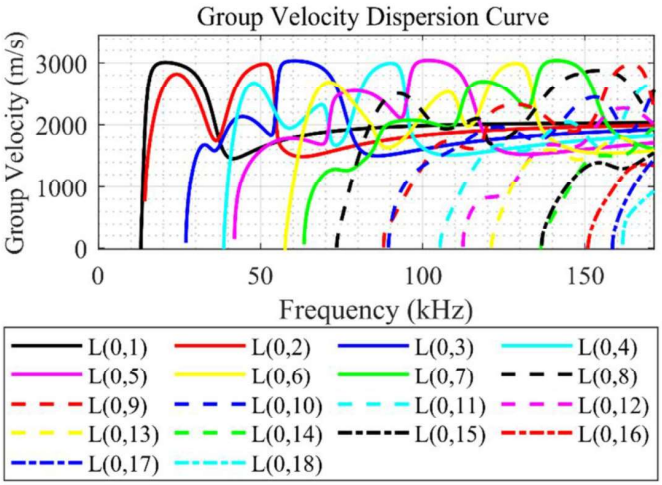

Figure 3.14 Group velocity dispersion curve for rebar embedded in concrete

In order to determine the time of arrival of sum combinational harmonic, i.e.$t_{f(a+b)}$, Short Time Fourier Transform (STFT) is applied on phase reversed time domain signal at the receiving end of rebar. STFT is shown for mode pair 1 and 2 in Figures 3.15(a) and 3.15(b). As phase reversal approach is applied on longitudinal receiving modes, time-frequency analysis is carried for longitudinal receiving modes for debonded specimen D1. Using group velocities of dominant longitudinal wave modes in their respective zones and peak amplitude of time of arrival for sum combinational harmonics, debonding location is estimated using equation 3.11. The time of arrival of $f(a+b)$ for mode pair 1 is 3.01×10^{-4}s and for mode

pair 2 is 3.99×10^{-4}s. The debonding location estimated using both mode pair for debonded specimen D1 is within its debonding location.

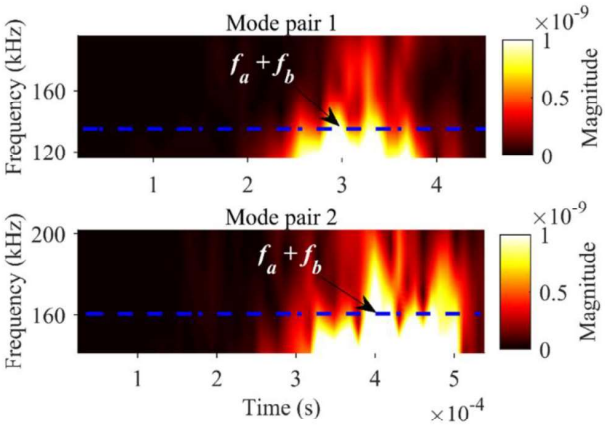

Figure 3.15 FE STFT for (a) mode pair 1 and (b) mode pair 2 at sum combinational harmonics using phase reversal approach

Table 3.4 Debonding location estimation using guided wave mixing for numerically debonded specimen

Debonded Case	**Mode pair**	**Frequencies**	**Time of arrival of $f_a + f_b$ (s)**	**Estimated Location l_a (mm)**	**Actual debonding location range (mm)**
N-D1-L1	1	50 kHz and 85 kHz	3.01×10^{-4}	220	150 – 350
N-D1-L2	2	60 kHz and 100 kHz	3.99×10^{-4}	200	150 – 350

To investigate the phenomenon of nonlinear guided waves in reinforced concrete beam which is numerically studied in section 3.3 and 3.4, experimental study is carried out in section 3.5. The experiments are carried to understand the ability of guided wave mixing in detecting and location debonding type damage in reinforced concrete beam.

3.4 Experiment

This section discusses the experimental study carried for guided wave mixing in reinforced concrete beams. Initially, the installation of PZT at rebar ends for exciting longitudinal and

measuring longitudinal and torsional wave modes are explained. The debonding created between steel rebar and concrete is studied using wave mixing of longitudinal wave mode pairs as discussed in section 3.2.

3.4.1 Installation of PZT discs and plates

The steel ribbed reo rebar selected for the study has 24mm diameter with longitudinal and transverse ribs. The longitudinal wave is excited using 2mm thick and 20mm diameter circular PZT disc attached to the rebar end as shown in Figure 3.16 (a). The similar PZT disc is used at the other end to receive the longitudinal guided wave signal. For receiving torsional wave modes, PZT plates are attached at the receiving rebar end as shown in Figure 3.16 (b) around the circumference of rebar. Due to deformed shape of rebar, the plates cannot be directly bonded onto the surface of rebar. In order to achieve smooth surface, the ribs were removed by chiselling 10mm length at rebar end. Each plate has dimension of 7mm x 2.7mm and 0.7mm thickness. The PZT plate accounts for the strain measurement in longitudinal and transverse direction as specified in Figure 3.16 (b). The transverse direction strain measurement will capture torsional guided wave modes in the rebar. The orientation of plate perpendicular to the axis of rebar will not be possible to bond plate on flat surface because of the curved circular rebar. Due to the only possible orientation as shown in Figure 3.16 (b), the plate will capture major strain component in longitudinal direction and other component in torsional direction. Unlike FE simulations, the torsional signal received using PZT plate in experiment will have longitudinal wave component as well.

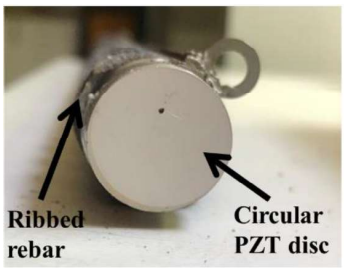

(a)

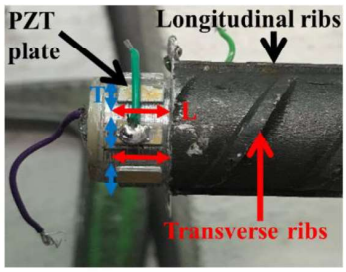

(b)

Figure 3.16 (a) Longitudinal PZT disc at ribbed rebar end (b) PZT plate for receiving torsional wave mode

3.4.2 Reinforced concrete beam specimens

The reinforced concrete beam specimen developed for this study is shown in Figure 3.5. The reinforced concrete beam has total length of 700mm with 100mm of bare rebar at each end. The beam has cross-section of 150mm × 150mm with 24mm diameter ribbed rebar at the center of cross-section. Only fully bonded and two debonded specimens are selected for experiments. The debonding is created from A-B using Mylar sheet wrapped around ribbed rebar to ensure that there will be no contact of concrete surface with rebar. After achieving 28 days compressive strength of concrete, it is tested for material properties. The PZT circular discs are attached to the excitation and receiving end of the rebar. While, the PZT plates are attached at the receiving end only. A set of 4 PZT plates are bonded equidistantly around the circumference of circular bar at the end.

3.4.3 Experimental setup and results

The experimental setup for detecting debonded damage using guided wave mixing is shown in Figure 3.17. The guided wave mixed signal for each mode pair as shown in Figure 3.6 is premixed and is generated through National Instrument (NI) system PXIe 1073 which is connected through computer system. The NI system has NI PXI-5412 as waveform generator. The generated signal is amplified using Ciprian amplifier HVA-800-A. The input signal is set to 0.6V which is amplified 400 times to acquire excitation signal at circular PZT to be 240V. While excited signal has longitudinal (L) wave modes only, the receiving guided wave signal is recorded in longitudinal (L) and torsional (T) direction using PZT disc and plate respectively at rebar end. The guided wave signal is measured and recorded using signal digitizer NI PXI-5105 and computer system. All bonded and debonded cases are tested by keeping voltage to

be constant at 240V. The experimental data is compared with FE for time domain and frequency analysis.

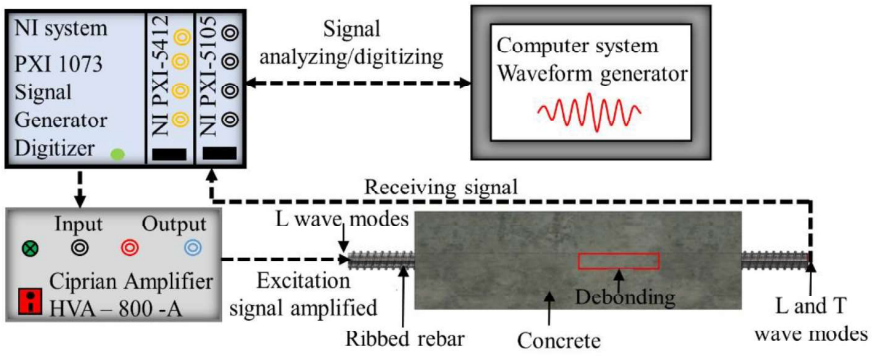

Figure 3.17 Experimental setup for guided wave mixing in rebar reinforced concrete

3.4.3.1 Time domain data for bonded and debonded specimen with FE comparison

The time domain data is acquired experimentally for longitudinal and torsional direction wave modes. For longitudinal wave mode, circular PZT disc shown in Figure 3.16 (a) acquires out of plane strain measurement as major displacements and therefore can be compared with out of plane longitudinal direction displacements acquired in FE. In order to receive torsional direction waves in experiment using PZT plate shown in Figure 3.16 (b), the strain measurements are observed both in torsional and longitudinal direction. For comparing the experimentally acquired torsional direction guided wave with FE data, longitudinal direction wave modes are added with torsional direction. Based on the dimensions of PZT plate, the torsional direction displacement are 40% in magnitude as compared to the longitudinal direction. Due to this, the proportion of longitudional and torsional guided wave modes are added together in FE to be compared with experimental data. For bonded specimen cases, time domain data is compared in longitudinal direction for mode pairs 1 and 2 are shown in Figure 3.18 (a) and 3.18 (b). Similarly, Figure 3.18 (c) and 3.18 (d) represents the time domain data for torsional direction wave modes incorporating longitudinal direction guided wave for mode pair 1 and 2 respectively in bonded specimen.

The experimental results for debonded specimen are also compared for time domain data. The guided wave signal for longitudinal direction wave are shown in Figure 3.19 (a) and 3.19 (b) for mode pairs 1 and 2 respectively. Similarly, the comparison of torsional direction guided wave are shown in Figure 3.19 (c) and 3.19 (d) for mode pairs 1 and 2 respectively.

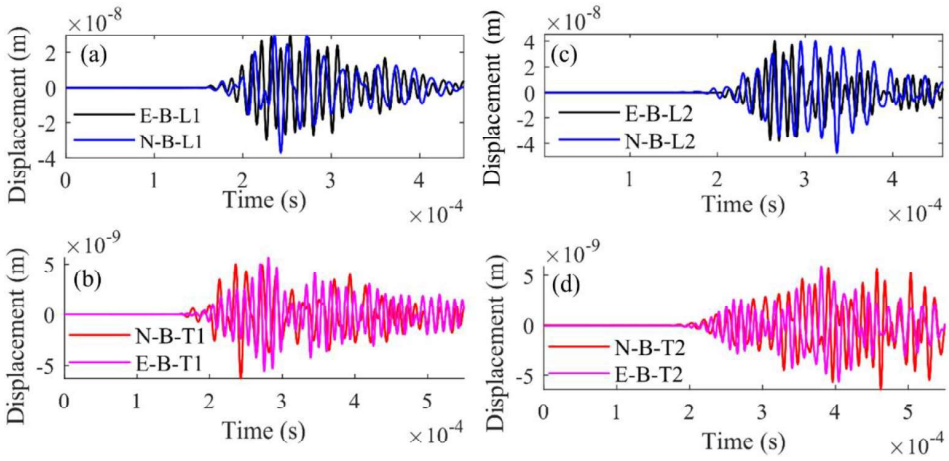

Figure 3.18 Experiment and FE Time domain signal for bonded case (a) longitudinal and (b) torsional receiving for mode pair 1 excitation, (c) longitudinal and (d) torsional receiving for mode pair 2 excitation

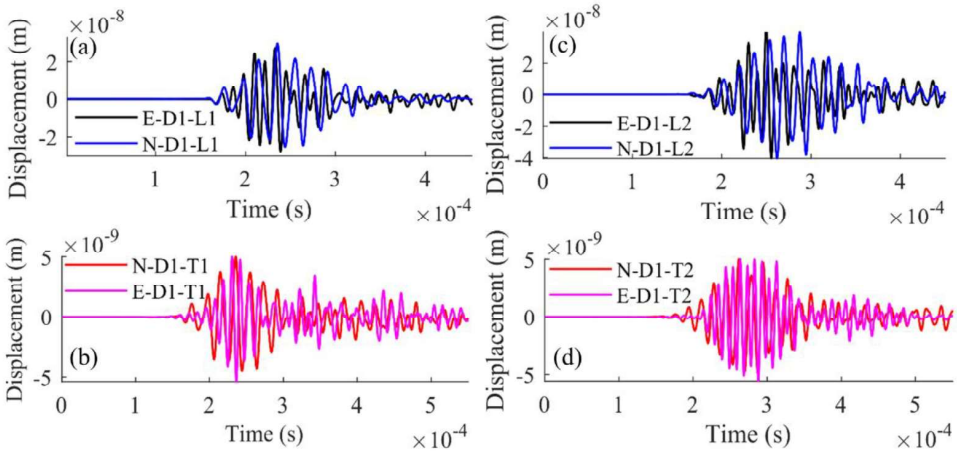

Figure 3.19 Experiment and FE Time domain signal for debonded case D1 (a) longitudinal and (b) torsional receiving for mode pair 1 excitation, (c) longitudinal and (d) torsional receiving for mode pair 2 excitation

The time domain signal represents good comparison with FE and experiment as seen in Figures 3.18 and 3.19. Due to larger group velocity of torsional wave modes as compared to longitudinal wave modes, the guided wave signal appears to arrive earlier in all cases where

torsional direction guided wave mode is also recorded. With torsional wave modes to be less dispersive in cylinder like structures, it can beneficial to detect debonding damage in reinforced concrete beam. For verifying and comparing the nonlinear feature of guided wave mixing, FFT is performed on time domain data acquired for bonded and debonded cases.

3.4.3.2 FFT for bonded and debonded specimen with FE comparison

FFT data is analysed experimentally and numerically for bonded and debonded case D1 for longitudinal and torsional receiving mode pairs. While considering bonded specimen, both longitudinal and torsional receiving wave for mode pairs 1 and 2 have shown the absence of combinational harmonics as shown in Figure 3.20 (a) and 3.20 (b) respectively. With debonded specimen D1, the sum combinational harmonics and higher harmonics are seen for both longitudinal and torsional direction receiving guided wave for mode pairs 1 and 2 as shown in Figure 3.21 (a) and 3.21 (b) respectively. The longitudinal receiving guided wave modes clearly show the presence of sum combinational harmonics. It is to be ascertain here that sum combinational harmonics in torsional direction guided wave signal is not only due to the addition of longitudinal guided wave signal which were added for comparison with experiment. Firstly, the numerical study has shown that signal received in torsional direction without addition of any longitudinal wave modes represents the presence of sum combinational harmonics as shown in Figure 3.10. Secondly, the phase matching condition shows the presence of torsional wave modes at sum combinational harmonics as shown theoretically in Figure 3.2. The amplitude of sum combinational harmonics for torsional receiving mode pairs appears to be larger than longitudinal receiving mode pairs. Therefore, guided wave mixed signal received in torsional direction is also essential in debonding damage detection in reinforced concrete beam.

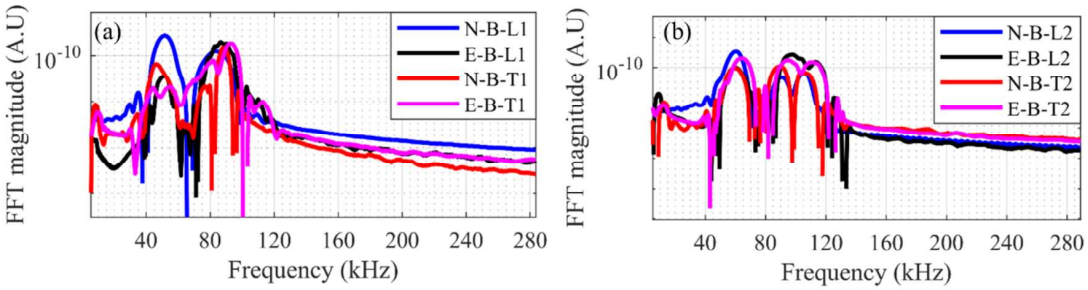

Figure 3.20 Experiment and FE FFT for bonded specimen with longitudinal and torsional receiving modes (a) mode pair 1 excitation (b) mode pair 2 excitation

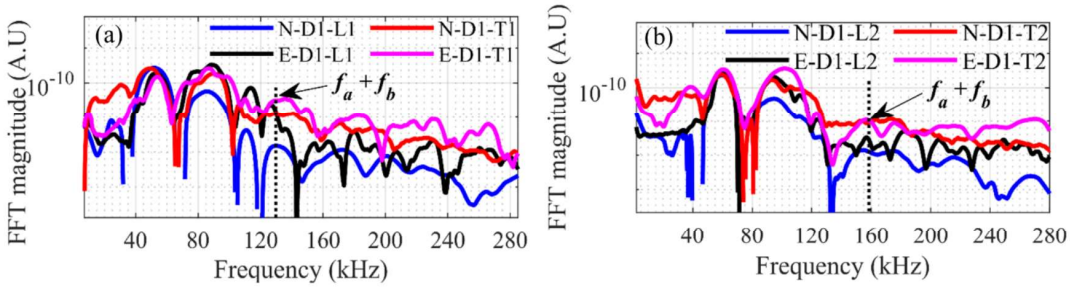

Figure 3.21 Experiment and FE FFT for debonded specimen D1 with longitudinal and torsional receiving modes (a) mode pair 1 excitation (b) mode pair 2 excitation

3.4.3.3 Phase reversal and location estimation with experimental data

As sum combinational harmonics are clearly observed using numerical simulations based on longitudinal guided wave modes, the experimental data is analysed using longitudinal receiving mode pairs for debonded specimen based on phase reversal approach. The advantage of phase reversal is that it reduces the presence of guided wave modes at excitation frequencies which are present in this structure type. For debonded specimen D1, the time domain data for longitudinal receiving wave mode for original and phase reversed signal is shown in Figure 3.22 (a) for mode pair 1 and Figure 3.22 (b) for mode pair 2 excitation. The sum of original and phase reversed signal for mode pair 1 and 2 are shown in Figure 3.22 (c) and 3.22 (d) respectively.

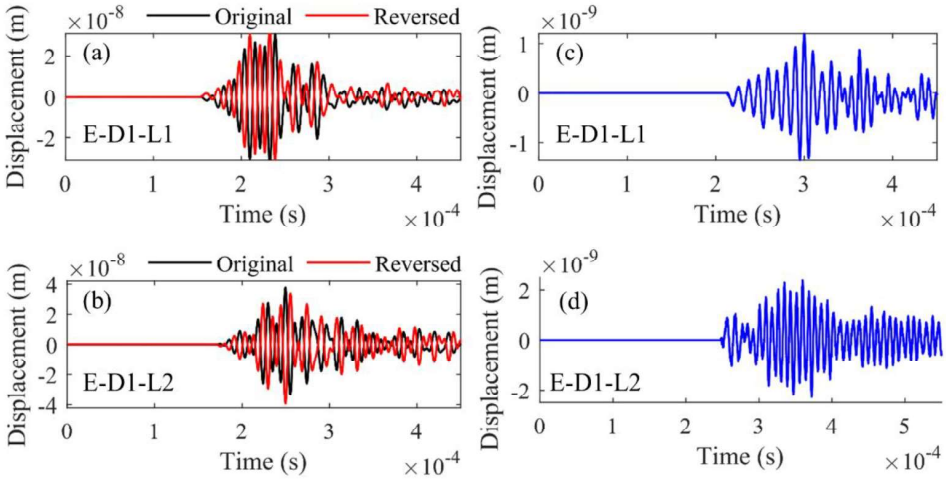

Figure 3.22 Experimentally D1 debonded specimen time domain data for original and phase reversed signal for (a) mode pair 1 and (b) mode pair 2, phase reversal sum signal for (c) mode pair 1 and (d) mode pair 2

For analysing the nonlinear feature experimentally, FFT is plotted for time domain data acquired using phase reversal approach. For debonded specimen D1 with longitudinal receiving mode pairs, both debonded cases E-D1-L1 and E-D1-L2 shows the presence of sum combinational harmonics for mode pair 1 and 2 as shown in Figure 3.23 (a) and 3.23 (b) respectively. The individual peaks at difference combinational harmonics are also observed for both mode pairs. With the presence of contact effect, second harmonics for both mixing frequencies are also generated in both mode pairs which are increased in phase reversal approach as seen in Figure 3.23. However, the presence of sum combinational harmonics indicates the presence of debonding damage without system nonlinearities.

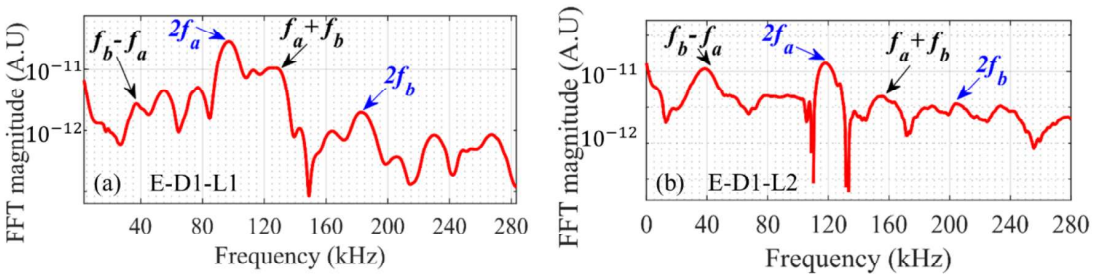

Figure 3.23 Experiment D1 debonded specimen FFT for (a) mode pair 1 and (b) mode pair 2 using phase reversal approach

The sum combinational harmonics at 135 kHz and 160 kHz for mode pairs 1 and 2 respectively can be analysed using STFT to indicate the location of debonding damage as observed numerically in section 3.3.5.2. STFT for experimental data using phase reversal approach are plotted for mode pair 1 and 2 in Figure 3.24 (a) and 3.24 (b) respectively.

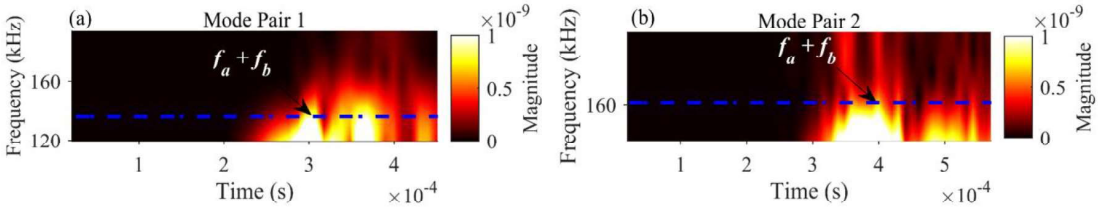

Figure 3.24 Experiment STFT for (a) mode pair 1 and (b) mode pair 2 at sum combinational harmonics using phase reversal approach

Using phase reversal approach, peak amplitude for time of arrival of sum combinational harmonics and group velocities of dominant mode pairs as highlighted in section 3.3.5.2, debonding location is estimated based on experimental data. Experimentally, the time of arrival of $f_a + f_b$ for mode pair 1 3.04×10^{-4}s and for mode pair 2 is 3.97×10^{-4}s. Using equation 3.11, the location of debonding l_a estimated experimentally for mode pair 1 is 207mm and for mode pair 2 is 205mm., which are in the debonding zone of specimen D1.

3.4.3.4 Nonlinear parameter using experimental data

Based on experimental data, the nonlinear parameter for guided wave mixing bonded and debonded cases is plotted against their respective numerically studied cases in Figure 3.25. All numerically bonded cases are represented by doted green bar and experimentally bonded cases are compared with purple filled bar. The nonlinear parameter is minimum in all bonded cases. For D2 debonded specimen, all numerical cases are represented in doted black bar against

experimental cases in yellow filled bar. Similarly, for D1 debonded specimen, doted blue line bar represents numerical cases and filled red bar represents all experimental cases.

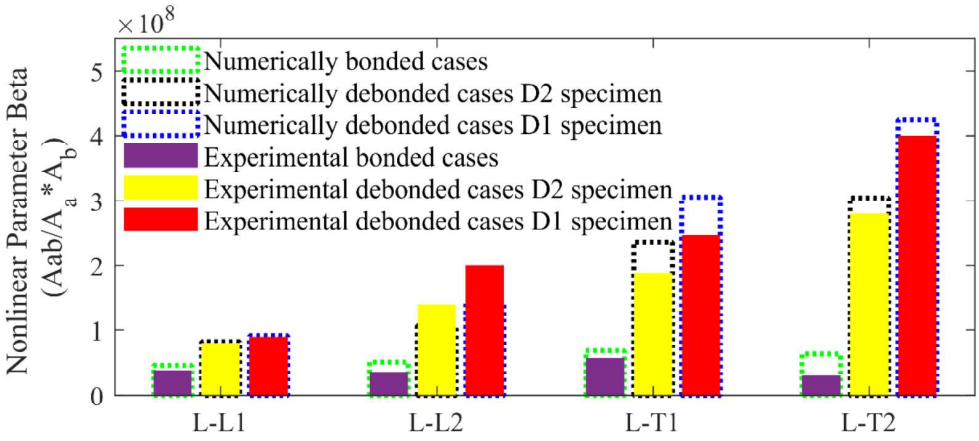

Figure 3.25 Nonlinear parameter for numerically and experimentally bonded and debonded cases

It is also noted experimentally that nonlinear parameter is increased with increase in debonding length. The red filled bar has slightly increased nonlinear parameter as compared to yellow filled bar, where D1 has 200mm of debonding length and D1 has 150mm of debonding length. The nonlinear parameter for torsional receiving guided wave modes is larger than longitudinal receiving guided wave modes both numerically and experimentally. Further, both mode pairs have indicated the presence of damage and increase in nonlinear parameter while receiving torsional guided wave modes. Therefore, the use of torsional guided wave modes at receiving rebar end is beneficial for damage detection.

3.5 Conclusion

In this study, nonlinear guided wave mixing has been studied numerically and experimentally to detect debonding damage in rebar reinforced concrete beam to avoid system nonlinearities. Longitudinal guided wave modes have been mixed at particular frequencies to observe combinational harmonics at sum frequencies. The excitation signal has premixed with

longitudinal wave modes, while receiving signal has been acquired in longitudinal and torsional direction wave modes at rebar end. The selection of mixing frequencies has been established based on phase matching and synchronism condition. After selection of two mode pairs, with mode pair 1 as 50 kHz and 85 kHz, while mode pair 2 as 60 kHz and 100 kHz, 4 bonded and 12 debonded cases have been defined numerically and experimentally taking into consideration of longitudinal and torsional receiving wave modes.

In numerical simulations, the debonding has been created using contact type effect, while in experiments mylar sheet has been wrapped around rebar in debonding region. For all debonded cases, numerical and experimental cases have shown the presence of sum combinational harmonics for both mode pairs. This study has also shown the absence of combinational harmonics in all bonded cases. The numerical and experimental data have been further analysed to clearly observe sum combinational harmonics using phase reversal approach for longitudinal receiving mode pairs. Phase reversal approach has been used to extract the combinational harmonics for all debonded cases. To locate debonding damage, phase reversal approach has been explored using wave number frequency analysis and short time Fourier transform to identify the dominant propagating guided wave modes. The debonding, which is located within the debonding zone of reinforced concrete beam, has estimated numerically and experimentally.

This study has shown that guided wave mixing of longitudinal wave modes could detect and locate debonding type damage in rebar reinforced concrete. Nonlinear parameter has been defined based on amplitude of sum combinational harmonics and mixing frequencies to quantify damage in debonded cases. The results in this study have shown that the nonlinear parameter is increased with debonding length. Further, the nonlinear parameter for torsional receiving wave modes has been found to be greater as compared to their respective longitudinal

receiving wave modes. It should be noted that torsional wave modes are important in identify debonding type damage in reinforced concrete beam.

Acknowledgement

This work was supported by Australian Research Training Program and Australian Research Council through DP200102300. The support is greatly appreciated.

3.6 References

1. Chen, J., et al., *Characterization of thermal damage in sandstone using the second harmonic generation of standing waves.* International Journal of Rock Mechanics and Mining Sciences, 2017. **91**: p. 81-89.
2. Soleimanpour, R. and C.T. Ng, *Locating delaminations in laminated composite beams using nonlinear guided waves.* Engineering Structures, 2017. **131**: p. 207-219.
3. Bermes, C., et al., *Nonlinear Lamb waves for the detection of material nonlinearity.* Mechanical Systems and Signal Processing, 2008. **22**(3): p. 638-646.
4. Jiao, J.P., et al., *Micro-crack detection using a collinear wave mixing technique.* Ndt & E International, 2014. **62**: p. 122-129.
5. Liu, P., et al., *Noncontact detection of fatigue cracks by laser nonlinear wave modulation spectroscopy (LNWMS).* Ndt & E International, 2014. **66**: p. 106-116.
6. Kim, G., et al., *Drying shrinkage in concrete assessed by nonlinear ultrasound.* Cement and Concrete Research, 2017. **92**: p. 16-20.
7. Chen, J., J. Ren, and T.Y. Yin, *Nondestructive evaluation of notched cracks in mortars by nonlinear ultrasonic technique.* Nondestructive Testing and Evaluation, 2016. **31**(2): p. 109-121.
8. Liu, M.H., et al., *Measuring acoustic nonlinearity parameter using collinear wave mixing.* Journal of Applied Physics, 2012. **112**(2).
9. Jones, G.L. and D.R. Korbett, *Interaction of Elastic Waves in an Isotropic Solid.* Journal of the Acoustical Society of America, 1963. **35**(1): p. 5-&.
10. Chen, Z.M., et al., *Mixing of collinear plane wave pulses in elastic solids with quadratic nonlinearity.* Journal of the Acoustical Society of America, 2014. **136**(5): p. 2389-2404.
11. Croxford, A.J., et al., *The use of non-collinear mixing for nonlinear ultrasonic detection of plasticity and fatigue.* Journal of the Acoustical Society of America, 2009. **126**(5): p. El117-El122.
12. Allen, J.C.P. and C.T. Ng, *Nonlinear Guided-Wave Mixing for Condition Monitoring of Bolted Joints.* Sensors, 2021. **21**(15).
13. Hasanian, M. and C.J. Lissenden, *Second order harmonic guided wave mutual interactions in plate: Vector analysis, numerical simulation, and experimental results.* Journal of Applied Physics, 2017. **122**(8).
14. Yeung, C. and C.T. Ng, *Nonlinear guided wave mixing in pipes for detection of material nonlinearity.* Journal of Sound and Vibration, 2020. **485**.
15. Li, W., et al., *Modeling and simulation of backward combined harmonic generation induced by one-way mixing of longitudinal ultrasonic guided waves in a circular pipe.* Ultrasonics, 2021. **113**: p. 106356-106356.
16. Zhao, Y.X., et al., *Experiment and FEM study of one-way mixing of elastic waves with quadratic nonlinearity.* Ndt & E International, 2015. **72**: p. 33-40.

17. Mustapha, S., et al., *Damage detection in rebar-reinforced concrete beams based on time reversal of guided waves.* Structural Health Monitoring-an International Journal, 2014. **13**(4): p. 347-358.
18. Beata, Z. and K. Rafał, *Debonding Size Estimation in Reinforced Concrete Beams Using Guided Wave-Based Method.* Sensors, 2020. **20**(2): p. 389.
19. Zhao, G.Q., et al., *Detection of Defects in Reinforced Concrete Structures Using Ultrasonic Nondestructive Evaluation with Piezoceramic Transducers and the Time Reversal Method.* Sensors, 2018. **18**(12).
20. Ervin, B.L., et al., *Estimation of general corrosion damage to steel reinforced mortar using frequency sweeps of guided mechanical waves.* Insight, 2006. **48**(11): p. 682-692.
21. Lu, Y., et al., *Guided waves for damage detection in rebar-reinforced concrete beams.* Construction and Building Materials, 2013. **47**: p. 370-378.
22. Sriramadasu, R.C., Y. Lu, and S. Banerjee, *Identification of incipient pitting corrosion in reinforced concrete structures using guided waves and piezoelectric wafer transducers.* Structural Health Monitoring-an International Journal, 2019. **18**(1): p. 164-171.
23. Zima, B. and R. Kędra, *Reference-free determination of debonding length in reinforced concrete beams using guided wave propagation.* Construction and Building Materials, 2019. **207**: p. 12.
24. Aseem, A. and C.T. Ng, *Debonding detection in rebar-reinforced concrete structures using second harmonic generation of longitudinal guided wave.* Ndt & E International, 2021. **122**.
25. Liu, M., et al., *Measuring acoustic nonlinearity parameter using collinear wave mixing.* Journal of Applied Physics, 2012. **112**: p. 024908.
26. Childress, J.D. and C.G. Hambrick, *Interactions Between Elastic Waves in an Isotropic Solid.* Physical Review, 1964. **136**(2A): p. A411-A418.
27. Johnson, P.A. and T.J. Shankland, *Nonlinear generation of elastic waves in granite and sandstone: Continuous wave and travel time observations.* Journal of Geophysical Research: Solid Earth, 1989. **94**(B12): p. 17729-17733.
28. Croxford, A.J., et al., *The use of non-collinear mixing for nonlinear ultrasonic detection of plasticity and fatigue.* The Journal of the Acoustical Society of America, 2009. **126**(5): p. EL117-EL122.
29. Cho, H., et al., *Nonlinear guided wave technique for localized damage detection in plates with surface-bonded sensors to receive Lamb waves generated by shear-horizontal wave mixing.* NDT & E International, 2019. **102**: p. 35-46.
30. Li, W.B., et al., *Theoretical analysis and experimental observation of frequency mixing response of ultrasonic Lamb waves.* Journal of Applied Physics, 2018. **124**(4).
31. Li, W.B., et al., *Numerical and experimental investigations on second-order combined harmonic generation of Lamb wave mixing.* Aip Advances, 2020. **10**(4).
32. Pavlakovic, B., et al., *Disperse: A general purpose program for creating dispersion curves.* Review of Progress in Quantitative Nondestructive Evaluation, Vols 16a and 16b, 1997. **16**: p. 185-192.
33. Wan, X., et al., *Numerical Simulation of Nonlinear Lamb Waves Used in a Thin Plate for Detecting Buried Micro-Cracks.* Sensors, 2014. **14**(5): p. 8528-8546.
34. Ankay, B. and C.Z. Zhang, *Acoustoelastic Evaluation of Ultra-High Performance Concretes.* 45th Annual Review of Progress in Quantitative Nondestructive Evaluation, Vol 38, 2019. **2102**.
35. Liu, Y., et al., *Higher order interaction of elastic waves in weakly nonlinear hollow circular cylinders. II. Physical interpretation and numerical results.* Journal of Applied Physics, 2014. **115**(21).
36. Ramadas, C., et al., *Modelling of attenuation of Lamb waves using Rayleigh damping: Numerical and experimental studies.* Composite structures, 2011. **93**(8): p. 2020-2025.
37. Li, W.B., et al., *Assessment of low-velocity impact damage in composites by the measure of second-harmonic guided waves with the phase-reversal approach.* Science Progress, 2020. **103**(1).
38. Jiao, J.P., et al., *Nonlinear Lamb wave-mixing technique for micro-crack detection in plates.* Ndt & E International, 2017. **85**: p. 63-71.

4. Chapter 4 (Paper 3). Detection and evaluation of heat damage in reinforced concrete beams using linear and nonlinear guided waves

Abstract

This study utilizes the linear and nonlinear features of guided waves (GWs) for detecting and evaluating heat damage in reinforced concrete (RC) beams. The RC beams with embedded sensors attached at rebar ends are experimentally studied using longitudinal GW at 200 kHz after heating the specimens in a furnace from 100°C to 300°C. For the studies investigating the effect of heat damage on the RC beams beyond 300°C, the rebar ends are exposed outside the concrete so that the longitudinal transducers can be attached there. These specimens are then experimentally studied using GW with an excitation frequency of 100 kHz. In this study, the RC beams are prepared as fully bonded and debonded specimens. The experimental study shows that heat damage in the RC beams causes debonding between rebar and concrete enabling GW signal to generate second harmonics. The experimental study also discussed the linear features of GW, which shows that the amplitude of the GW signal increases with elevated temperatures in the RC beams. To distinguish material nonlinearity and contact nonlinearity, two types of nonlinear parameters are defined in this study. The nonlinear parameter due to the contact acoustic nonlinearity (CAN) effect in the RC beams is defined as β, while the nonlinear parameter due to material nonlinearity is defined as β_m. The study shows that β_m is negligible in comparison to β at relevant heated temperatures. With the increase in temperature, the nonlinear parameter β is significantly increased at elevated temperatures. The peak amplitude of the nonlinear parameter β is observed at the maximum heated temperature 800°C for both bonded and debonded specimens.

Keywords: Heat damage detection, reinforced concrete beam, guided wave, embedded sensors, debonding

Statement of Authorship

Title of Paper	Linear and nonlinear longitudinal guided waves for heat damage study with embedded sensors and exposed transducers in reinforced concrete beams
Publication status	☐ Published ☐ Accepted for Publication ☒ Submitted for Publication ☐ Unpublished and unsubmitted work written in manuscript style
Publication Details	Aseem, A. and C.T. Ng, *Detection and evaluation of heat damage in reinforced concrete beams using linear and nonlinear guided waves.* Structural Health Monitoring-an International Journal, 2023.

Principal Author

Name of Principal Author (Candidate)	Ahmed Aseem		
Contribution to the Paper	Conceptualization, Theoretical study, Conducting experimental measurements, Signal processing and data analysis, Writing the original draft and editing.		
Overall percentage (%)	80%		
Certification:	This paper reports on original research I conducted during the period of my Higher Degree by Research candidature and is not subject to any obligations or contractual agreements with a third party that would constrain its inclusion in this thesis. I am the primary author of this paper.		
Signature		Date	16-07-2023

Co-Author Contributions

By signing the Statement of Authorship, each author certifies that:

i. the candidate's stated contribution to the publication is accurate (as detailed above);

ii. permission is granted for the candidate in include the publication in the thesis; and

iii. the sum of all co-author contributions is equal to 100% less the candidate's stated contribution.

Name of Co-Author	Ching-Tai Ng		
Contribution to the Paper	Supervision, writing – review and editing.		
Signature		Date	18-07-2023

Please cut and paste additional co-author panels here as required.

4.1 Introduction

Reinforced concrete (RC) structures are subjected to various damages, such as debonding, delamination, corrosion, cracks, and defects etc. which can lead to deterioration and affect the serviceability of the structure. In the worst case, it can lead to catastrophic failure. Many studies used non-destructive techniques to identify damages in RC structures. Linear and nonlinear guided waves (GWs) have been proven to be useful in detecting damage in RC structures. They can identify debonding and delamination in RC [1-6]. GWs can also detect corrosion damages at steel rebars in RC beams [7, 8]. Lu et al. and Mustapha et al. studied damage in RC using GWs [9, 10]. Aseem and Ng detected the debonding between steel rebar and concrete using nonlinear features of GWs [11]. The presence of surface cracks and notched cracks were also detected using GWs [12, 13].

The studies focused on GWs in the literature are limited to damage detection at room temperature, at which the mechanical properties of steel and concrete do not deteriorate. These damages are studied by creating debonding, corrosion, cracks and other defects. However, the temperature change can also affect the structural integrity of RC structures. Chang et al. demonstrated the reduction in residual compressive strength, ultimate stress and elastic modulus of concrete after heating the samples from 100^{o}C to 600^{o}C, where they tested the mechanical properties of concrete after each heating interval [14]. Later, this phenomenon was well explained in [15]. At elevated temperatures, the water vapours are generated inside the concrete, and they tend to migrate to lower-pressure regions, i.e. outside the concrete. Due to this activity, the generated pore pressure can develop cracks in concrete and result in spalling of concrete at high temperatures. It was shown that the relative compressive strength of ordinary concrete reduced by 20-30% after it is heated from 100^{o}C to 300^{o}C, and around 70% reduction when the temperature increases to 600^{o}C. The splitting tensile strength is also

reduced by 70% after heating the concrete to 600^{o}C. Ozbolt et al. (2014) also numerically showed the reduction in relative Young's modulus, compressive strength and tensile strength of concrete from 100^{o}C to 800^{o}C [16]. A sharp reduction of 80% in the mechanical properties of concrete is observed at 800^{o}C. Ghazaly et al. [17] and Shamseldein et al. [18] also studied the reduction in bond strength of RC with heated temperature. With the reduction in mechanical properties, the serviceability of concrete structures is also affected. The flexural capacity of concrete beams is reduced by around 40% when they are heated up to 800^{o}C [19, 20]. It showed the reduction in the compressive, tensile and bending capacity of steel fibre-RC. The reduction in splitting tensile strength of concrete at elevated temperature reflects the reduction in the bond strength of the concrete. The reduction in bonding between rebar and concrete at increased temperature affects the integrity of the RC structure. The generation of debonding between rebar and concrete at heated temperatures can affect the serviceability and feasibility of the RC structure. If the RC structure is required to be made serviceable after fire or heat damage, it is necessary to investigate the debonding damage and condition of the concrete.

There were very limited studies in the literature focused on investigating the damage of RC beams subjected to heated damage using non-destructive testing. Monte et al. used ground penetrating radar to study the development of water pore pressure in concrete subjected to heated temperature, which can result in the spalling of concrete [21]. Ground penetrating radar has proven to be useful in detecting cracks or delamination in RC structures as studied by Miramini et al. [22]. Lee et al. used the impact echo method to study heat-damaged slabs [23]. The change in ultrasonic pulse velocity across the various depth of the slab can also predict the damage state. The velocity tends to be faster at distance further from the exposed heated surface of the slab, while the ultrasonic pulse velocity is lowest at the heated face. Similarly, acoustic emission (AE) energy has been used by Xargay et al. to determine the damage state of high-strength concrete (HSC) and HSC with fibre-reinforced [24]. The study shows the increase in

AE energy with the elevated temperature for HSC samples. Cobola et al. have demonstrated the use of nonlinear ultrasonic spectroscopy to study concrete nonlinearity subjected to heat damage [25]. For heated samples, the non-harmonics are increased because of concrete material nonlinearity at elevated temperatures. Aseem et al. investigated the fire-damaged RC building using an ultrasonic pulse velocity test and a conventional rebound hammer test [26]. With the reduction in concrete core compressive strength of fire damaged structural members, the ultrasonic pulse velocity is also reduced.

Therefore, the above studies reflect the material degradation of fire-damaged concrete using various non-destructive techniques. It is noted that mechanical properties, such as flexural, compressive, and tensile strength of heat-damaged concrete are also reduced. However, these studies have not investigated the degradation in bonding between steel rebar and concrete of fire-damaged RC beams. The presence of debonding can significantly reduce the flexural and shear strength of the RC structure. The serviceability of the RC structure is reduced due to the generation of debonding damage. Due to debonding between steel rebar and concrete, contact surfaces are generated at the interfaces of steel and concrete. These contact surfaces can generate higher harmonics as discussed by Solodov et al. [27].

This paper first investigates the effect of heat damaged specimens on bonding between steel rebar and concrete using linear and nonlinear longitudinal GWs, and then uses them to detect and evaluate the heat damage. In Section 4.2, the methodology is discussed for detecting heat damage using linear and nonlinear features. The ability of nonlinear features to detect debonding or contact-type damage is explained. In Section 4.3, an experimental study is discussed, and experimental case studies are defined for bonded and debonded RC specimens at heated temperatures. Section 4.4 discusses the results obtained from experimental case studies. The heated temperature shows the generation of second harmonics in receiving the

GW signal. The nonlinear parameter defined in Section 4.2 is then calculated for results obtained in the experimental case studies. In Section 4.5, a conclusion is derived for this experimental study.

4.2 Methodology

Linear and nonlinear GWs are used to detect damage due to elevated temperature in the RC beam. The linear features of GWs, such as time of arrival and amplitude of the longitudinal GW can give us an indication of the presence of damage. The nonlinear features, such as the generation of second or higher harmonics, are sensitive to heat damage.

For damage detection using longitudinal GWs in RC beams, piezoceramic transducers (PZTs) are attached at the cross-section of embedded rebar ends as shown in Figure 4.1. The longitudinal GWs are exited at one rebar and received at the other rebar end. At room temperature, the rebar in the intact sample is fully bonded with concrete. In the unheated RC beam, there is no indication of damage via GWs. When the beam is heated in the oven, the pore water pressure develops resulting in the generation of micro cracks. Due to the development of micro-cracks and the degradation of concrete material at elevated temperatures, the bonding between steel and concrete is depreciated. It can cause debonding between steel rebar and concrete surfaces. The debonding behaves as contact surfaces for propagating longitudinal GWs in embedded rebar. The generation of second harmonics due to contact nonlinearity is explained in the literature [27].

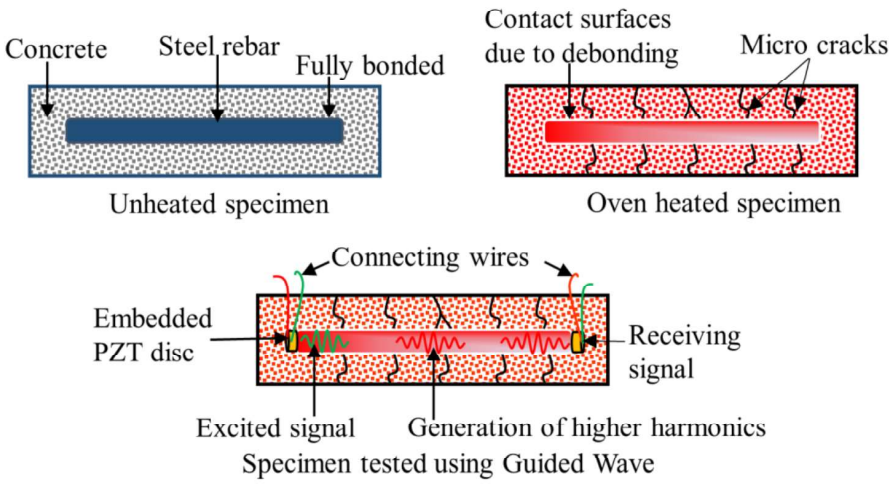

Figure 4.1 Heat damage detection using longitudinal GWs in RC beam

4.2.1 Reinforced concrete beam with embedded rebar ends

In RC structures, steel rebars are embedded inside the concrete. If the structure is subjected to fire damage, the embedded rebars cannot be accessed for installing PZTs. To overcome this problem, PZTs are attached at rebar ends before casting the RC, and hence, they are embedded in the specimens as shown in Figure 4.2. The RC beam with embedded rebar ends is referred to as specimen type 1 in this study. Fully bonded and debonded samples are monitored using linear and nonlinear GWs at elevated temperatures as shown in Figures 4.2(a) and 4.2(b). An artificial debonding is created between steel rebar and concrete as shown in Figure 4.2(b). The epoxy used to glue the PZTs to the rebar in this study has high temperature resistance, which will be discussed in Section 4.3. The mechanical properties of piezoceramic material and epoxy change when the temperature is beyond 300°C, and hence, specimen type 1 is heated up to 300°C in this study. PZTs have high sensitivity and are beneficial for studying the sensitivity of the nonlinear features of GWs. However, piezoelectric materials undergo thermal instability and degradation in piezoelectric and electromechanical properties beyond their curie

temperature T_C. Beyond this temperature, the material is also depolarized along with thermal expansion at elevated temperatures [28].

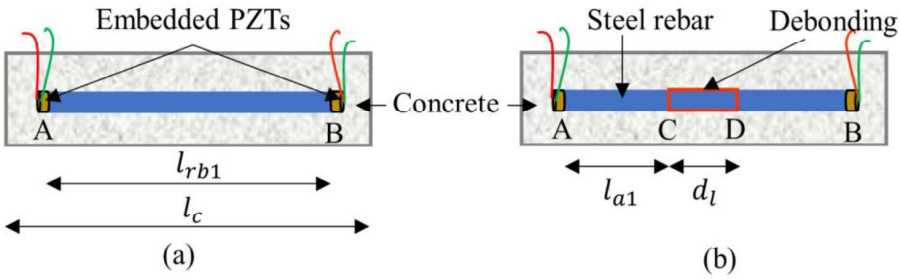

Figure 4.2 (a) Fully bonded and (b) debonded specimen with embedded rebar ends for heat damage study

Considering this limitation of embedded PZTs at elevated temperatures, they are used to monitor the heat damage from room temperature to 300°C in this study. It should be noted that RC members in fire damaged structures can be exposed to higher temperatures, e.g. 1,000°C, as found in the literature. At higher elevated temperatures, the mechanical properties of RC members are deteriorated and can have a significant impact on the bonding of rebar and concrete. To study this damage effect by considering experimental constraints at elevated temperatures, the embedded rebar is exposed outside the concrete as discussed in the section below.

4.2.2 Reinforced concrete beam with exposed rebar ends

To monitor the heat damage beyond 300°C using the linear and nonlinear GWs, embedded rebars are exposed outside the concrete beam and are connected to longitudinal transducers. The transducers are attached to rebar ends after each heating interval to excite and receive GW signals as shown in Figure 4.3. Both bonded and debonded specimens are prepared for the RC beam with exposed rebar ends. The RC beam with exposed rebar ends is labelled as specimen type 2 in this study.

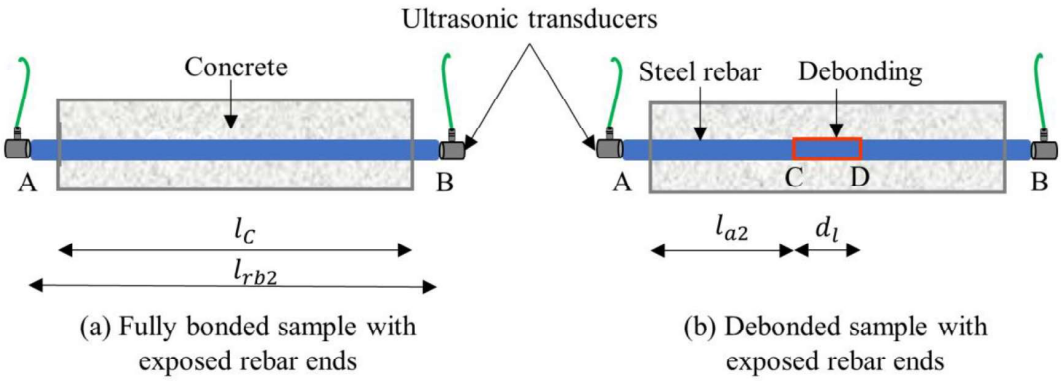

Figure 4.3 (a) Fully bonded and (b) debonded specimen with exposed rebar ends for heat damage study

4.2.3 Linear and nonlinear features for heat damage detection

For the RC beam with rebar ends embedded inside the concrete as shown in Figure 4.2, the longitudinal GWs signal is excited at location A with PZT and received at location B with PZT. The time of arrival of the GW signal at location B for specimen type 1 can be written as

$$t_{a1} = \frac{l_{rb1}}{V_{gc}} \tag{4.1}$$

where

t_{a1} = time of arrival of longitudinal wave mode in specimen type 1

l_{rb1} = length of embedded rebar in specimen type 1

V_{gc} = group velocity of longitudinal wave mode for rebar embedded in concrete

In exposed rebar specimen type 2 as shown in Figure 4.3, the longitudinal GWs are excited at exposed rebar end A with transducer and received at exposed rebar end B. For this specimen type 2, the time of arrival of the longitudinal GW can be written as

$$t_{a2} = \frac{2l_e}{V_{ge}} + \frac{l_c}{V_{gc}} \tag{4.2}$$

where

t_{a2} = time of arrival of longitudinal wave mode in specimen type 2

l_e = length of exposed rebar in specimen type 2

l_{rb1} = length of embedded rebar in specimen type 2

V_{gc} = group velocity of longitudinal wave mode for rebar embedded in concrete

V_{ge} = group velocity of longitudinal wave mode for exposed bare rebar

Apart from the linear features, the nonlinear feature, second harmonic, is used in this study to detect heat and debonding damage. Due to the contact-type damage from heated samples, the second harmonics are received at the rebar end as shown in Figure 4.1. Nonlinear parameter β is defined to quantify the damage relatively at elevated temperature, which is defined as $\beta = A_2/A_1$. The amplitude of the second harmonics generated due to heated temperatures is sourced from contact nonlinearity and material nonlinearity. At elevated temperatures, the material properties, microstructure and behaviour of steel rebar change in comparison to the unheated rebar. Nonlinear GWs have also been studied by many researchers to detect these changes in structures. For GW propagating in steel rebar with heat damage, material nonlinearity needs to be considered while quantifying the damage. The amplitude of second harmonics due to material nonlinearity in steel rebar can contribute towards the total amplitude of the second harmonics generated for heated damage in the RC beam. Considering classical nonlinear elastic theory, the nonlinear stress-strain relation for a longitudinal propagating GW can be written as [29]

$$\sigma_{xx} = E_0 \varepsilon_{XX}(1 + \beta_m \varepsilon_{XX}) \tag{4.3}$$

where σ_{xx} is the stress, E_0 is the linear young's modulus, ε_{XX} is the strain, β_m is the second order material nonlinearity acoustic parameter. Using the equation of motion as $\rho \frac{\partial^2 u}{\partial t^2} = \frac{\partial \sigma}{\partial x}$ and perturbation method, the second order material nonlinearity parameter β_m is defined as

$$\beta_m = \frac{8A_2}{A_1^2 x k^2} \tag{4.4}$$

where x represents the propagation distance for the wave and k is the wave number written as $k = \omega/C_l$, in which ω is the fundamental frequency and C_l is the longitudinal velocity. Considering constant values of $\frac{8}{xk^2}$ at elevated temperatures, β_m can be written as A_2/A_1^2. To study the material nonlinearity of bare rebar, β_m is calculated for each heated interval for bare steel rebar, which is compared to the nonlinear parameter due to heat damage generating debonding or contact in the RC beam.

4.2.4 Guided wave dispersion curves

The study focuses on longitudinal GWs for heat damage detection in the rebar and RC beam. Longitudinal GWs are dispersive. There is a larger number of GW modes in embedded rebar than in bare rebar. Dispersion curves are plotted using DISPERSE software to understand the presence of longitudinal GW modes in bare and embedded rebar as shown in Figure 4.4 (a) and 4.4(b) respectively. A circular steel rebar of 24 mm diameter with material properties as shown in Table 1 is modelled in DISPERSE to trace the dispersion curve [30]. For rebar embedded in concrete, the cross-section of the beam is selected as 75 mm × 75 mm with 24 mm diameter circular rebar at the center. The outer concrete in the embedded rebar is defined as a radial feature to trace longitudinal GW modes.

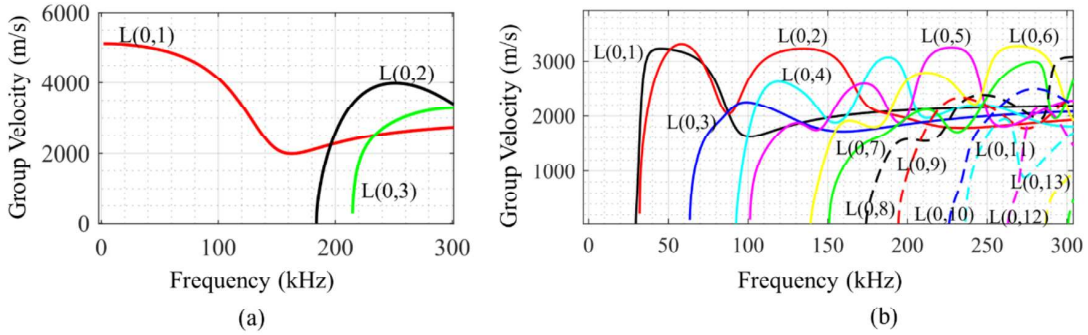

Figure 4.4 Longitudinal group velocity dispersion curve for (a) bare rebar and (b) RC beam specimen

Based on the dispersion curve, there are fewer longitudinal GW modes at lower frequencies, i.e. below 100 kHz. To avoid multiple longitudinal GW modes at a higher frequency, a low frequency is used in this study for the excitation of the GW signal. Considering the size of the specimen selected for this study, the excitation frequency cannot be below 50 kHz for longitudinal wave modes to propagate through the embedded and bare rebar. The experimental setup and case studies are discussed in Section 4.3.

4.3 Experimental study

The experimental study is carried out in this section to investigate the debonding in the RC beam due to heat damage. The bare rebar, specimen type 1 and 2 are subjected to heated damage at elevated temperatures. The bare rebar and specimens are tested using a GW signal at an undamaged state and after every heated elevated temperature.

4.3.1 Installation of PZTs for embedded rebar specimen

For the embedded rebar specimen, the PZTs are attached using high temperature resistant epoxy. Before carrying out the study for embedded rebar specimens, the propagation of longitudinal GW in bare rebar is studied to excite and receive GW signal using high temperature resistant epoxy. A plain steel rebar of 24 mm diameter having 300 mm length is

used for the bare rebar and specimen type 1 study . PZTs are attached at the rebar ends as shown in Figure 4.5. As PZTs used in this study have an operating temperature around 300°C with a curie temperate of 350°C, the bonding epoxy and electric wires must be suitable to work after being heated up to this temperature. The silver conductive epoxy resin generally used for bonding PZTs has an operating temperature up to 90°C along with electric copper wires. To achieve an operating temperature of 300°C, Duralco 4703 high temperature epoxy resin is used to bond PZTs with rebar. This epoxy resin provides high bond strength with ceramics and high temperature stability. As this resin has electrical resistivity and non-conductive properties, it cannot be used for bonding electric wires to PZT or rebar. For achieving electric current flow, silver conductive epoxy is used to attach the high temperature wires to PZT or rebar, which is then protected by high temperature epoxy resin as shown in Figure 4.5. The high temperature wires used in this study are ceramic fiber thermocouple cables, which can be heated up to 1200°C.

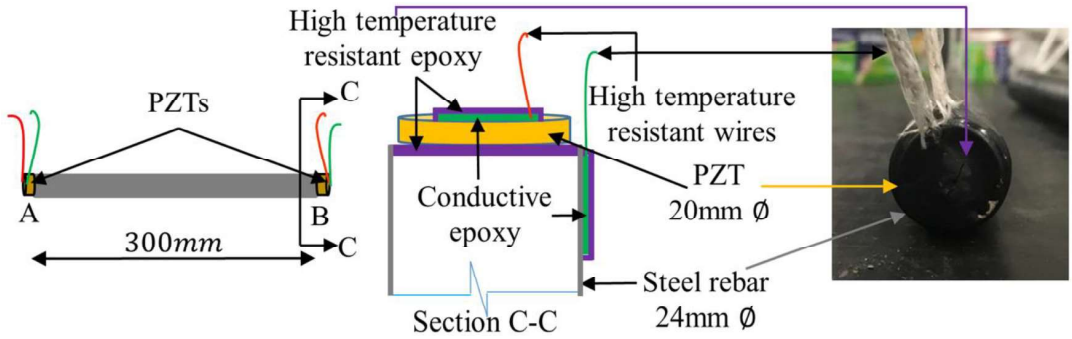

Figure 4.5 Installation of PZTs and high temperature resistant wires using epoxy at rebar ends for heat damage study

Duralco 4703 is prepared by mixing resin and hardener, which is then cured as per manufacturer specification and applied to the desired areas on PZTs and rebar as shown in Figure 4.5. After installation of PZTs to rebar ends, the bare rebar is tested for GW signal.

4.3.2 Experimental setup

A GW study is carried out using National Instrument (NI) system PXIe 1073. The GW signal is generated using signal generator NI PXI 5412. The signal is amplified using CIPRIAN Amplifier, which is then excited using PZT for bare rebar and specimen type 1. After propagation of GW signal through bare or embedded rebar, it is received through NI PXI 5105. After initial testing of bare rebar and concrete beam specimens, they are heated at regular intervals in an electric furnace. Within each heated interval, the bare rebar and the specimen are tested for GW signal as shown in Figure 4.6. The bare rebar and specimens are uniformly heated at the rate of 10°C/min to reach every heated interval before GW testing. The heated intervals range from 100°C to 300^0 C for specimen type 1 and 100°C to 800°C for bare rebar and specimen type 2. When the temperature at the heated interval is obtained, it is maintained for 2 hours before cooling it down to 100°C at 10°C/min. The chamber door is then opened to cool the specimen at ambient temperature.

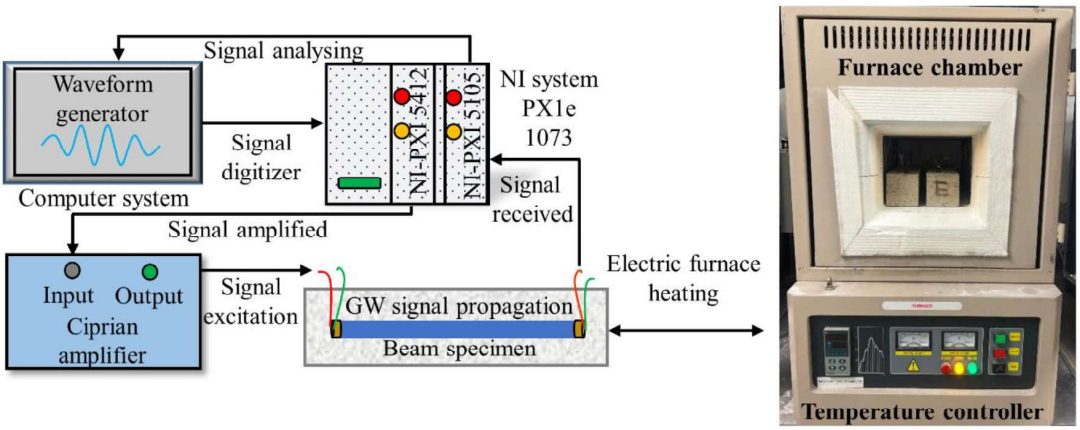

Figure 4.6 Experimental setup of heat damage study for rebar and RC beam

4.3.3 Validation of bare rebar for guided wave signal

Before casting the rebar with embedded ends in concrete for specimen type 1, the bare rebar with PZTs attached using high-temperature epoxy is tested for GW signal. The high temperature-epoxy resin is firmly bonded with PZTs for excitation and receiving of GW signal. The experimental setup used for testing bare rebar is shown in Figure 4.6, where the concrete beam specimen is replaced by bare rebar. An 80 kHz Hann windowed signal with 10 cycles is excited at the bare rebar end and received at the other rebar end. The input voltage is set to 0.6V, which is amplified 400 times to 240V. The measured time domain signal is presented in Figure 4.7 (a). Based on the group velocity dispersion curve for bare rebar, L(0,1) GW mode propagates at 80 kHz as shown in Figure 4.4. The group velocity of time domain signal in Figure 7 (a) is found to be similar to L(0,1) GW mode in group velocity dispersion curve for bare rebar. The time-frequency plot obtained using Short Time Fourier Transform (STFT) [31] for the time domain signal is shown in Figure 4.7(b). Time-frequency data for L(0,1) GW mode from the dispersion curve is superimposed on the time-frequency plot of the GW signal in bare rebar. It reflects the propagation of L(0,1) GW mode at 80 kHz frequency. The first pulse received is L(0,1) GW mode confirming the propagation of longitudinal GW signal using high-temperature epoxy and wires.

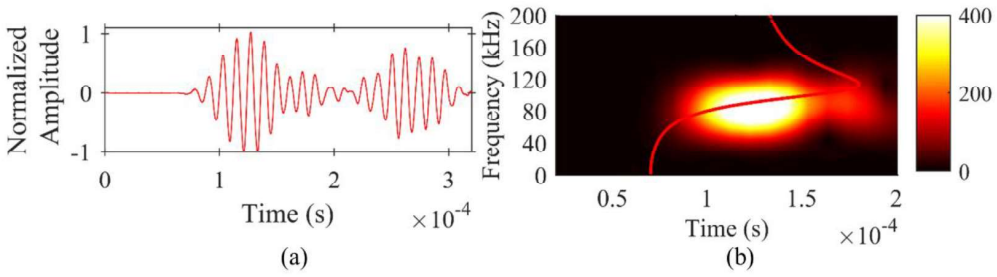

Figure 4.7 Time domain and (b) time-frequency spectrum of 80 kHz excitation signal in bare rebar

4.3.4 Reinforced concrete beam specimen with embedded rebar ends

The RC beam specimen type 1 and 2 are cast in the laboratory. For specimen type 1, the length of the concrete beam l_c is 400 mm as shown in Figure 4.2(a). The cross-section of the specimen is 75 mm × 75 mm. The length of the embedded rebar is 300 mm represented as l_{rb} in Figure 4.2(a) with a 50 mm cover at both ends. The steel rebar of 24 mm diameter having high-temperature epoxy and wires for PZTs at both ends is used for specimen type 1. The rebar is placed at the center of the cross-section as shown in Figure 4.8(a). The normal strength concrete with proportions of cement, sand and coarse aggregate as 1:2:4 is prepared. The mechanical properties of concrete are shown in Table 4.1. Figure 4.8(b) shows the final specimen type 1 prepared in the laboratory.

Table 4.1 Material properties for concrete and steel rebar

Material	Density (kg/m^3)	Elastic Modulus (GPa)	Poisson's ratio
Steel	7890	210	0.33
Concrete	230	32	0.13

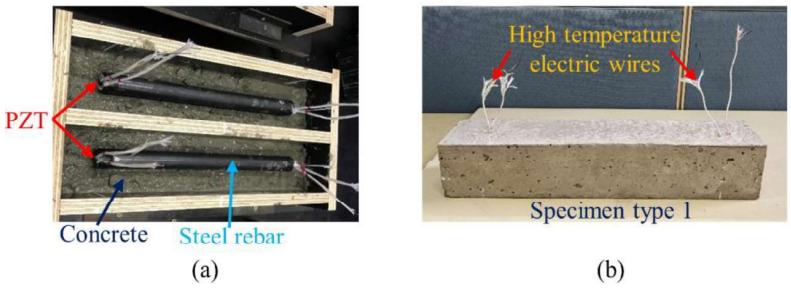

Figure 4.8 (a) Cast-in situ specimen type 1 and (b) cured specimen type with high-temperature wires

The size of the specimen is restricted to account for the heating furnace chamber size. Initially, the fully bonded specimen type 1 is studied for GW signal at room temperature. The exposed wires are connected to the NI setup as shown in Figure 4.6. For specimen type 1, the travel distance for the GW signal is only 300 mm. By considering the wavelength of GW at a

higher frequency, a 200 kHz 10-cycle Hann windowed signal is excited at end A with a voltage of 240V. The received time domain signal at end B is shown in Figure 4.9(a). Fast Fourier Transform (FFT) is applied on the time domain signal and is shown in Figure 4.9(b). There are no second harmonics generated in the fully bonded specimen type 1 as there is no contact effect between steel rebar and concrete.

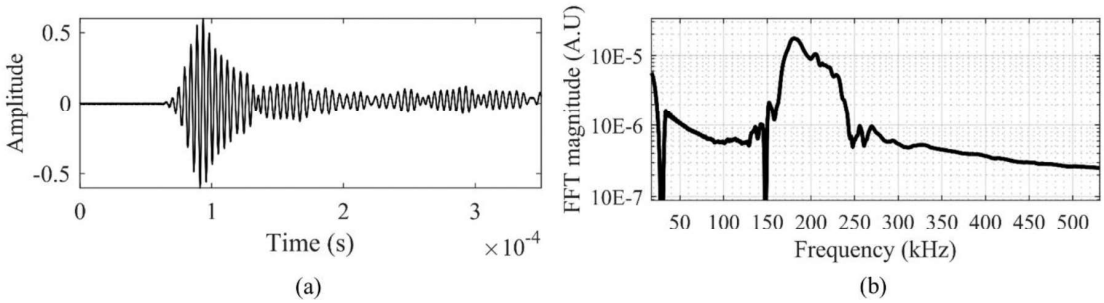

Figure 4.9 (a) Time domain and (b) frequency domain for fully bonded specimen type 1 without heat damage

The debonding is created using a Mylar sheet wrapped around the steel rebar at a distance of 100 mm shown as CD in Figure 4.2(b). The debonded specimen is prepared to study and monitor the effect of heat damage on the inherent debonded specimen. The debonding between steel rebar and concrete produces contact surfaces for longitudinal GW to generate second harmonics. A similar 200 kHz 10-cycle Hann windowed signal is excited at end A for specimen type 1 with debonding as shown in Figure 4.2(b). The time domain signal is shown in Figure 4.10 (a). With the FFT transform of this time domain signal, the presence of second harmonics at 400 kHz as shown in Figure 4.10 (b).

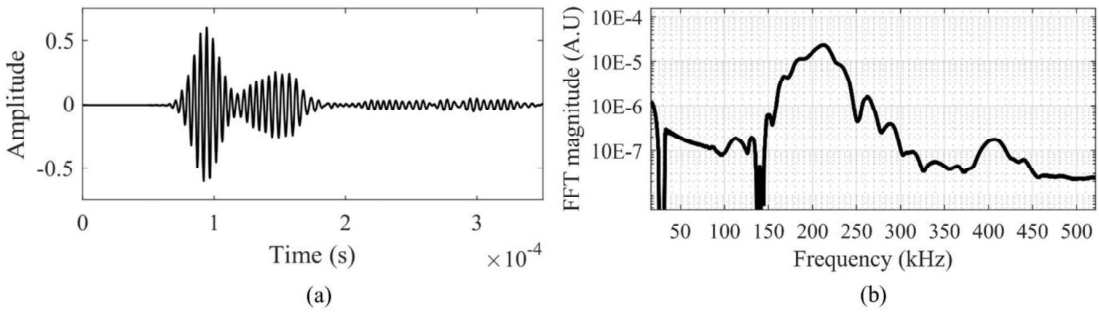

Figure 4.10 (a) Time domain and (b) frequency domain for debonded specimen type 1 without heat damage

Second harmonics are generated due to debonding in specimen type 1. It is worth mentioning from these results that embedded PZTs can be used to detect and monitor debonding type damage in RC structures using longitudinal GWs. These results for bonded and debonded specimens are acquired without any heat damage at room temperature. For heat damage, case studies are defined in Section 4.3.6 with results shown in Section 4.4. For shorter rebar length in specimen type 1, the greater excitation frequency is selected due to shorter wavelength, while specimen 2 has greater rebar length and lower frequency is selected for GW study.

4.3.5 Reinforced concrete beam specimen with exposed rebar ends

As specimen type 1 can only be heated up to 300°C due to the operational temperature limit of PZTs and wires, specimen type 2 is prepared in the laboratory with exposed rebar ends to study the effect of heat damage on bonding between steel rebar and concrete beyond 300°C. The total length of the steel rebar shown as l_{rb2} in Figure 4.3(a) is 400 mm with 50 mm of exposed rebar at either end. The cross-section of specimen type 2 is similar to specimen type 1 with 24 mm diameter steel rebar at the centre of the cross-section. The longitudinal and cross-section view for specimen type 2 are shown in Figures 4.11(a) and 4.11(b), respectively.

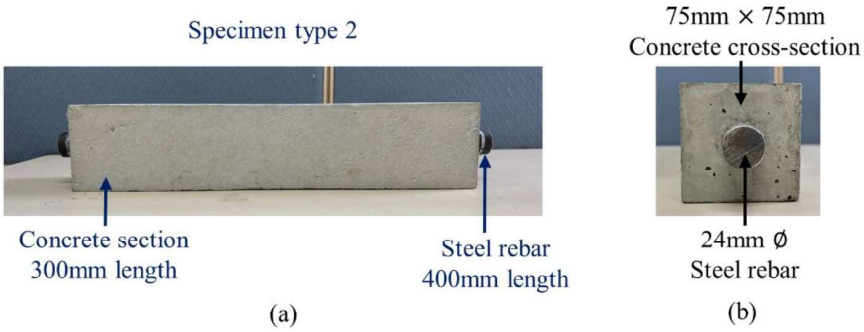

Figure 4.11 (a) Longitudinal and (b) cross-section view for specimen type 2 with exposed rebar ends

For excitation and receiving of longitudinal GW, G series ULTRAN transducers are attached to the exposed rebar ends. ULTRAN G series GC200-D13 is connected to excite 100 kHz 10-cycle Hann windowed signal. The GW signal is received at rebar end B using GC500D-13 as shown in Figure 4.12(a). The frequency domain represents the absence of second harmonics reflecting that the specimen is fully bonded as shown in Figure 4.12(b). The amplitudes of the time domain signal and FFT for specimen type 2 are larger than that of specimen type 1. As PZTs are embedded and surrounded by concrete in specimen type 1, the amplitude of the GW signal propagated in the embedded rebar is smaller for similar excitation voltage in specimen type 2. On contrary, specimen type 2 has bare rebar ends.

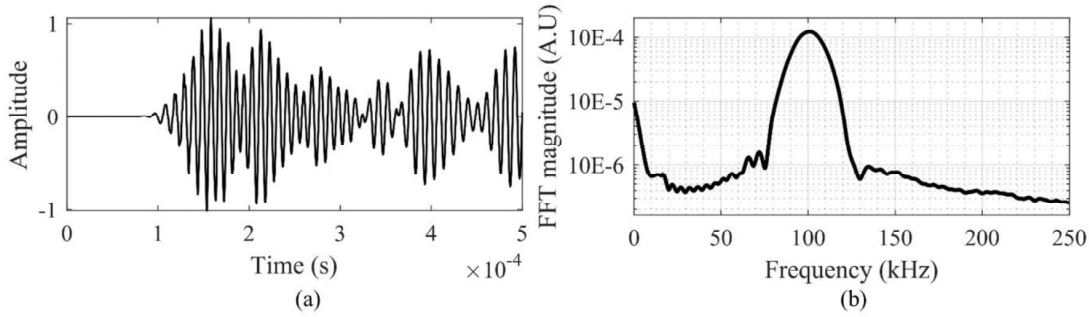

Figure 4.12 (a) Time domain and (b) frequency domain for fully bonded specimen type 2 without heat damage

The specimen type 2 is also prepared with debonding length d_l of 100 mm as shown in Figure 4.3(b). The distance to the debonding l_{a2} is 125 mm. With a similar experimental setup, the debonded specimen type 2 is excited with a 100 kHz 10-cycle Hann windowed signal. The time domain signal is shown in Figure 4.13(a). In debonded specimen type 2, the presence of second harmonics is clearly observed as shown in Figure 4.13(b).

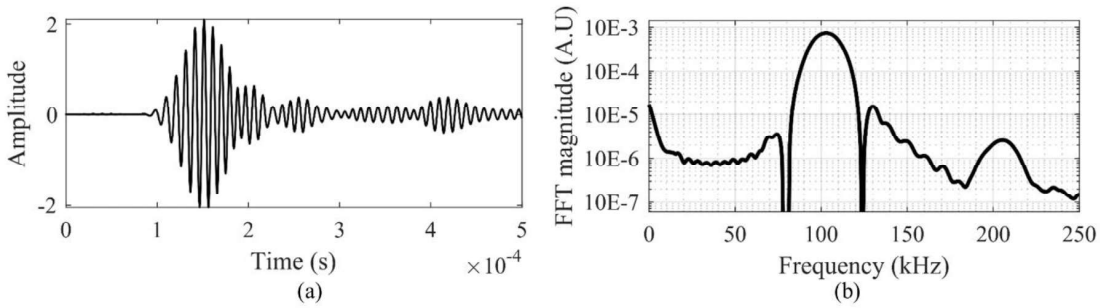

Figure 4.13 (a) Time domain and (b) frequency domain for debonded specimen type 2 without heat damage

The time domain signals for bonded and debonded specimen type 2 are also different. The GW signal for a fully bonded specimen is more dispersive and has a greater number of GW modes as compared to the debonded specimen. It is understood that GW can detect debonding with the presence of second harmonics.

4.3.6 Experimental case studies

The bonded and debonded specimen type 1 and 2 are analysed for heat damage study using GW. Specimen type 1 for fully bonded and debonded are heated up to 300°C. The debonding length in debonded specimen type 1 is 100 mm. Specimens 1B and 1D are heated up to each interval as shown in Table 4.2 and then cooled to room temperature for GW testing. For specimen type 2, the GW study is carried out using exposed rebar ends, for which the maximum heated temperature is 800°C. For GW study using specimen type 2, the transducers are attached to exposed rebar ends after the specimen is cool down in each heated interval. Specimen type

2 is heated until the cracks widely open and break the RC beam specimen as shown in Section 4.4.3. The linear and nonlinear GW study can give an indication of the effect of debonding between steel rebar and concrete for both fully bonded and debonded specimens. The time domain and FFT data for each case study are shown in Section 4.4.

Table 4.2 Heat damage cases for bonded and debonded specimen type 1 and 2

Specimen type	**Rebar ends**	**Bonded**	**Debonded**		**Excitation frequency**	**Heated temperature**
		Cases	**Cases**	**Debonded length**		
Specimen type 1	Embedded	1B1	1D1	100 mm	200	Room
		1B2	1D2	100 mm	200	100^0C
		1B3	1D3	100 mm	200	200^0C
		1B4	1D4	100 mm	200	300^0C
Specimen type 2	Exposed	1B1	1D1	100 mm	100	Room
		1B2	1D2	100 mm	100	100^0C
		1B3	1D3	100 mm	100	200^0C
		1B4	1D4	100 mm	100	400^0C
		1B5	1D5	100 mm	100	600^0C
		1D6	1D6	100 mm	100	800^0C

The nonlinear study investigates the presence of second harmonics in heat damaged and debonded cases, which is due to the initial debonding or debonding generated due to heat damage. As discussed in Section 4.2, the second harmonics can be generated due to material nonlinearity. When the specimen is heated, the temperature change can produce material nonlinearities in embedded rebars through which GW is propagated. If there is any material nonlinearity due to heat damage in the rebar, it can be monitored using GW study on bare rebar. To study material nonlinearity in bare rebar, the case studies are defined in Table 4.3.

Table 4.3 Heat damage cases for bare rebar type 1 and 2

Bare rebar				
Rebar type	**Cases**	**Excitation Frequency (kHz)**	**Rebar length**	**Heated temperature**
Rebar type 1	1R1	200	300	Room
	1R2	200	300	100°C
	1R3	200	300	200°C
	1R4	200	300	300°C
Rebar type 2	2R1	100	400	Room
	2R2	100	400	100°C
	2R3	100	400	200°C
	2R4	100	400	400°C
	2R5	100	400	600°C
	2R6	100	400	800°C

The rebar type 1 is 300 mm in length, which is similar to the embedded rebar in specimen type 1. The rebar type 2 is 400 mm in length, which is similar to the rebar in specimen type 2. These rebars are subjected to heated intervals as shown in Table 4.3 to determine any second harmonics generated due to material nonlinearity.

4.4 Results and discussions

The linear and nonlinear GW results are discussed for RC beam specimens and the bare rebar in this section. The heat damage has an impact on the time domain signal for the RC beam specimen. The heat damage creates debonding between steel rebar and concrete to generate second harmonics. The bonded and debonded specimen type 1 are similar to each other except the debonding length is 100 mm. Similarly, the bonded and debonded specimen type 2 have similar characteristics except the debonded has 100 mm of debonding length. The bonded and debonded specimen are tested for heat damage to understand the linear and nonlinear characteristics of GW signal with and without debonding in the RC beam.

4.4.1 Second harmonics due to heat damage in specimen type 1

After initial GW testing of fully bonded specimen type 1 at room temperature, it is heated at 100°C, 200°C and 300°C. After each heated interval, the bonded specimen is tested for GW signal at 200 kHz with an input voltage of 240V. The time domain data received for fully bonded specimen type 1 heated cases is shown in Figure 4.14(a). The FFT for each heated case for fully bonded specimen type 1 is shown in Figure 4.14(b). The time domain signal is normalized to plot the frequency data. Figure 4.14(a) shows an increase in second harmonics magnitude at 400 kHz with the increase in temperature. The maximum amplitude of second harmonics is observed for 1B4 at 300°C. It is obvious that heat damage has created debonding between steel rebar and concrete to generate contact surfaces for second harmonics. The amplitude of the time domain signal is also increased for heated cases, and the maximum amplitude happens in case 1B4.

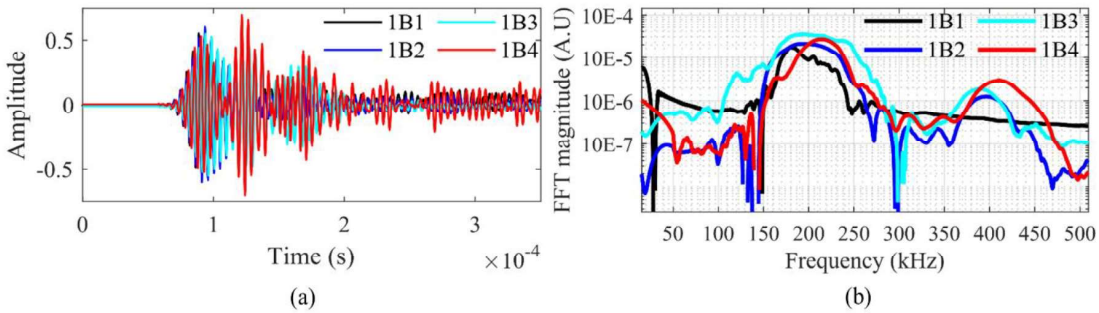

Figure 4.14 (a) Time domain and (b) frequency domain for fully bonded specimen type 1 at heat damaged cases

Similarly, specimen type 1 with 100 mm of debonding is considered in the heat damage cases to observe the time domain signal and second harmonics. The excitation signal is 200 kHz with 240V for each heated case. The time domain signal for debonded specimen type 1 at heat damaged cases is shown in Figure 4.15(a). Initially, the second harmonics are produced due to the artificial debonding created in the specimen for case 1D1. The heated cases 1D2,

1D3 and 1D4 show an increase in the amplitude of second harmonics as shown in Figure 4.15(b). It depicts that further debonded regions are produced in embedded rebar due to heat damage to generate second harmonics. The heat damage case ID4 shows the maximum amplitude of second harmonics at 300°C.

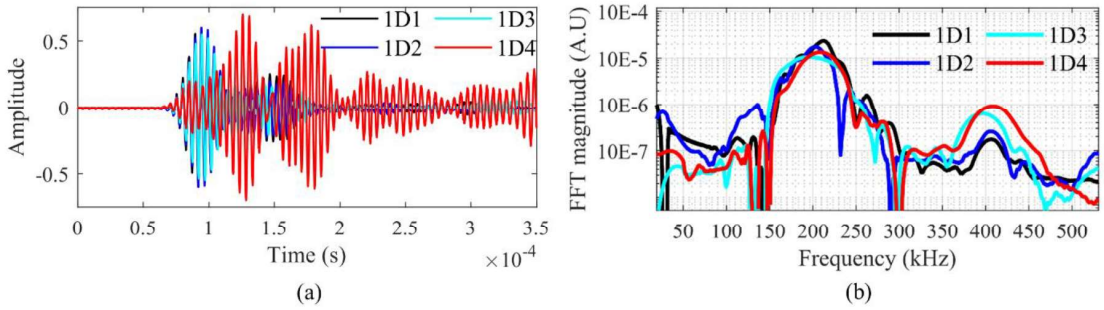

Figure 4.15 (a) Time domain and (b) frequency domain for debonded specimen type 1 at heat damaged cases

4.4.2 Second harmonics due to heat damage in specimen type 2

The embedded PZTs could not be tested for GW after the specimen was heated beyond 300°C due to its limitation. To overcome this issue, specimen type 2 with exposed rebar ends is heated beyond 300°C to monitor the GW signal for linear and nonlinear study. The specimen type 2 with fully bonded and debonded are heated up to 800°C. The specimen type 2 case studies for heated temperature are defined in Table 4.2. The excitation frequency for specimen type 2 is 100 kHz at 240V. The time domain signal for fully bonded specimen type 2 cases is shown in Figure 4.16(a). The time domain signals are normalized to plot the data in the frequency domain as shown in Figure 4.16(b). The time domain signal represents a significant increase in amplitude for cases 2B5 and 2B6. In the frequency domain, the second harmonics appear for cases 2B2, 2B3, 2B4, 2B5 and 2B6 at 200 kHz. The maximum amplitude of second harmonics for fully bonded specimen type 2 is noted for case 2B6 at 800°C.

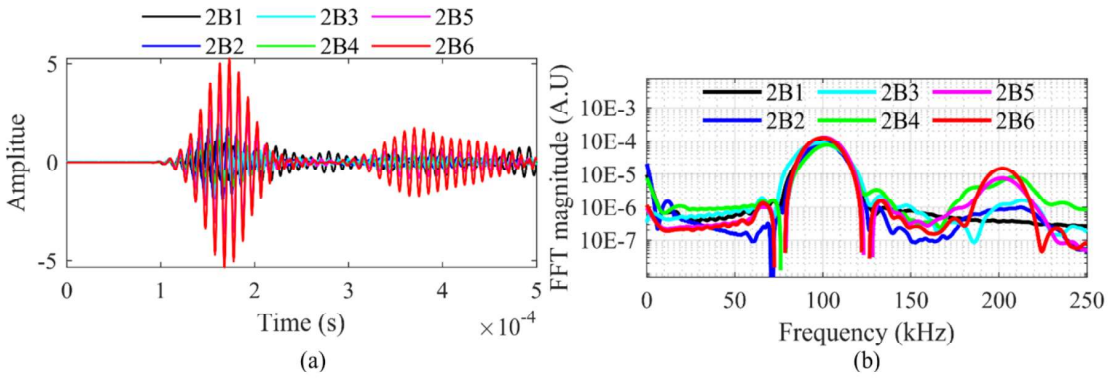

Figure 4.16 (a) Time domain and (b) frequency domain for fully bonded specimen type 2 at heat damaged cases

The debonded specimen type 2 with 100 mm of debonding is heated for cases as shown in Table 4.2. The specimen is tested for GW signal at 100 kHz with 240V after each heated case. The time domain signal for debonded specimen type 2 cases is shown in Figure 4.17(a). The amplitude of the time domain signal is significantly increased for heated cases 2D5 and 2D6 at 600°C and 800°C respectively. The time domain signal is normalized to attain FFT as shown in Figure 4.17(b). The debonded heated cases 2D2, 2D3, 2D4, 2D5 and 2D6 show an increase in the amplitude of second harmonics. The maximum amplitude of second harmonics is observed for 2D6 at 800°C.

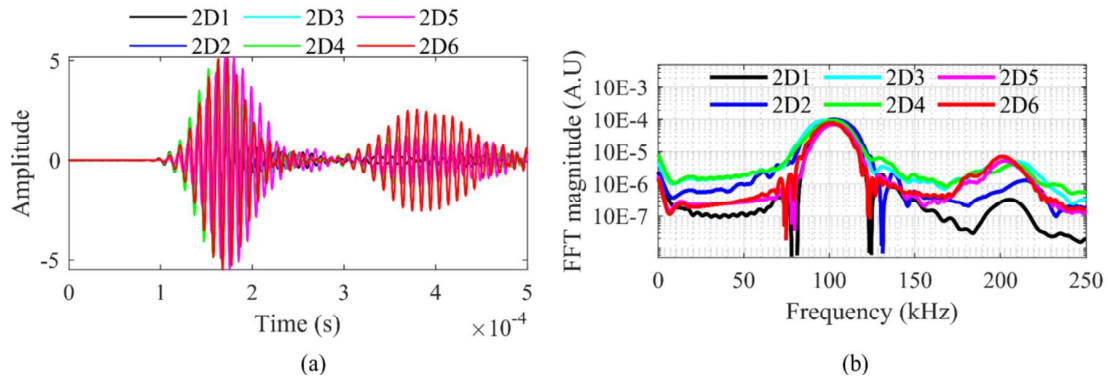

Figure 4.17 (a) Time domain and (b) frequency domain for debonded specimen type 2 at heat damaged cases

The bonded and debonded specimen type 1 and 2 showed an increase in the amplitude of second harmonics with elevated temperatures. Therefore, the second harmonic is a useful indicator of the severity of heat damage which deteriorates the bonding between steel and concrete.

4.4.3 Linear feature for heat damage in reinforced concrete specimen

Sections 4.4.1 and 4.4.2 show the amplitude for the time domain signal of both specimen type 1 and 2 with the temperature. The peak amplitudes of time domain signals are plotted for bonded and debonded specimen type 1 and 2 at their respective heated temperatures as shown in Figure 4.18. For specimen type 1, the amplitude of time domain signal is lesser than specimen type 2 as the PZTs are embedded inside the concrete. With similar excitation voltage for specimen type 1 and 2, specimen type 1 has greater energy leakage to surrounding concrete as compared to specimen type 2, which has exposed rebar ends. The amplitude is slightly increased at the elevated temperature beyond 200^0C for specimen type 1. For both bonded and debonded specimen type 2, the amplitude of GW is significantly increased from heated intervals of 200°C to 800°C. For specimen type 2, the debonded specimen has a sharp increase in amplitude as compared to the bonded specimen. It has been acknowledged that heat damage has generated debonding between steel and concrete which results in a reduction of leaking GW energy into surrounding concrete. Due to this phenomenon, a larger amplitude of the GW signal is observed as the temperature progress.

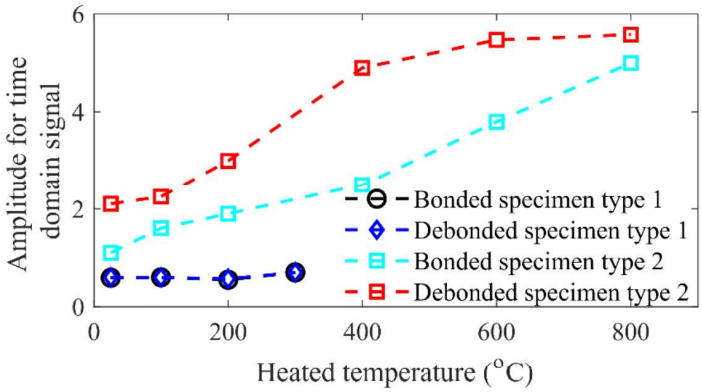

Figure 4.18 Change in the amplitude of GW signal for bonded and debonded specimen type 1 and 2 with elevated heat temperatures

Apart from heat damage creating debonding between steel and concrete, it also has an impact on the concrete surrounding the rebar. With the increase in heated temperature, cracks appear on the concrete surface mainly beyond 200°C. These cracks tend to widen at increased temperature. The spalling of concrete is also observed beyond 400°C. The pattern of cracks for the bonded and debonded specimen is different. For bonded specimens, the cracks appeared near the edges at the approximate 1/3 location of the beam as shown in Figure 4.19(a). However, for debonded specimens, the crack appears at the center of debonding location, which was already known as shown in Figure 4.19(b). For progressive heat, the damage is concentrated at the center of debonding location in the debonded specimen. Considering this, in fully bonded specimens the cracks tend to appear at the location, where the bonding of concrete with steel is weaker. At 1,000°C, the concrete beam specimens are fully cracked and divided into sections as shown in Figure 4.19(c). After 1,000°C, the steel rebar is manually pulled out of the concrete with ease showing no or minimal bonding with the surrounding concrete. As the steel rebar is pulled out, the concrete section is broken by itself and divided into sections. Figure 4.19(c) shows the cross-section of concrete at cracked locations showing the progress of the crack throughout the cross-section. It is therefore important to consider that heat damage creates debonding between steel rebar and concrete. The experimental results also

reflect that structural health monitoring of RC can be carried out when they are exposed to fire or heat damage.

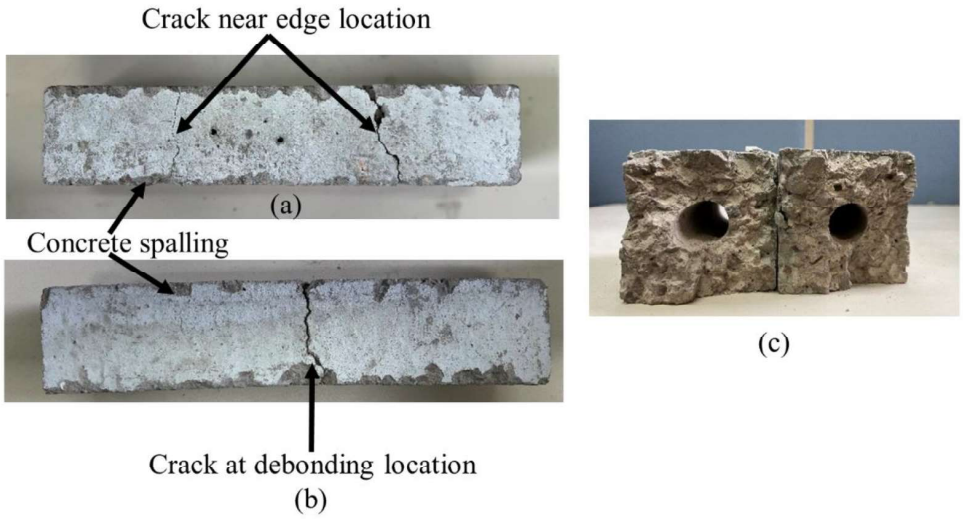

Figure 4.19 Crack pattern for (a) bonded and (b) debonded specimen type, (c) concrete cross-section at cracked location

4.4.4 Rebar heat damage

The amplitude of second harmonics generated due to heat damage of bonded and debonded specimen type 1 and 2 have components of heat damage due to material nonlinearity of embedded rebar. To study the second harmonics due to material nonlinearity in rebar because of heat damage, the bare rebar cases are defined in Table 4.3. The rebar type 1 and 2 are tested for GW signal using ULTRAN transducers. ULTRAN G series GC200-D13 is used to excite the GW signal ULTRAN G series GC500D-13 is used to receive the GW signal using a similar experimental setup instead of the RC beam as shown in Figure 4.6. The excitation signal used for specimen type 1 is used for rebar type 1 with excitation voltage to be consistent at 240V. The time domain signal for rebar type 1 at heated intervals is shown in Figure 4.20(a). At heated intervals, the frequency domain does not show any significant second harmonics as shown in

Figure 4.20(b). The amplitude of the received signal is slightly reduced for heated case 1R4 at 300°C.

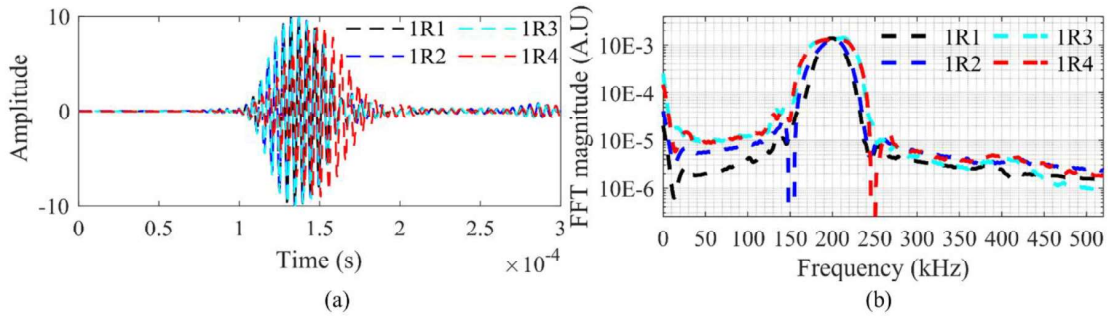

Figure 4.20 (a) Time domain and (b) frequency domain for rebar type 1 in heat damaged cases

Similarly, the rebar type 2 is heated for temperature intervals as shown in Table 4.3. The excitation signal in rebar type 2 is similar to specimen type 2. The amplitude of the received signal slightly decreases at higher temperature with a consistent excitation voltage of 240V as seen in Figure 4.21(a). Again, the rebar type 2 did not show any significant second harmonics at heated temperature as seen in Figure 4.21(b).

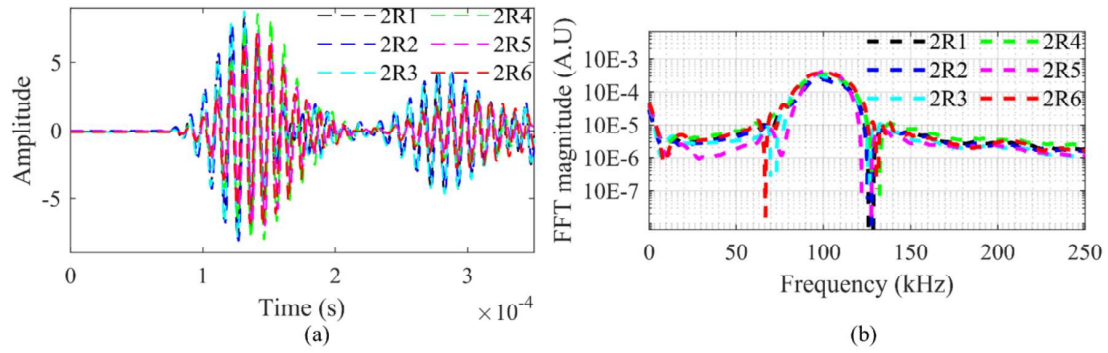

Figure 4.21 (a) Time domain and (b) frequency domain for rebar type 2 in heat damaged cases

As the steel rebar undergoes changes in material properties and nonlinearity at elevated temperatures, the longitudinal guided waves did not show the presence of any nonlinear

features. Therefore, the nonlinear parameter calculated for material nonlinearity in bare rebar will not have a significant magnitude in comparison to the nonlinear parameter due to contact heat damage.

4.4.5 Nonlinear parameter

Based on heated damage, the nonlinear parameter β_m due to material nonlinearity and β due to contact damage is discussed in this section. Due to heat damage, β_m is calculated for bare rebar while β is calculated for the concrete beam specimen as discussed in Section 4.2.3. The rebar type 1 and specimen type 1 are compared together for β_m and β respectively, while rebar type 2 and specimen type 2 are compared together for β_m and β, respectively. The bonded specimen type 1 β and rebar type 1 β_m are shown in Figure 4.22(a). Due to the difference in magnitude of time domain signal amplitude between rebar and concrete beam specimen, the nonlinear parameter β_m and β is normalized for peak amplitude in the concrete beam specimen type. A_1 is the amplitude of FFT at excitation frequency, where A_2 is the amplitude of the generated second harmonics. Similarly, the debonded specimen type 1 β and rebar type 1 β_m are plotted in Figure 4.22(b). For bonded specimen type 1, β is slightly reduced between 100°C and 200°C. It is due to the increase of debonding contact gap at an increased temperature between rebar and concrete making the GW signal unable to generate a larger amplitude of second harmonics. However, the increase in β is observed at 300°C. It should be noted that further cracks and debonding are generated as the temperature is progressively increased. For the debonded specimen type 1, β is increased from 100°C to 300°C.

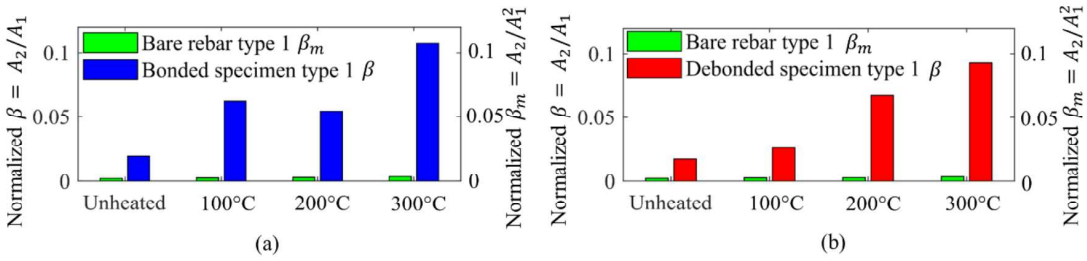

Figure 4.22 Nonlinear parameter βm for bare rebar type 1 and β for (a) bonded and (b) debonded specimen type 1

For rebar type 2 and specimen type 2, the heated temperature is from 100°C to 800°C. The β value of the bonded specimen type 2 is plotted along with β_m value of the rebar type 2 in Figure 4.23. It can be seen that contact type β for bonded specimen type 2 increases with elevated temperature.

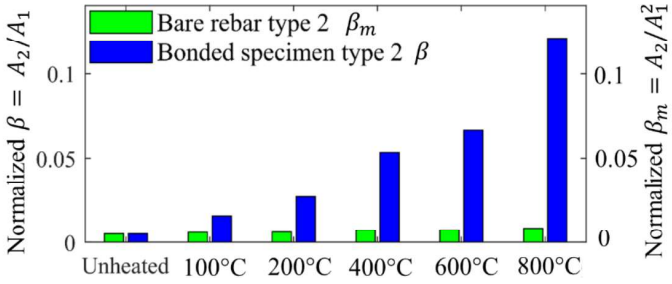

Figure 4.23 Nonlinear parameter βm for bare rebar type 2 and β for bonded specimen type 2

The β value of the debonded specimen type 2 is plotted along with β_m value of the rebar type 2 in Figure 4.24. The nonlinear parameter β significantly increases for debonded specimen type 2 at 200°C. It has been slightly reduced at 300°C as seen for bonded specimen type 1. The reduction in β value is linked to the contact gap between rebar and concrete. Mainly, β value of the debonded specimen type 2 still shows the presence of significant heat damage at 400°C, which progressively increases up to 800°C.

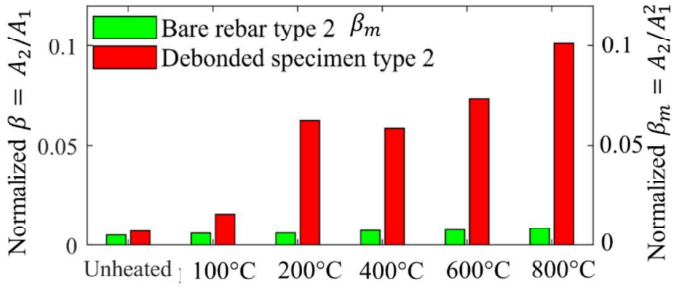

Figure 4.24 Nonlinear parameter βm for bare rebar type 2 and β for debonded specimen type 2

After 800°C, the bonded and debonded specimen type 2 were cracked due to excessive heat damage at 1,000°C as discussed in Section 4.4.3. The nonlinear parameter β shows that nonlinear GW can detect debonding damage generated due to heated temperature in RC beams. The severity of damage can also be monitored as the nonlinear parameter β increases at elevated temperature.

4.5. Conclusion

Linear and nonlinear GW features are studied experimentally to detect heat damage in the RC beams. The RC specimens are heated in a furnace to study debonding damage between rebar and concrete. Specimen type 1 has rebar ends fully embedded inside the concrete while specimen type 2 has embedded rebars, whose ends are exposed outside the beam for attaching transducers. Specimen type 1 has embedded sensors attached to rebar inside the concrete, which can be subjected to heat damage at 300°C. For specimen type 2, the GW signal is propagated after the cool down of the specimen from the heated temperature. Therefore, specimen type 2 is tested up to 800°C before the cracks open in the RC beam at 1,000°C.

For both specimen type 1 and 2, the bonded and debonded specimen are prepared. The debonding is created using a Mylar sheet wrapped around the steel rebar. For specimen type 1, a 200 kHz excitation signal is used for the GW study with the heated temperature at 100°C,

200°C and 300°C. The debonded specimen type 1 shows the presence of second harmonics at room temperature as compared to bonded specimen type 1. This reflects that the embedded sensors can detect debonding between steel rebar and concrete in RC beams. The second harmonics are observed at heated temperatures for both bonded and debonded specimen type 1. Specimen type 2 is tested for GW signal using ULTRAN transducers at the exposed rebar ends. Specimen type 2 is heated at 100°C, 200°C, 400°C, 600°C and 800°C temperature. The excitation frequency for specimen type 2 is 100 kHz. Both bonded and debonded specimen type 2 show that the presence of second harmonics at heated temperature. The presence of second harmonics in bonded and debonded specimen type 1 and 2 at elevated temperature reflects the development of debonding between steel rebar and concrete due to heat damage.

The linear features of the GW signal are also compared in this study. The peak amplitude of GW signals is compared for bonded and debonded specimen type 1 and 2 at elevated temperatures. The study has shown that the amplitude of the GW signal increases with an increase in heated temperature.

To quantify heat damage at elevated temperature, β is calculated for RC specimens at heated temperatures due to contact nonlinearity, while β_m is calculated for bare rebar at heated temperatures due to material nonlinearity. To achieve this, a separate heat damage experimental study is carried out on the bare rebar type 1 and 2 similar to rebars in specimen type 1 and 2, respectively. These two parameters are calculated separately to distinguish any material nonlinearity from rebar due to heat damage. The study has shown that ratio of β_m for its respective β heated case at increased temperatures is very marginal. This result has reflected that the amplitude of any second harmonics of longitudinal GW generated due to material nonlinearity in rebars is very minimal. The nonlinear parameter β for bonded and debonded specimen type 1 and 2 have significantly increased beyond 200°C. The peak amplitude of β is

observed for bonded and debonded specimen type 2 at 800°C. Therefore, the heat damage in the RC beam creates cracks and debonding between steel rebar and concrete enabling GW to generate second harmonics.

Acknowledgement

This work was funded by the Australian Research Council (ARC) DP200102300 and DP210103307 grants. The authors are grateful for the support.

4.6 References

1. Beata, Z. and K. Rafał, *Debonding Size Estimation in Reinforced Concrete Beams Using Guided Wave-Based Method.* Sensors, 2020. **20**(2): p. 389.
2. Zhu, X.Q., H. Hao, and K.Q. Fan, *Detection of delamination between steel bars and concrete using embedded piezoelectric actuators/sensors.* Journal of Civil Structural Health Monitoring, 2013. **3**(2): p. 105-115.
3. Soleimanpour, R. and C.T. Ng, *Locating delaminations in laminated composite beams using nonlinear guided waves.* Engineering Structures, 2017. **131**: p. 207-219.
4. Wu, F. and F.K. Chang, *Debond detection using embedded piezoelectric elements in reinforced concrete structures - Part I: Experiment.* Structural Health Monitoring-an International Journal, 2006. **5**(1): p. 5-15.
5. Wu, F. and F.K. Chang, *Debond detection using embedded piezoelectric elements for reinforced concrete structures - Part II: Analysis and algorithm.* Structural Health Monitoring-an International Journal, 2006. **5**(1): p. 17-28.
6. Ou, G., et al., *Identifi cation of de-bonding between steel bars and concrete using wavelet techniques: Comparative study.* Australian Journal of Structural Engineering, 2013. **14**(1): p. 43-56.
7. Majhi, S., et al., *Corrosion detection in steel bar: A time-frequency approach.* NDT & E International, 2019. **107**: p. 102150.
8. Sriramadasu, R.C., Y. Lu, and S. Banerjee, *Identification of incipient pitting corrosion in reinforced concrete structures using guided waves and piezoelectric wafer transducers.* Structural Health Monitoring-an International Journal, 2019. **18**(1): p. 164-171.
9. Lu, Y., et al., *Guided waves for damage detection in rebar-reinforced concrete beams.* Construction and Building Materials, 2013. **47**: p. 370-378.
10. Mustapha, S., et al., *Damage detection in rebar-reinforced concrete beams based on time reversal of guided waves.* Structural Health Monitoring-an International Journal, 2014. **13**(4): p. 347-358.
11. Aseem, A. and C.T. Ng, *Debonding detection in rebar-reinforced concrete structures using second harmonic generation of longitudinal guided wave.* Ndt & E International, 2021. **122**.
12. Chen, J., C.L. Yang, and Q.Q. Guo, *Evaluation of surface cracks of bending concrete using a fully non-contact air-coupled nonlinear ultrasonic technique (vol 51, 104, 2018).* Materials and Structures, 2019. **52**(2).
13. Chen, J., J. Ren, and T.Y. Yin, *Nondestructive evaluation of notched cracks in mortars by nonlinear ultrasonic technique.* Nondestructive Testing and Evaluation, 2016. **31**(2): p. 109-121.

14. Chang, Y.F., et al., *Residual stress–strain relationship for concrete after exposure to high temperatures.* Cement and Concrete Research, 2006. **36**(10): p. 1999-2005.
15. Behnood, A. and M. Ghandehari, *Comparison of compressive and splitting tensile strength of high-strength concrete with and without polypropylene fibers heated to high temperatures.* Fire Safety Journal, 2009. **44**(8): p. 1015-1022.
16. Ozbolt, J., et al., *3D numerical analysis of reinforced concrete beams exposed to elevated temperature.* Engineering Structures, 2014. **58**: p. 166-174.
17. Ghazaly, N., et al., *Evaluation of bond strength between steel rebars and concrete for heat-damaged and repaired beam-end specimens.* Engineering Structures, 2018. **175**: p. 661-668.
18. Shamseldein, A., et al., *Assessment and restoration of bond strength of heat-damaged reinforced concrete elements.* Construction and Building Materials, 2018. **169**: p. 425-435.
19. Colombo, M., M. di Prisco, and R. Felicetti, *Mechanical properties of steel fibre reinforced concrete exposed at high temperatures.* Materials and Structures, 2010. **43**(4): p. 475-491.
20. Esfahani, M., et al., *Experimental investigation of residual flexural capacity of damaged reinforced concrete beams exposed to elevated temperatures.* Engineering Structures, 2021. **240**.
21. Lo Monte, F., et al., *Ground-Penetrating Radar monitoring of concrete at high temperature.* Construction and Building Materials, 2017. **151**: p. 881-888.
22. Miramini, S., et al., *Health Assessment of a Pedestrian Bridge Deck using Ground Penetrating Radar.* Electronic Journal of Structural Engineering, 2018. **18**(1): p. 30-37.
23. Lee, C., et al., *Interpretation of Impact-Echo Testing Data from a Fire-Damaged Reinforced Concrete Slab Using a Discrete Layered Concrete Damage Model.* Sensors, 2020. **20**(20).
24. Xargay, H., et al., *Acoustic Emission behavior of thermally damaged Self-Compacting High Strength Fiber Reinforced Concrete.* Construction and Building Materials, 2018. **187**: p. 519-530.
25. Chobola, Z., M. Matysík, and I. Plšková, *Detection of Reinforced Concrete Thermal Damage by Nonlinear Ultrasonic Spectroscopy.* Solid state phenomena, 2019. **296**: p. 143-148.
26. Aseem, A., et al., *Structural health assessment of fire damaged building using non-destructive testing and micro-graphical forensic analysis: A case study.* Case Studies in Construction Materials, 2019. **11**.
27. Solodov, I.Y., N. Krohn, and G. Busse, *CAN: an example of nonclassical acoustic nonlinearity in solids.* Ultrasonics, 2002. **40**(1): p. 621-625.
28. Zhang, S. and F. Yu, *Piezoelectric Materials for High Temperature Sensors.* Journal of the American Ceramic Society, 2011. **94**(10): p. 3153-3170.
29. Zhao, Y.X., et al., *Generation mechanism of nonlinear ultrasonic Lamb waves in thin plates with randomly distributed micro-cracks.* Ultrasonics, 2017. **79**: p. 60-67.
30. Pavlakovic, B., et al., *Disperse: A general purpose program for creating dispersion curves.* Review of Progress in Quantitative Nondestructive Evaluation, Vols 16a and 16b, 1997. **16**: p. 185-192.
31. Sharma, G.K., et al., *Short time Fourier transform analysis for understanding frequency dependent attenuation in austenitic stainless steel.* Ndt & E International, 2013. **53**: p. 1-7.

5. Conclusions

5.1 Summaries and contributions of this thesis

In this thesis, a comprehensive study has been carried out to detect debonding type damage in reinforced concrete beam using linear and nonlinear features of guided waves. The effect of heat damage on rebar and concrete bonding is also monitored using linear and nonlinear guided waves. In Chapter 1, the advantages of SHM are elaborated in reinforced concrete structures, which can help to detect damage before any catastrophic failure. For detecting damage using non-destructive testing, advantages of linear and nonlinear guided waves are highlighted which has been used by many researchers in various kinds of structures. The propagation of guided wave modes in cylindrical structures like rebar are mentioned. Mainly, longitudinal and torsional guided wave modes are used in this thesis for damage detection. Nonlinear features as second harmonics and guided wave mixing have their own advantages which are mentioned to detect debonding type damage in rebar embedded in concrete.

In Chapter 2, numerical and experimental study has been carried out to detect and locate debonding damage using second harmonics generation. The theoretical study has shown that when propagating guided wave interacts with contact nonlinearity or damage, this phenomenon generates higher harmonics. A 3D FE model of reinforced concrete beam has been generated in ABAQUS and longitudional guided waves have been propagated through rebar embedded in concrete. The guided wave modes interacting with damage in reinforced concrete beam have generated second harmonics which were absent in fully bonded specimen. This chapter has also shown that by using STFT and wave-number frequency analysis, the location of debonding can be estimated. The experiments have been conducted and the results match well with numerical study representing that debonding between rebar and concrete in reinforced concrete beam can be detected and located using second harmonics generation.

Further, the thesis advances the nonlinear technique of damage detection using guided wave mixing in the reinforced concrete beam. Chapter 3 has outlined the advantages of nonlinear guided wave mixing where system nonlinearities can be avoided over second harmonics generation. A comprehensive numerical and experimental study has been carried out in this paper to detect debonding in reinforced concrete using guided wave mixing. The theoretical study has shown that synchronism condition of propagating guided wave mode pairs has to be met to generate combinational harmonics. For developing a 3D FE model of the reinforced concrete beam, ribbed steel rebar has been used in this paper.

Two longitudinal guided wave mode pairs have been selected, whose synchronism condition were satisfied for producing sum combination harmonics in the presence of debonding, damage or material nonlinearity. The receiving longitudinal and torsional guided wave modes have shown the presence of sum combinational harmonics in debonded specimens which are absent in bonded specimens. Phase-reversal technique has further shown the clear presence of sum combinational harmonics in debonded specimens. The torsional receiving mode pair appears to be more sensitive to damage than the longitudinal mode pair. The experimental case studies have also shown that guided wave mixing can detect debonding damage in reinforced concrete beams. The location of debonding has also been estimated accurately numerically and experimentally using guided wave mixing.

Reinforced concrete structures can also be subjected to heat or fire damage which can affect the bonding between steel rebar and concrete. Nonlinear guided waves could play an important role in monitoring the debonding between rebar and concrete due to heat damage. This comprehensive study has been undertaken in Chapter 4. The experimental study used reinforced concrete beam specimens of two types where one has PZT sensors attached to rebar embedded inside the concrete while the other specimen has rebar exposed outside concrete for attaching longitudinal transducers. Using an electric furnace, the specimen with an embedded

sensor was heated from 100°C to 300°C due to the limitation of embedded sensors, while the exposed rebar specimen was heated from 100°C to 800°C and they were tested using longitudinal guided waves. Linear study showed that the amplitude of guided wave signal was increased with an increase in temperature. Further, the nonlinear study has been conducted using second harmonics which had clearly shown that second harmonics were generated due to elevated temperature and the amplitude of second harmonics also tends to increase with hearted temperature. The bare rebars had also been tested at heated temperature from 100°C to 800°C for linear and nonlinear guided waves which showed that the second harmonics were absent at heated temperature. It concluded that second harmonics in the reinforced concrete specimen at heated temperature had been generated from contact nonlinearity due to debonding between rebar and concrete rather than from any material nonlinearity in rebar.

5.2 Recommendations

This thesis has studied the linear and nonlinear features of guided waves for damage detection in steel rebar embedded in concrete. Longitudinal guided waves are used for excitation in various damage detection studies. The research work can further be advanced in the following areas;

1. In circular steel rebar, there are longitudinal, torsional and flexural propagating guided wave modes. This research has utilized longitudinal excited guided waves for detecting and locating damage. The ability of flexural guided wave modes to detect damage in embedded rebar using nonlinear techniques can be potentially studied. As found in this study, torsional guided waves are sensitive to debonding damage but they require larger excitation amplitude to propagate through embedded rebar. Therefore, it is another

direction to explore torsional guided waves excitation in embedded rebars for debonding damage detection.

2. The steel rebar in reinforced concrete structures can be spliced or bent in civil structures. The ability of longitudinal guided waves to travel through spliced or bent sections can be studied in the future. The detection of damage before and after the spliced or bent section can be explored.
3. In this thesis, the collinear one-way guided wave mixing is studied. However, there is potential to study two-way collinear guided wave mixing for damage detection embedded rebars. By satisfying phase-matching conditions, the excitation waves form either ends of rebars can be focused to interact in damaged area.
4. The reinforced concrete structures are also subjected to static or moving loads such as bridges. The ability of guided waves to detect damage in such scenarios can be studied in the future.
5. This thesis investigates the presence of damage at one location in a reinforced concrete beam. Further efforts can be made using guided waves to locate damage at multiple locations in embedded rebar in concrete.
6. In reinforced concrete bridges and buildings, the PZT sensors can be installed to rebars before casting of concrete. This practice can give us useful information in detecting debonding, corrosion or damage due to fire in rebar reinforced concrete during lifecycle of the structure.
7. Apart from debonding damage, the ability of nonlinear features of guided waves can be explored to determine crack damage, material nonlinearity and material strength of concrete due to varying live loads in structures such as bridges and buildings.